Neuron

Article

Spatial context non-uniformly modulates inter-laminar information flow in the primary visual cortex

Graphical abstract

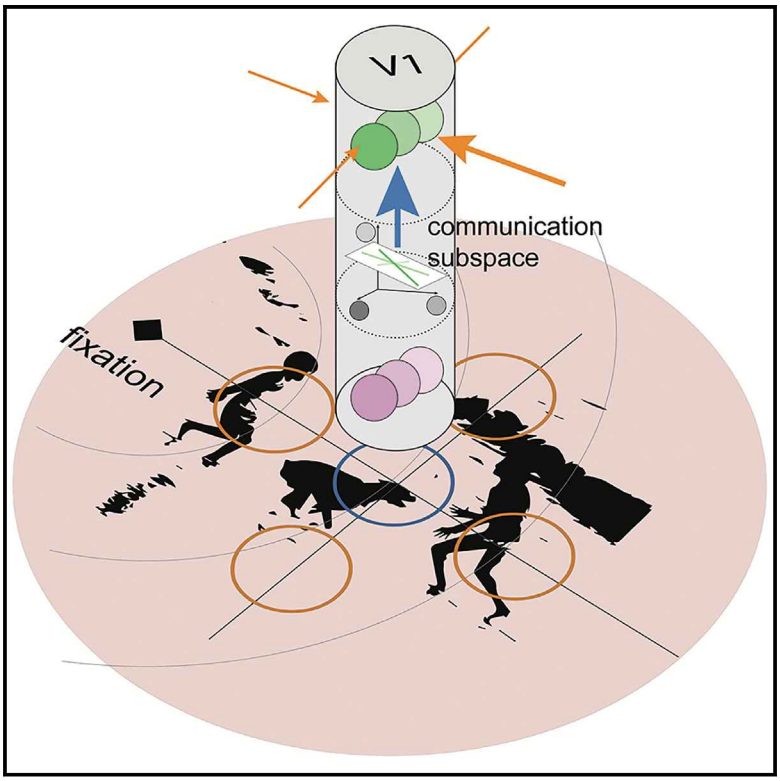

Authors

Xize Xu (徐锡泽), Mitchell P. Morton, Sachira Denagamage, Nyomi V. Hudson, Anirvan S. Nandy, Monika P. Jadi

Correspondence

xize.xu@yale.edu (X.X.), anirvan.nandy@yale.edu (A.S.N.), monika.jadi@yale.edu (M.P.J.)

In brief

Using simultaneous, layer-specific population recordings from primate primary visual area V1, Xu, Morton, et al. show that the spatial configuration of contextual stimuli differentially modulates inter-laminar information flow by changing its efficacy but not its structure. This non-uniform modulation is mediated by a location-dependent output-layer-targeting signal.

Highlights

- Inter-laminar information flow in V1 occurs along communication subspaces
- Structure of inter-laminar subspace is preserved across spatial locations of visual context
- Visual context degrades efficacy of information flow in a location-dependent manner
- The degradation is driven by a novel signal targeting the output layers

Xu et al., 2024, Neuron *112*, 1–15
December 18, 2024
https://doi.org/10.1016/j.neuron.2024.09.021

CellPress

Please cite this article in press as: Xu et al., Spatial context non-uniformly modulates inter-laminar information flow in the primary visual cortex, Neuron (2024), https://doi.org/10.1016/j.neuron.2024.09.021

Neuron

CellPress

Article

Spatial context non-uniformly modulates inter-laminar information flow in the primary visual cortex

Xize Xu (徐锡泽),[1,2,5,7,*] Mitchell P. Morton,[1,4,7] Sachira Denagamage,[1,4] Nyomi V. Hudson,[1] Anirvan S. Nandy,[1,3,4,5,6,8,*] and Monika P. Jadi[1,2,4,6,8,9,*]

[1]Department of Neuroscience, Yale University, New Haven, CT 06510, USA
[2]Department of Psychiatry, Yale University, New Haven, CT 06510, USA
[3]Department of Psychology, Yale University, New Haven, CT 06511, USA
[4]Interdepartmental Neuroscience Program, Yale University, New Haven, CT 06510, USA
[5]Kavli Institute for Neuroscience, Yale University, New Haven, CT 06510, USA
[6]Wu Tsai Institute, Yale University, New Haven, CT 06510, USA
[7]These authors contributed equally
[8]Senior author
[9]Lead contact
*Correspondence: xize.xu@yale.edu (X.X.), anirvan.nandy@yale.edu (A.S.N.), monika.jadi@yale.edu (M.P.J.)
https://doi.org/10.1016/j.neuron.2024.09.021

SUMMARY

Our visual experience is a result of the concerted activity of neuronal ensembles in the sensory hierarchy. Yet, how the spatial organization of objects influences this activity remains poorly understood. We investigate how inter-laminar information flow within the primary visual cortex (V1) is affected by visual stimuli in isolation or with flankers at spatial configurations that are known to cause non-uniform degradation of perception. By employing dimensionality reduction approaches to simultaneous, layer-specific population recordings, we establish that information propagation between cortical layers occurs along a structurally stable communication subspace. The spatial configuration of contextual stimuli differentially modulates inter-laminar communication efficacy, the balance of feedforward and effective feedback signaling, and contextual signaling in the superficial layers. Remarkably, these modulations mirror the spatially non-uniform aspects of perceptual degradation. Our results suggest a model of retinotopically non-uniform cortical connectivity in the output layers of V1 that influences information flow in the sensory hierarchy.

INTRODUCTION

Spatial vision is the ability to perceive visual objects within three-dimensional space, and its dysfunction is detrimental to our ability to interact with the visual world. Our visual experience relies on the coordinated activity of neuronal ensembles in the sensory hierarchy of the cortex.[1] Yet, how the spatial organization of objects influences information flow between neuronal populations in this hierarchy remains incompletely understood.

Visual perceptual performance varies as a function of visual field location, which is best at the center of gaze, degrades with eccentricity, and varies with radial angle. This asymmetry is paralleled by the asymmetric neural organization at multiple stages of the visual system (see Himmelberg et al.[2] for a review). Thus, a comprehensive characterization of the neural correlates of spatial vision requires empirical investigations without the assumption of spatial isotropy. Phenomena such as visual crowding—the inability to recognize objects among clutter—offer a powerful framework for such investigations. Visual crowding is thought to be the primary limitation on object perception in peripheral vision.[3] The crowding zone, which refers to the spatial extent over which flankers affect target identification, shows distinct spatially non-uniform characteristics, as identified by psychophysical studies.[4,5] This suggests non-uniform information processing along the visual hierarchy.

Understanding the neural basis of spatially non-uniform context integration requires identification of where the effects arise in the visual hierarchy and how information flow along this hierarchy is modulated by context. Neuronal spiking activity recorded from anesthetized monkeys indicates that visual crowding impairs feature representations as early as the primary visual cortex (area V1).[6,7] Human imaging studies show modulation of activity in V1[8,9] as well as in higher visual areas.[10–13] More importantly, inter-areal correlations are disrupted by spatial context integration,[14] suggesting modulation of information flow along the hierarchy. Despite extensive psychophysical

Please cite this article in press as: Xu et al., Spatial context non-uniformly modulates inter-laminar information flow in the primary visual cortex, Neuron (2024), https://doi.org/10.1016/j.neuron.2024.09.021

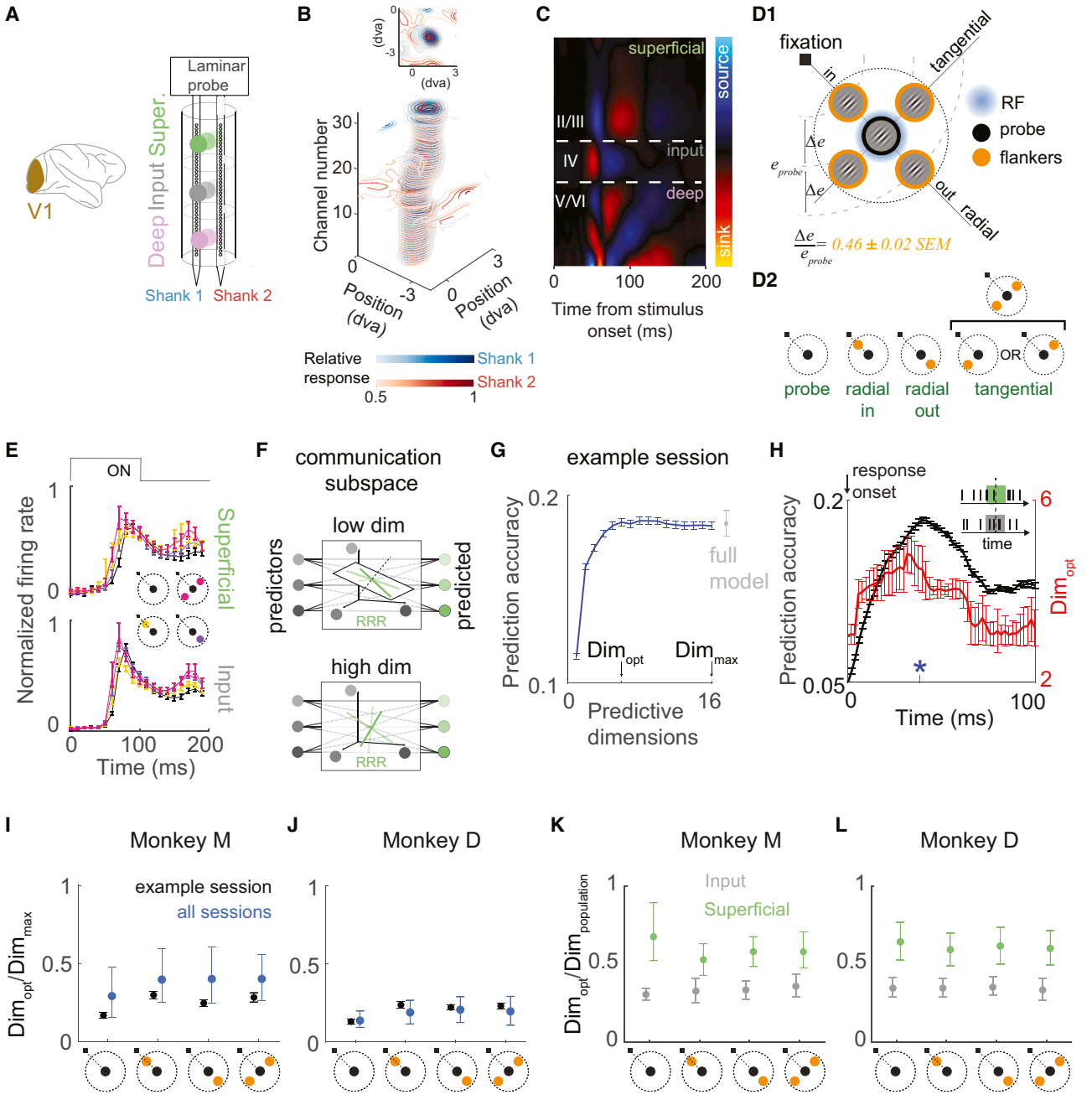

Figure 1. Characterization of inter-laminar information flow in V1

(A) Illustration of electrophysiological recordings with high-density 2-shank laminar probes.

(B) Example receptive field contours along the two shanks on the laminar probe. Top: vertical view. Dva, degrees of visual angle.

(C) Example current source density (CSD).

(D) Visual stimulation protocol. (D1) Schematic of visual stimulation for the passive fixation task. e_{probe}, parafoveal eccentricity of probe presentation; Δe, center-to-center distance between the probe and flankers. D2: summary of stimulus conditions. In subsequent results, "tangential" refers to one of the two tangential locations shown in (D1), indicated by a common symbol shown here.

(E) Normalized peri-stimulus time histograms (PSTHs; see STAR Methods) of recorded units in the superficial (top) and input (bottom) layers under various visual conditions. Top: visual stimulation protocol.

(F) Illustration of a low-dimensional communication subspace between cortical layers. The activity of each neuron in the superficial layer (illustrated by green circles) is predicted as a linear combination of the population activity in the input layer (illustrated by gray circles), which is equivalent to its projection onto a certain axis (shown as a green line/superficial neuron) in the activity space of input layer population. The axes for prediction either span the entire input layer activity space (bottom row) or are constrained in a low-dimensional subspace (top row), referred to as "communication subspace." The activity along the subspace is sufficient

(legend continued on next page)

Please cite this article in press as: Xu et al., Spatial context non-uniformly modulates inter-laminar information flow in the primary visual cortex, Neuron (2024), https://doi.org/10.1016/j.neuron.2024.09.021

studies and computational modeling,[15–26] the neural basis of the perceptual asymmetry of spatial context integration remains incompletely understood. Understanding how the organization of objects influences information flow along the visual hierarchy is thus critical to our understanding of spatial vision.

Information flow in the visual hierarchy is both inter-areal as well as inter-laminar because the laminar organization of neuronal populations,[1,27] with their stereotypical patterns of intra- and inter-areal projections,[28–30] is a canonical motif of cortical organization. The neurophysiological aspects of these lamina-specific circuits have been extensively characterized in the context of surround modulation, namely the change in neuronal activity in response to visual stimulation of classical and extra-classical receptive fields.[31–40] Geniculate feedforward connections, intra-V1 horizontal connections, and inter-areal feedback connections to V1 have all been shown to contribute to surround modulation in V1 at different spatiotemporal scales (see Angelucci et al.[41] for a review). However, a prevailing assumption in most of these studies has been the spatially uniform nature of the surrounding context. In V1, receptive field sizes and spatial frequency preference vary with eccentricity. In addition, the distribution of cortical tissue devoted to visual space varies with polar angle (see Himmelberg et al.[2] for a review). Such asymmetric neural organization suggests the possibility of non-uniform processing within V1 acting as a substrate for the non-uniform psychophysical effects observed in phenomena such as visual crowding.[4,5] In this study, we investigated how the spatial configuration of visual stimuli modulates inter-laminar information flow in V1 by analyzing functional communication between neuronal populations. We specifically focused on communication between two populations: input-layer neurons that receive geniculate inputs and project locally to superficial layers and superficial-layer neurons that project to higher-order visual areas as well as to local deep layers.

We performed laminar recordings from awake macaque V1 with visual stimuli presented either in isolation or with a flanking stimulus at various locations known to cause non-uniform perceptual impairment in peripheral vision. We characterized information flow from the input to the superficial layer, which is a key pathway in the feedforward propagation of sensory information. Using dimensionality reduction techniques to identify communication subspaces,[42] we found that the information flow from the input to superficial layers occurs along a structurally stable communication subspace under different visual conditions. Flanking stimuli modulated the efficacy of inter-laminar information flow in a location-specific manner by changing both its efficacy and the balance of feedforward and effective feedback signaling. Moreover, our analysis revealed a non-uniform contextual signal in the superficial layers triggered by flankers.

RESULTS

To characterize inter-laminar information flow in V1, we simultaneously recorded the spiking activity in the input layer (unit count: 27.9 ± 3.2 SEM) and in the primary downstream target, the superficial layer (unit count: 21.9 ± 5.0 SEM) in two awake macaque monkeys (Figure 1A; 14 sessions from monkey M, 8 sessions from monkey D). The recorded neurons consisted of well-isolated single units and multi-unit clusters, which had retinotopically aligned receptive fields (Figure 1B), implying a high probability of direct interactions. Laminar identity was established using current source density (CSD) analysis[43] (Figure 1C). Monkeys were trained to fixate on the center of the screen and passively view a probe stimulus (100 ms stimulus duration, 200–250 ms inter-stimulus interval) at the receptive field of the recording site, either in isolation (probe condition) or with a flanking stimulus (flanked condition) at one of four spatial locations relative to the probe (Figure 1D1), based on which three flanked conditions were defined (Figure 1D2). In both the radial-in and radial-out flanked conditions, the flanker was positioned on the radial axis connecting the probe and the fixation point, either between the probe and the fixation point or past the probe, respectively. In the tangential flanked condition, the flanker was positioned on either side of the probe along the axis orthogonal to the radial axis.

Given the rich temporal dynamics of the V1 units (Figure 1E), we hypothesized that the dynamics of inter-laminar information flow were also time variant and therefore conducted analysis on a moment-by-moment basis. Neuronal activity was measured as spike counts in 50-ms bins during the appropriate stimulus processing range of V1 neurons, which we refer to as the responsive period (see STAR Methods). Leveraging trial-to-trial response variabilities to repeated stimuli, we characterized inter-laminar information flow by assessing the extent to which variability of mean-subtracted neuronal activity in the superficial layer could be predicted by the correponding activity in the input layer.

Information propagation between cortical layers occurs along a communication subspace

Information propagation across cortical areas has been shown to occur along a ''communication subspace.''[42,44] That is, only a low-dimensional subspace of the upstream area neural

to capture the inter-laminar communication. Any perturbation of input layer activity orthogonal to this subspace (black dotted line) will not change the predicted population activity of the superficial layer.

(G) Predicting superficial layer population activity (16 units) from input layer population activity (34 units) using reduced-rank regression (RRR) with varying number of predictive dimensions (blue curve) or a full regression model (gray circle) for an example session. Error bars indicate the standard error across multiple draws of trials and the corresponding cross-validation folds. For all prediction analyses presented, the RRR model performs as well as the full model (Figure S1).

(H) Temporal evolution of the optimal dimensionality (red) and its prediction accuracy (black) computed by RRR for the example session used in (G) (see STAR Methods). Blue asterisk: time around which the window analyzed in (G) was centered. Error bars indicate the standard error across multiple draws of trials.

(I) The ratio between Dim_{opt} and Dim_{max} under various visual conditions for an example session (black) or across all sessions (blue) from monkey M. Error bars indicate the 95% confidence interval for the mean ratio averaged across the responsive period.

(J) Same as (I) for results from monkey D.

(K and L) The ratio between Dim_{opt} and the dimensionality of the population activity ($Dim_{population}$) in the superficial layer (green) or the input layer (gray) across all sessions from monkey M (K) and monkey D (L).

Please cite this article in press as: Xu et al., Spatial context non-uniformly modulates inter-laminar information flow in the primary visual cortex, Neuron (2024), https://doi.org/10.1016/j.neuron.2024.09.021

population activity space is informative of the downstream area activity (illustrated in Figure 1F). It is important to note that a subspace of neural activity is different from a subnetwork. Whereas a subnetwork comprises a subset of neurons, a subspace of neural activity corresponds to a subset of population activity patterns, which may involve non-trivial activities of all neurons within the network. The dimensionality of the communication subspace from V1 to V2 has been shown to be consistently lower than the dimensionality of the target population activity.[42] Based on these results, we hypothesized that inter-laminar information propagation also occurs along subspaces and that this is not simply due to the low dimensionality of either the source or target population activity. Specifically, we tested whether the inter-laminar interaction between the input and superficial layers in V1 was limited to a subspace of the neural activity space of the input layer by employing reduced-rank regression (RRR),[45,46] a multivariate linear regression model with a constraint enforcing a small number of latent predictive factors (see STAR Methods). For an example session under the radial-in condition (Figure 1G), only 6 dimensions (Dim_{opt}) were needed to achieve prediction performance that is as good as a full linear regression model (ridge regression; see STAR Methods), which was lower than the maximal possible prediction dimensionality (Dim_{max}) determined by the minimum between the number of units in the source and target populations. Moment-by-moment analysis for this session revealed that this result held throughout the responsive period of V1 (Figure 1H). Furthermore, this result was consistent across visual conditions, sessions, and monkeys (Figures 1I and 1J), implying that inter-laminar information flow in V1 shared the low-dimensional property exhibited by inter-areal information flow. We next tested whether this signature of inter-laminar information flow was due to a low complexity of population activity either in the source population (the input layer) or in the target population (the superficial layer). We used factor analysis to assess the complexity of population activity in either layer (see STAR Methods). The analysis revealed that the dimensionality of activity in either population was consistently higher than the number of predictive dimensions (Figures 1K and 1L). Thus, the observed low dimensionality of inter-laminar interactions cannot be explained by the complexity of population activity in the input or superficial layer but rather reflected the nature of inter-laminar information flow.

We next investigated the impact of stimulus configuration on the structure and efficacy of the communication subspace underlying inter-laminar information flow. Potentially, inter-laminar information flow can be modulated by the spatial configuration of stimuli in two ways that are not mutually exclusive: (1) the structure of the communication subspace is changed, which would be observable as the degraded prediction performance under a given visual condition when the corresponding input layer data were projected onto the communication subspace identified from a different visual condition, and (2) the efficacy of the communication subspace is changed, which would be observable as differential prediction accuracies across visual conditions. To test these possibilities, we performed RRR to characterize the communication subspace and computed its prediction accuracy on a moment-by-moment basis for each visual condition.

Structure of communication subspace is preserved across flanker locations

Testing whether the structure of inter-laminar information flow is changed requires characterizing the difference between communication subspaces identified from different visual conditions. To ensure a fair comparison across visual conditions, populations in the input and the superficial layers used to conduct prediction analysis were fixed and the sample sizes were matched across visual conditions. These protocols prevented the number of analyzed neurons and trials from differentially affecting the analysis result.[42,47] We first investigated the relative alignment between the subspaces across different visual conditions by using the measure of principal angle (Figure 2A), which computes angles between sequentially aligned pairs of basis vectors, each within one of the subspaces. The smallest principal angle is referred to as the "leading principal angle." Small principal angles indicate a similar orientation of subspaces and imply that much of the structure of the communication subspace is preserved across visual conditions. By performing RRR using data from a sliding time window of 50 ms, we identified the communication subspace for each visual condition and computed the principal angles between all possible pairs. To assess whether the obtained principal angles were significantly small, we compared them with the principal angles between randomly generated subspaces while preserving the dimensionalities of the computed communication subspaces (see STAR Methods). The leading principal angles between the communication subspaces identified from the probe and any of the flanked conditions were consistently below chance level (Figure 2B). The result held for all other visual condition comparisons (Figure S2A). Because the regression could be prone to overfitting, we calculated within-condition principal angles (see STAR Methods), which provided an estimate of the minimal principal angle that could be realistically obtained, and compared these with the cross-condition principal angles. The levels of the within-condition principal angles (Figure 2B, black curves) were consistently comparable with the cross-condition principal angles (Figure 2B, colored curves), providing further evidence for similar communication subspaces across visual conditions.

To characterize the influence of the relative alignment between communication subspaces across visual conditions on the strength of interaction, we performed cross-prediction analysis using the projection of the data from the source (input layer) population for a given visual condition onto the communication subspaces identified across different visual conditions using a multivariate linear regression model (Figure 2A). Throughout the responsive period, the projected data gave similar prediction performance across all visual conditions from which the communication subspace was identified, and these were significantly above what would be expected by chance (Figures 2C and S2B). Thus, the extent to which the input layer activity was informative of the superficial layer activity was similar among the communication subspaces identified from different visual conditions. Taken together, these two results indicate that the structure of inter-laminar information flow in a linear framework is preserved across different spatial configurations of visual stimuli.

Please cite this article in press as: Xu et al., Spatial context non-uniformly modulates inter-laminar information flow in the primary visual cortex, Neuron (2024), https://doi.org/10.1016/j.neuron.2024.09.021

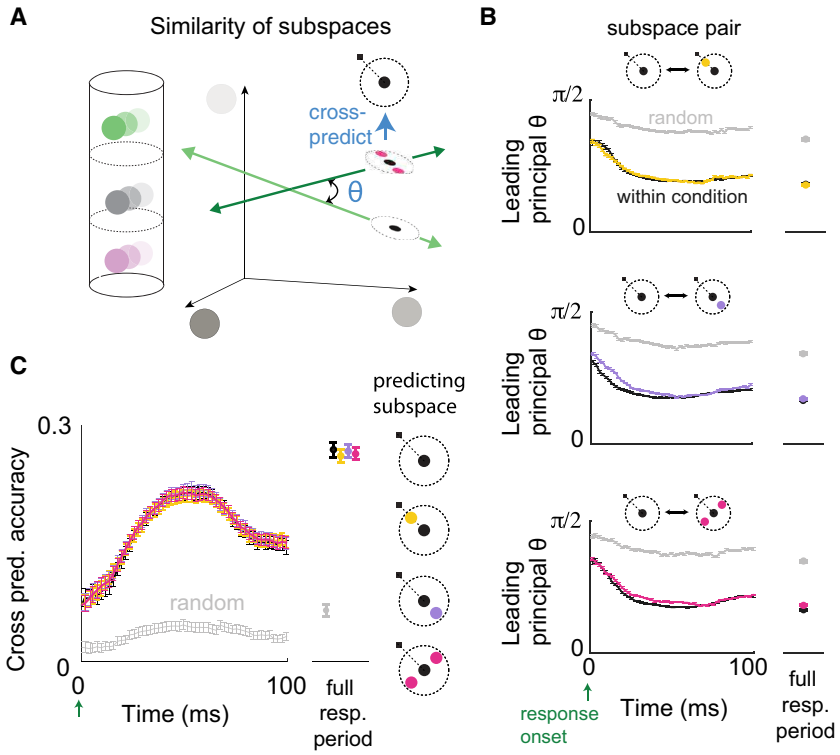

Figure 2. Similarity of inter-laminar communication subspace across visual conditions

(A) Illustration of principal angle measure and cross-prediction analysis for comparing two subspaces. Each axis represents the activity of an input layer neuron used to predict superficial layer activity. Green lines represent input-to-superficial communication subspaces identified from two visual conditions.

(B) Temporal evolution of leading principal angle between the communication subspaces identified for all visual conditions (averaged across all sessions). Gray: chance level alignment between subspaces (see STAR Methods). Black: within-condition leading principal angles (see STAR Methods).

(C) Cross-prediction analysis for neural activity in probe condition, using projection onto subspaces identified from one of the four visual conditions. Error bars indicate the 95% confidence interval for the mean. Difference between conditions was inferred using estimation statistics framework (see STAR Methods). Black: within-condition prediction. Yellow, purple, magenta: across-condition prediction. Gray: chance level (see STAR Methods). Also shown in (B) and (C) on the right, are the results calculated using the activities from the full responsive period (a 100-ms time bin starting from response onset). For other visual condition comparisons, see Figure S2.

Efficacy of inter-laminar information flow is degraded in the presence of flankers

We next investigated how the spatial configuration of visual stimuli influenced the efficacy of inter-laminar information flow, as characterized by inter-laminar prediction accuracies. We started by comparing the probe condition against the flanked condition (data pooled across all possible locations of flankers). Temporal dynamics of prediction accuracy were obtained as the predictive performance at optimal dimensionality under RRR employed on a moment-by-moment basis. As shown in Figure 3A for a representative session, under either visual condition, the inter-laminar prediction accuracy initially increased and then decayed during the responsive period. To quantify the difference in the prediction accuracies across visual conditions for each session, we introduced a prediction modulation index (PMI; see STAR Methods). For the example session in Figure 3A, the corresponding PMI was significantly negative during the entire responsive period (Figure 3B), indicating that the prediction accuracy was weakened in the presence of flankers. Despite an inter-subject difference in the initial temporal profile of the PMI, the degradation of inter-laminar prediction accuracy was consistent across sessions for both monkeys (Figure 3C), implying a weaker efficacy of information flow.

Degradation in the efficacy of inter-laminar information flow is mediated by layer-specific signals

We tested two non-mutually exclusive hypotheses about how the presence of flankers might weaken inter-laminar prediction accuracy (schematized in Figure 4A): hypothesis *I*, the flanked condition causes the activation of a novel signal targeting the input layer, or hypothesis *II*, the flanked condition causes the activation of a novel signal targeting the superficial layer. To disentangle these possibilities, we investigated the temporal relationship between layer-specific activity and the degradation in prediction accuracy. On a moment-by-moment basis, we performed the RRR analysis using data from the two layers at different temporal delays (Figure 4B1) and thereby determined the temporal evolution of PMI as a function of delay. It is important to note here that delays associated with both inter-laminar signal conduction and intra-laminar recurrent processing would factor into this temporal analysis. If hypothesis *I* were true, the timing of the degradation and hence the temporal profile of the PMI would be independent of the inter-laminar delay being considered (Figure 4B2, left). In contrast, if hypothesis *II* were true, i.e., if the novel signal targeted the superficial layer, the timing of the degradation would depend on the offset of the superficial layer data analyzed and therefore shift earlier with increasing temporal delay (Figure 4B2, right). Based on these observations, we estimated the time of degradation of prediction accuracy by determining the decrease onset time (DOT) of PMI followed by persistently negative components and related it with the temporal delay being considered. As shown in Figure 4C, for two representative sessions from the two monkeys, the DOTs of PMI became earlier with increasing temporal delay. Across sessions, the correlation between the DOTs of PMI and the temporal delay was consistently negative and close to −1 for both monkeys (Figure 4D), indicating a dependence as predicted by hypothesis *II*. This result suggests that the degradation of prediction accuracy in the presence of flankers was mainly due to a novel signal targeting the superficial layer.

Please cite this article in press as: Xu et al., Spatial context non-uniformly modulates inter-laminar information flow in the primary visual cortex, Neuron (2024), https://doi.org/10.1016/j.neuron.2024.09.021

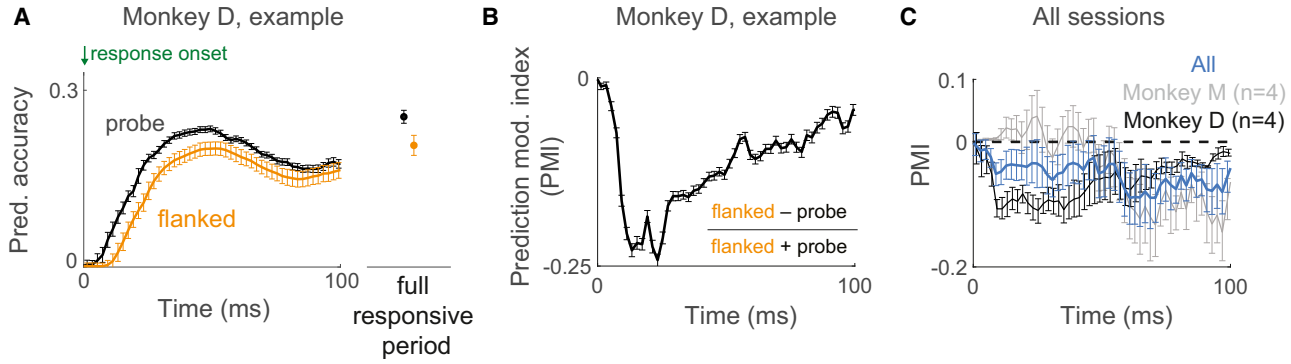

Figure 3. Efficacy of inter-laminar information flow across visual conditions

(A) The temporal evolution of input-superficial prediction accuracies under the probe (black) and the flanked conditions (orange) for an example session from monkey D. Error bars indicate the standard error across multiple draws of trials. Results calculated using the activities from the full responsive period (a 100-ms time bin starting from response onset) are shown on the right.

(B) The temporal evolution of the prediction modulation index (PMI; see STAR Methods). Error bars indicate 95% confidence interval for the mean. Difference between conditions was inferred using estimation statistics framework (see STAR Methods).

(C) Same as (B) for results across sessions from each monkey (gray: monkey M; black: monkey D) or across the two monkeys (blue).

Degradation in the efficacy of inter-laminar information flow is sensitive to flanker location

Two robust characteristics of visual crowding identified by psychophysical studies are the asymmetry and anisotropy of crowding zones, the spatial extent over which flankers affect target recognition. First, a flanker more eccentric than the target stimulus (radial-out condition) has a greater perceptual crowding effect than an equally spaced inward (less eccentric) flanker (radial-in condition).[5] Second, the crowding zone is elongated along the radial axis so that radially positioned flankers produce a stronger crowding effect than tangential ones (tangential condition).[4] We reasoned that these perceptual asymmetries could be due to asymmetries in inter-laminar prediction accuracy in V1. To investigate this possibility, we first compared the inter-laminar prediction accuracies between the probe and the different flanked conditions. The degradation due to the presence of flankers was consistent across all flanker locations, yet the extent of degradation varied (Figure 5A). To further characterize this, we compared the prediction accuracy under the flanked condition associated with the strongest perceptual crowding effects (the radial-out condition) against the other flanked conditions (the radial-in and the tangential conditions). To ensure a fair comparison across visual conditions, we additionally aligned the temporal prediction accuracy data to account for different response latencies across conditions. We found that the prediction accuracy degraded in the radial-out condition compared with the radial-in (Figure 5B) and the tangential conditions (Figure 5E) over most of the responsive period. Despite an inter-subject variability in the temporal profile of the prediction degradation caused by the radial-out condition relative to the radial-in condition, such degradation was consistent across all sessions for both monkeys. Moreover, applying the inter-laminar temporal delay analysis as above, we found that the prediction degradation with radial-out flankers emerged earlier with increasing temporal delay (Figures 5C, 5D, 5F, and 5G), consistent with a hypothesis of a superficial-layer-targeting signal that is dominant in the radial-out condition.

Bi-directional information flow depends on flanker location

Prediction analysis using RRR was motivated by the anatomical model of lamina-specific circuits, and thus assumed a direction of information flow from the input layer (source) to the superficial layer (target). We next sought to understand how information flow in either direction was affected by the spatial configuration of visual stimuli. We investigated this by employing canonical correlation analysis (CCA; see STAR Methods) to relate the population activities in the input and superficial layers at different time delays on a moment-by-moment basis (Figure 6A), which we refer to as population correlation. Positive or negative delays between the population activities from each layer allowed a bi-directional analysis of inter-laminar information flow. This methodology has been previously applied[48] to study the structure of interactions between cortical areas, finding that the balance was feedforward dominated shortly following stimulus onset and then became feedback dominated. For each visual condition, we calculated the population correlation between activities in the two layers as a function of time and time delay between layers (Figure 6B). To quantify the strength of interaction in each direction, we computed a "feedforward correlation" by taking the mean over correlations for all positive delays (input layer leading superficial layer; STAR Methods) and similarly for "effective feedback correlation" for negative delays (superficial layer leading input layer). For a representative example session under the probe condition (Figure 6B), whereas the feedforward correlation increased steadily from the time of response onset and then gradually decayed, the effective feedback correlation was consistently lower than the feedforward correlation, indicating a feedforward-dominant interaction throughout the responsive period.

We quantified the degree to which the inter-laminar interaction was dominant in either direction of signaling by defining a direction dominance index (DDI; see STAR Methods), where a positive DDI indicates the dominance of feedforward signaling and a negative DDI indicates the dominance of effective feedback

Please cite this article in press as: Xu et al., Spatial context non-uniformly modulates inter-laminar information flow in the primary visual cortex, Neuron (2024), https://doi.org/10.1016/j.neuron.2024.09.021

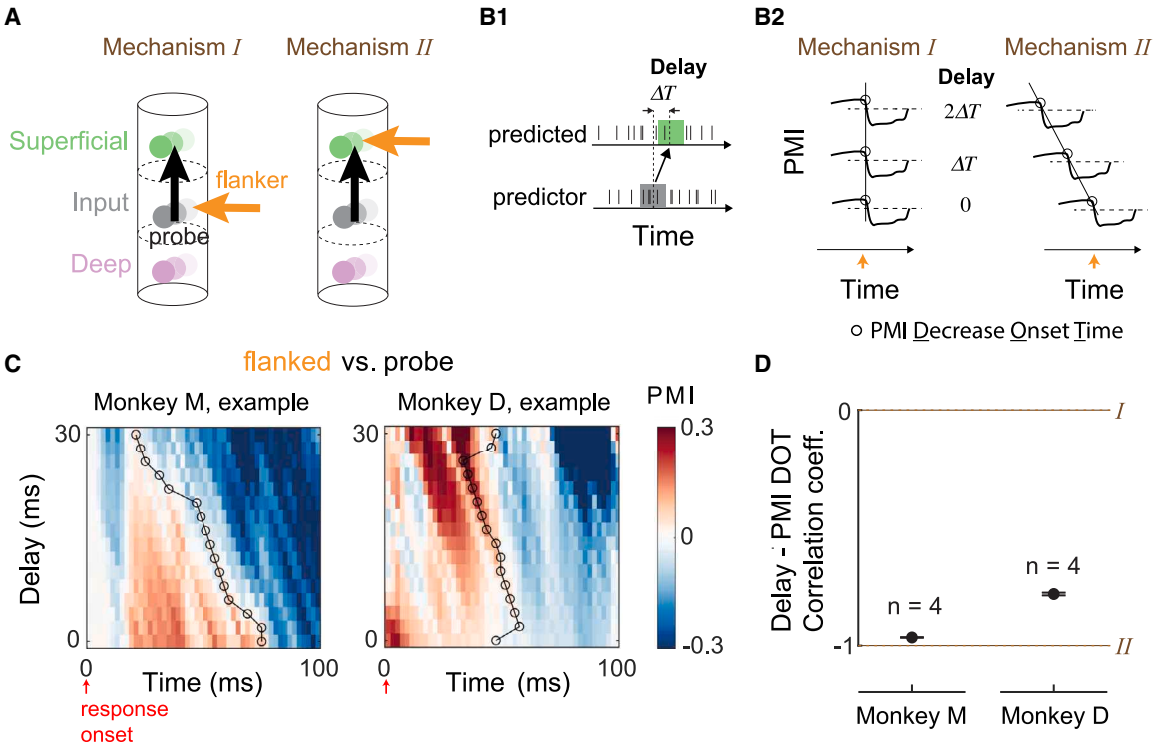

Figure 4. Mechanism of degradation in the efficacy of inter-laminar information flow

(A) Illustration of two possible mechanisms: flanker causes the activation of a novel signal (orange arrow) targeting the input (mechanism *I*) or superficial layer (mechanism *II*).

(B) Delay analysis protocol and potential outcomes. (B1) RRR was conducted on a moment-by-moment basis using input (at t) and superficial layer activity at non-negative temporal delays (t + delay). (B2) Illustration of delay-induced changes in PMI dynamics, as implied by mechanisms *I* and *II*. Orange arrows: the time when the hypothetical novel signal caused by the flanker arrived at the input (mechanism *I*) or superficial (mechanism *II*) layer.

(C) Temporal evolution of inter-laminar PMI under the probe and the flanked conditions at various inter-laminar temporal delays for example sessions from two monkeys. PMIs that are neither significantly positive nor negative are colored in white (the corresponding 95% confidence interval for the mean PMI includes zero). Black circles: decrease onset times (DOTs) of PMI at each level of delay.

(D) Correlation between inter-laminar temporal delay and the DOTs of PMI across all sessions from each monkey. Error bars indicate 95% confidence interval for the mean.

signaling. The larger the magnitude of DDI, the more biased the interaction was toward one direction. To investigate the impact of stimulus configuration on the balance of the inter-laminar feedforward and effective feedback signaling, we determined the temporal evolution of DDI separately for each visual condition. In the same example session as above, under both the probe and the flanked conditions, the DDI increased steadily and gradually decayed, remaining significantly positive throughout the responsive period (black and orange curves in Figure 6C). Thus, the interaction became more feedforward dominated in the early phase of the responsive period and then returned to a more balanced interaction. Remarkably, the DDI was less positive under the flanked condition, indicating that the balance was shifted away from the feedforward direction in the presence of a flanker. This result was robust across sessions for each monkey (Figure 6D). Furthermore, similar analysis revealed that this modulation was flanker-position dependent. In the visual condition associated with the strongest perceptual crowding effect (the radial-out condition), the balance was shifted away from the feedforward direction compared with both the radial-in and tangential conditions (Figure 6E). Thus, the non-uniformity in stimuli-specific prediction accuracy analysis (Figure 5) was mirrored by the modulation of the interplay between inter-laminar feedforward and effective feedback signaling. Interestingly, the inter-subject difference in the temporal profile of the difference in DDI across visual conditions (probe vs. flanked and radial-out vs. radial-in) was similar to that in PMI obtained from the prediction analysis, such that both the shift of balance (Figures 6D and 6E) and the degradation of inter-laminar prediction accuracy (Figures 3C and 5B) emerged later during the responsive period for monkey M compared with monkey D.

Strength of contextual drive to the superficial layer is location specific

To test the hypothesis that our observations are a reflection of a signal that targets the superficial layers and is sensitive to flanker locations, we next examined the relative strength of this signal evoked by flanker-only stimuli at different locations. For each flanker-only condition, we determined the level of charge sinks by integrating over time the early current sinks in the superficial

Please cite this article in press as: Xu et al., Spatial context non-uniformly modulates inter-laminar information flow in the primary visual cortex, Neuron (2024), https://doi.org/10.1016/j.neuron.2024.09.021

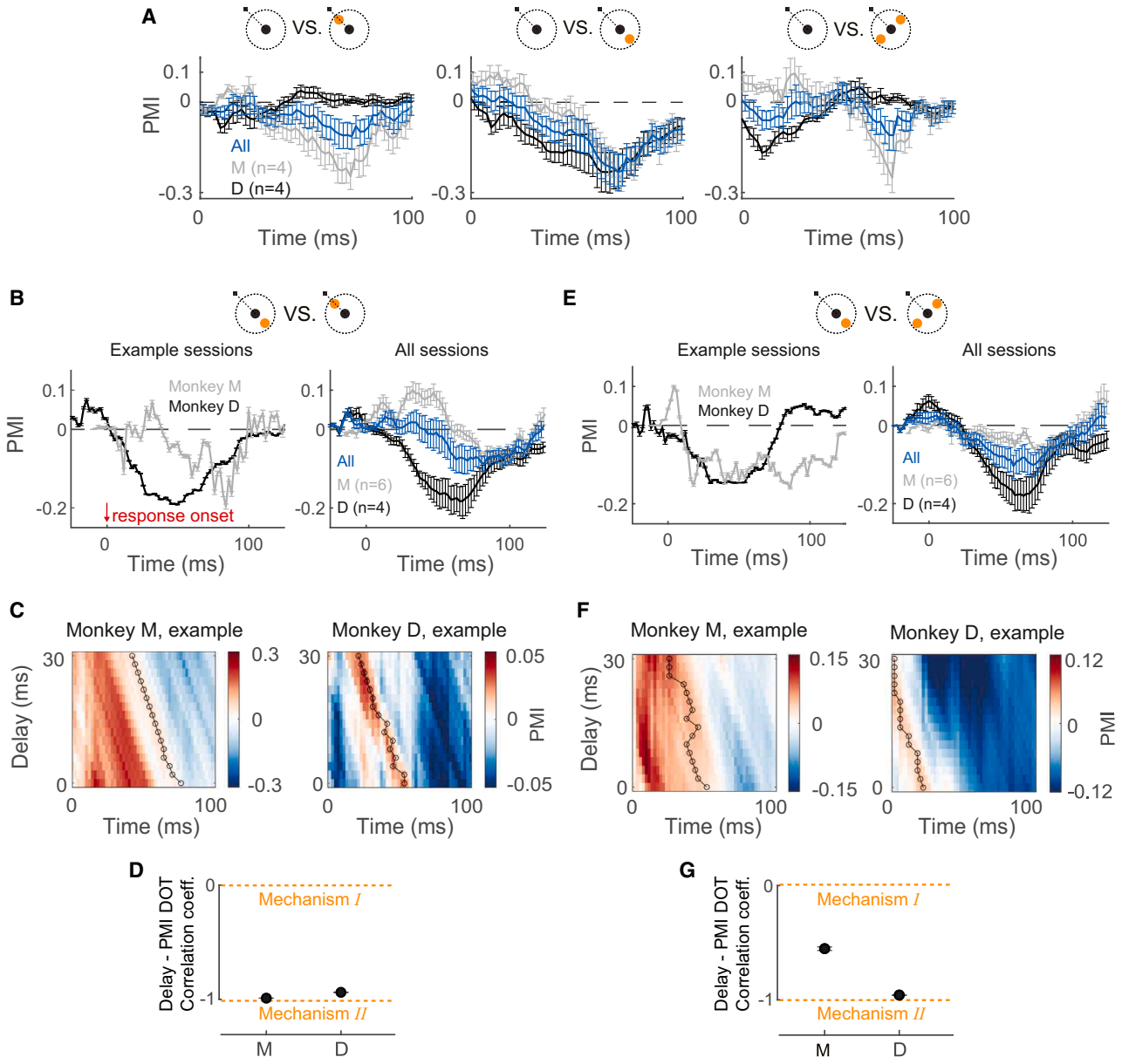

Figure 5. Efficacy of inter-laminar information flow as a function of flanker location

(A) Same as Figure 3C, comparing the prediction accuracy under the probe condition against each flanked condition (from left to right: radial-in, radial-out, and tangential).

(B) Temporal evolution of RRR PMI comparing the radial-out and radial-in conditions for example sessions (left) or across all sessions (right), from monkeys M (gray), D (black), or both (blue). Negative PMIs imply a degradation of prediction accuracy in the radial-out condition compared with the radial-in condition. Error bars indicate 95% confidence interval for the mean.

(C) Example sessions showing temporal evolution of PMI as a function of inter-laminar delay (see Figures 4B and 4C) for the visual conditions compared in (B).

(D) Correlation between inter-laminar temporal delay and the DOTs of PMI across all sessions from each monkey.

(E–G) Same as (B)–(D), comparing the modulation of inter-laminar prediction accuracy under the radial-out and tangential conditions. For comparison between the radial-in and tangential conditions, see Figure S3A.

layer obtained from the CSD response (Figures 7A–7C; see STAR Methods), which reflected the subthreshold integrated input to local neurons.[43,49] For both monkeys, flankers at the radial-out position evoked stronger charge sinks compared with flankers at the radial-in or tangential positions (Figure 7D), thus providing direct evidence for a location-dependent superficial-layer-targeting signal that differentially impacts the representation of the probe. Similar results were obtained from spike-based analysis, such that the radial-out flanker-only condition evoked higher levels of activity (Figure 7E). This provides

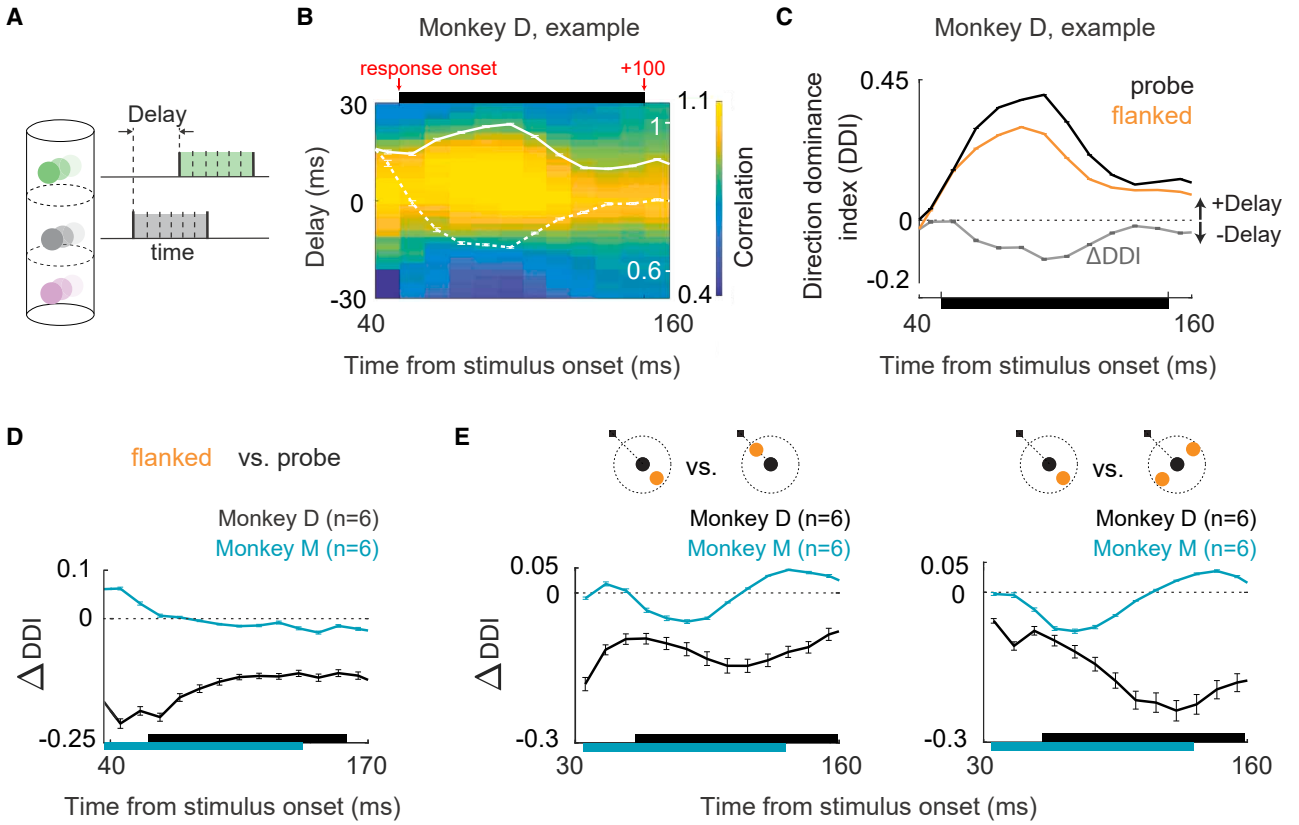

Figure 6. Balance of bi-directional inter-laminar information flow and its modulation in the presence of flankers

(A) Canonical correlation analysis (CCA) protocol for estimating temporal evolution of population correlations.

(B) CCA-based population correlation as a function of time and inter-laminar delay during the visually responsive period. Overlaid solid and dotted traces (white) show the average correlation at positive and negative sides of delay, respectively. Error bars indicate the standard error across multiple draws of trials.

(C) Temporal evolution of the direction dominance index (DDI; see STAR Methods) under the probe and the flanked conditions for an example session. Also shown is the difference between DDIs across conditions (gray trace).

(D) Temporal evolution of the difference in the DDIs under the probe and the flanked conditions for all sessions from each monkey.

(E and F) Same as (D) for results comparing DDIs separately under different types of flanked stimuli (E: radial-out vs. radial-in; F: radial-out vs. tangential). In (B)–(E), corresponding visually responsive periods estimated as 100 ms from the response onsets are marked by horizontal bars. In (C)–(E), error bars indicate 95% confidence interval for the mean.

further evidence for stronger inputs to the superficial layer as a potential mechanism underlying the observed non-uniformity. These results support a hypothesis that the observed degradation in the efficacy of inter-laminar information flow and the shift in feedforward-feedback signaling balance are mediated by retinotopically non-uniform cortical connectivity in the output layers of V1 (Figure 7F).

DISCUSSION

We leveraged simultaneous laminar recordings to understand how the spatial configuration of visual contextual stimuli affected inter-laminar information flow in V1 of the macaque. V1 activity has been extensively studied as a locus of surround modulation[34–41] and, more recently, has been implicated as a bottleneck impairing perception under visual crowding.[6–9,13] We established that information flow across V1 laminar populations is constrained to a communication subspace. We demonstrated that the efficacy of inter-laminar information flow was degraded in the presence of contextual stimuli. This degradation was not accompanied by changes in the structure of the subspace of neural activity along which the information flow occurs. Furthermore, we found that the balance between the inter-laminar feedforward and effective feedback signaling was non-uniformly shifted in the presence of flankers. Strikingly, these modulations matched the spatially non-uniform aspects of perceptual degradation, such that a greater degree of modulation was associated with a flanker at the visual location that is known to exert a stronger perceptual impairment. Finally, we found that the spatial configuration of contextual stimuli differentially modulated contextual signaling in the superficial layers. Our results suggest a model in which degraded information flow along the sensory hierarchy, mediated by retinotopically non-uniform connectivity in the output layers of V1, underlies the perceptual impairments in spatial vision.

Contextual modulation of information flow

Despite decades of research at the level of perception, investigation into the neural mechanisms of non-uniform perceptual

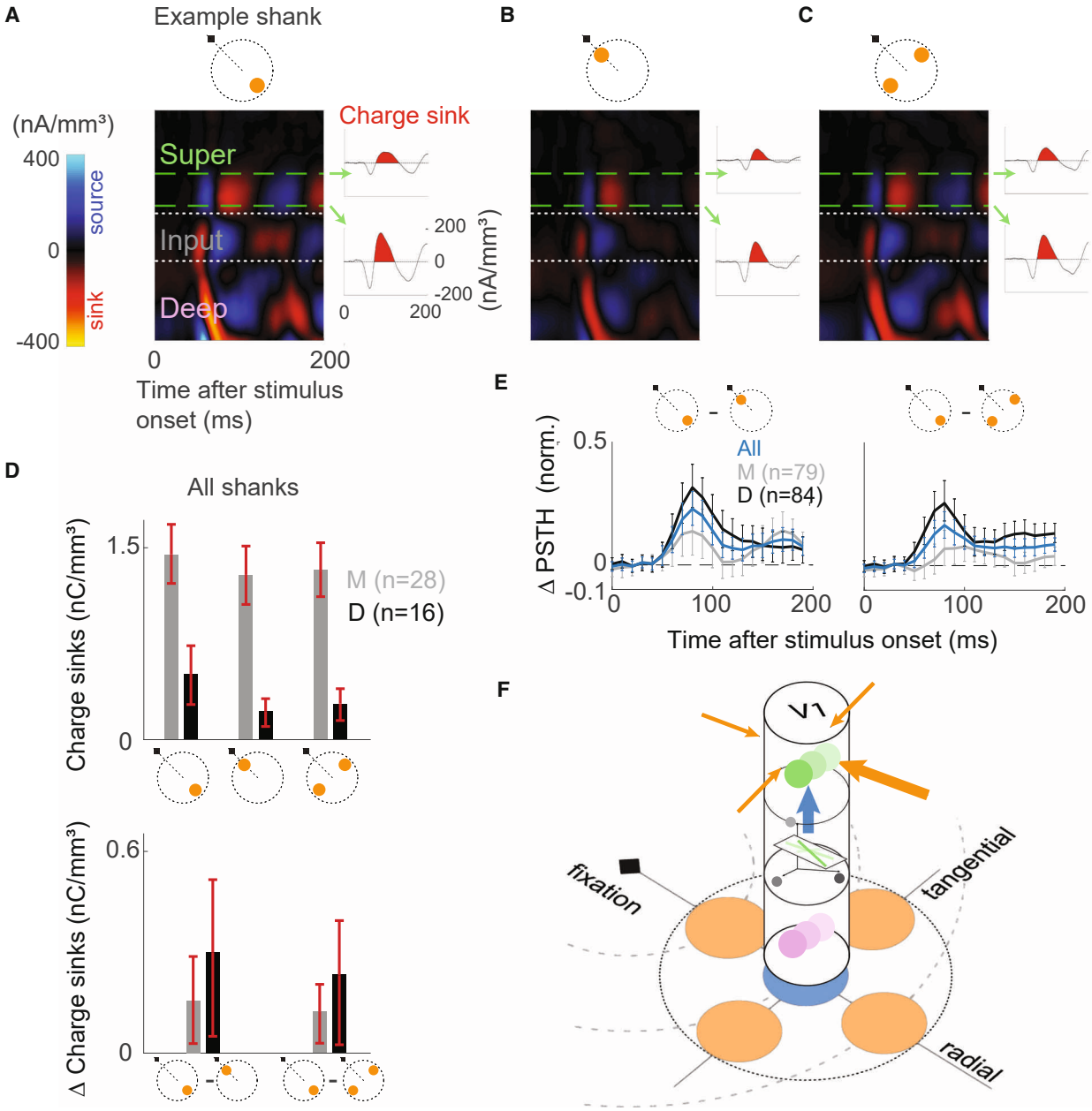

Figure 7. Retinotopically non-uniform context integration in V1

(A) An example of estimated CSD across V1 layers evoked by flanker presented by itself at the radial-out position. Dotted white lines indicate laminar boundaries (see STAR Methods). Traces on the right show temporal evolution of the CSD signal at two recording sites on the example shank, marked by the green dashed lines. Red shade: the earliest charge sink.

(B and C) Same as (A), with the flanker presented at the radial-in and tangential positions, respectively.

(D) Top: level of early charge sinks under different flanker-only conditions across all sessions from each monkey. Bottom: within-shank difference in the level of early charge sinks between the radial-out and radial-in conditions (left) and the radial-out and tangential conditions (right). Error bars indicate 95% confidence interval for the mean. Difference between conditions was inferred using estimation statistics framework (see STAR Methods). For comparison between the radial-in and tangential conditions, see Figure S3B.

(E) Difference in the normalized PSTH of superficial layer units between the radial-out flanker-only and radial-in flanker-only conditions (left) and the radial-out flanker-only and tangential flanker-only conditions (right). Error bars indicate 95% confidence interval for the mean difference (see STAR Methods). Normalized PSTHs for each condition are shown in Figure S4.

(F) Summary of findings.

Please cite this article in press as: Xu et al., Spatial context non-uniformly modulates inter-laminar information flow in the primary visual cortex, Neuron (2024), https://doi.org/10.1016/j.neuron.2024.09.021

degradation in peripheral vision has received limited attention. The most studied hypothesis is that the perceptual degradation is mediated by changes in the tuning properties of neurons and therefore leads to information loss about target features as early as the input and superficial layers of V1.[6,7,50] The observed impairment of information encoding has been shown to be greater with flankers positioned at visual configurations that exert stronger crowding effects, either with shorter target-flanker distance or at a radial-out location relative to the target stimulus. However, modulation of neural responses and changes in information coding do not necessarily imply changes in signaling efficacy along processing stages in the visual hierarchy. Our results demonstrate that inter-laminar information flow in V1, a key mechanism of hierarchical signaling, is disrupted by spatial context, which may account for the accumulation of information loss along the visual hierarchy.

Although we address degraded inter-laminar information flow in V1, our results do not rule out the possibility of additional mechanisms responsible for visual crowding in higher visual areas. A stronger information loss in area V4 has been observed with crowding due to the summation of signals within the larger receptive fields of V4 neurons compared with V1.[7] Other relevant studies relying on coarser measures of neural activity, such as fMRI, found that inter-areal temporal correlations (between V1, V2, V3, V4, and the visual word form area) are lower with crowded letters compared with uncrowded letters.[14] Such deterioration in the extrastriate cortex can only compound the degradation of signaling that we identified within V1, as higher visual areas ultimately rely on V1 inputs for their computations.[1] Given reports of the similar extents of anatomical horizontal (recurrent within V1) and feedback (from V2 to V1) projections in the visual cortex,[51] cortical magnification can partially explain the inward-outward asymmetry of perceptual degradation due to crowding but not the full extent of the radial-tangential anisotropy.[21] This suggests the existence of additional "functional" non-uniformities in the peri-columnar network.

Source of non-uniform context signal

The dependence of the PMI temporal profile on the inter-laminar delay suggested that the degradation of prediction accuracy in the presence of flankers was mainly due to a novel signal targeting the superficial layer. This result is broadly consistent with a recent study[37] that examined the laminar profile of current sinks in the CSD upon stimulation of the receptive field surround with isotropic annular gratings and found, based on onset latency measurements, that the processing of such spatial context initiates in the superficial and deep layers. Our results significantly extend this prior work by (1) characterizing the effect of such a mechanism on information propagation along the intra-V1 hierarchy and (2) showing that such a mechanism could also be a template for non-uniform contextual modulation. Further experiments are needed to be able to pinpoint the source of this implicated input, which could non-exclusively be horizontal connections from superficial-layer neurons outside the recorded V1 column or feedback connections from higher visual areas. Both possibilities are supported by previous studies in the context of surround modulation where optogenetic inactivation of horizontal connections in mouse L2/3 V1[52] or marmoset V2 feedback connections to V1[53] reduced the amplitude of surround modulation. Moreover, each type of connection was shown to contribute to the processing of spatial context at different spatiotemporal scales.[37,41] It is important to note that our results do not conflict with previous work suggesting the contribution of geniculate feedforward connections, which primarily terminate in the input layer of V1, to the processing of contextual stimuli,[34,40,54–57] but imply a weaker effect of such connections on the efficacy of input-superficial information flow compared with connections terminating in the superficial layers. Interestingly, our observation of an intermediate level of negative correlation (close to neither 0 nor −1) between the time when degradation emerged and the temporal delay being considered for the comparison between the tangential and radial-out conditions from one monkey (Figure 5G), suggests the influence of potentially both types of connections on the anisotropy. Thus, the mechanism underlying the non-uniform aspect of the modulation of inter-laminar information flow by contextual stimuli could vary with the specific locations of flankers being compared.

Features of inter-laminar information flow

Our study has identified two signatures of inter-laminar flow in V1: low-dimensionality and effective feedback signaling. By employing RRR, we demonstrated that the interaction between the input and superficial layers occurred through a low-dimensional communication subspace, akin to inter-areal interactions[42,44] but in contrast to interactions within the superficial layer of V1.[42] The low-dimensional structure could confer the computational benefit of flexible and selective routing of activity to downstream targets.

The interplay of feedforward and feedback signaling is a hallmark of cortical information processing.[58–60] Such interplay is not only prominent at the inter-areal level but is also implicated at the local circuit level within V1.[40,53,61] Extensive studies have attempted to infer feedback interactions between brain areas by relating activities between areas with temporal delay,[48,62–66] computing phase delays in local field potentials (LFPs) or multi-unit neuronal activity (MUA)[61,67–69] and comparing the timing of neuronal response onsets[70–72] as well as the emergence of certain neuronal response properties[73–76] across areas. Yet, feedback interactions among within-area laminar circuits in general, and between the input and superficial layers in particular, remain unknown. Here, we characterized inter-laminar interactions along both feedforward and feedback directions by applying CCA with varying temporal delay between layers. Notably, we observed substantial levels of correlation over a range of negative delays, especially at the initial and late phases of the responsive period, implying an effective feedback component (superficial leading input) in the inter-laminar interaction. This result is consistent with the implication of a previous study that examined the laminar profile of the MUA for the alpha rhythm and found that MUA in the superficial and deep layers preceded MUA in the input layer.[61] Given that the dendritic arbors of the input layer (L4C) neurons are locally confined, and the descending axons of the superficial-layer neurons mainly pass through the input layer with very weak branching,[28,29,77] the identified effective feedback signaling is less likely to be

relayed via a direct superficial-input anatomical connection. Instead, certain types of neurons in the deep layer, the primary target of projections from neurons in the superficial layer, have been shown to send extensive axonal projections into the input layer,[28,78,79] which form an indirect superficial-input pathway via the deep layer and could serve as an anatomical substrate for the identified effective feedback signaling.

RESOURCE AVAILABILITY

Lead contact

Further information and requests for resources should be directed to and will be fulfilled by the lead contact, Monika P. Jadi (monika.jadi@yale.edu).

Materials availability

This study did not generate new unique reagents.

Data and code availability

All data tables have been deposited to Figshare (https://doi.org/10.6084/m9.figshare.27055252). Raw electrophysiology data are available upon request. All analysis was performed using MATLAB software from MathWorks.

ACKNOWLEDGMENTS

This research was supported by NIH/NEI R01 EY032555, a NARSAD Young Investigator grant, a Ziegler Foundation grant, and Yale Orthwein Scholar funds to A.S.N.; NIH/NEI R01 EY034605 and R00 EY025026 to M.P.J.; Kavli postdoctoral fellowship and Swartz postdoctoral fellowship in theoretical neuroscience to X.X.; NIH/NINDS training grants T32-NS007224 and T32-NS041228 to M.P.M. and S.D.; and an NIH/NEI core grant for vision research P30 EY026878 to Yale University. We want to thank the veterinary and husbandry staff at Yale for excellent animal care. We would like to dedicate this to the memory of Bosco S. Tjan.

AUTHOR CONTRIBUTIONS

X.X., A.S.N., and M.P.J. conceptualized the project. M.P.M. and A.S.N. designed the experiments, and A.S.N. supervised the data collection. M.P.M., N.V.H., and S.D. collected data and performed preliminary analyses. X.X. conducted the statistical analysis. M.P.J. supervised the analysis. X.X., A.S.N., and M.P.J. wrote the manuscript.

DECLARATION OF INTERESTS

The authors declare no competing interests.

STAR★METHODS

Detailed methods are provided in the online version of this paper and include the following:

- KEY RESOURCES TABLE
- EXPERIMENTAL MODEL AND STUDY PARTICIPANT DETAILS
- METHOD DETAILS
  - Surgical procedures
  - Electrophysiology
  - Behavioral control and eye tracking
  - Receptive field mapping
  - Current source density mapping
  - Experimental task
- QUANTIFICATION AND STATISTICAL ANALYSIS
  - Normalized peri-stimulus time histograms (PSTHs)
  - Response onset estimation
  - Unit selection for regression analysis
  - Data preparation for regression analysis
  - Regression
  - Factor analysis
  - Principal angle
  - Cross-prediction analysis
  - Population correlation analysis

SUPPLEMENTAL INFORMATION

Supplemental information can be found online at https://doi.org/10.1016/j.neuron.2024.09.021.

Received: March 9, 2024
Revised: August 19, 2024
Accepted: September 25, 2024
Published: October 22, 2024

REFERENCES

1. Felleman, D.J., and Van Essen, D.C. (1991). Distributed Hierarchical Processing in the Primate Cerebral Cortex. Cereb. Cortex *1*, 1–47. https://doi.org/10.1093/cercor/1.1.1-a.
2. Himmelberg, M.M., Winawer, J., and Carrasco, M. (2023). Polar angle asymmetries in visual perception and neural architecture. Trends Neurosci. *46*, 445–458. https://doi.org/10.1016/j.tins.2023.03.006.
3. Levi, D.M. (2008). Crowding—An essential bottleneck for object recognition: A mini-review. Vision Res. *48*, 635–654. https://doi.org/10.1016/j.visres.2007.12.009.
4. Toet, A., and Levi, D.M. (1992). The two-dimensional shape of spatial interaction zones in the parafovea. Vision Res. *32*, 1349–1357. https://doi.org/10.1016/0042-6989(92)90227-A.
5. Petrov, Y., Popple, A.V., and McKee, S.P. (2007). Crowding and surround suppression: Not to be confused. J. Vis. *7*, 12.1–12.9. https://doi.org/10.1167/7.2.12.
6. Henry, C.A., and Kohn, A. (2020). Spatial contextual effects in primary visual cortex limit feature representation under crowding. Nat. Commun. *11*, 1687. https://doi.org/10.1038/s41467-020-15386-7.
7. Henry, C.A., and Kohn, A. (2022). Feature representation under crowding in macaque V1 and V4 neuronal populations. Curr. Biol. *32*, 5126–5137.e3. https://doi.org/10.1016/j.cub.2022.10.049.
8. Millin, R., Arman, A.C., Chung, S.T.L., and Tjan, B.S. (2014). Visual Crowding in V1. Cereb. Cortex *24*, 3107–3115.
9. Chen, J., He, Y., Zhu, Z., Zhou, T., Peng, Y., Zhang, X., and Fang, F. (2014). Attention-Dependent Early Cortical Suppression Contributes to Crowding. J. Neurosci. *34*, 10465–10474. https://doi.org/10.1523/JNEUROSCI.1140-14.2014.
10. Chicherov, V., Plomp, G., and Herzog, M.H. (2014). Neural correlates of visual crowding. NeuroImage *93*, 23–31. https://doi.org/10.1016/j.neuroimage.2014.02.021.
11. Bi, T., Cai, P., Zhou, T., and Fang, F. (2009). The effect of crowding on orientation-selective adaptation in human early visual cortex. J. Vis. *9*, 13.1–1310. https://doi.org/10.1167/9.11.13.
12. Anderson, E.J., Dakin, S.C., Schwarzkopf, D.S., Rees, G., and Greenwood, J.A. (2012). The neural correlates of crowding-induced changes in appearance. Curr. Biol. *22*, 1199–1206. https://doi.org/10.1016/j.cub.2012.04.063.
13. Kwon, M., Bao, P., Millin, R., and Tjan, B.S. (2014). Radial-tangential anisotropy of crowding in the early visual areas. J. Neurophysiol. *112*, 2413–2422. https://doi.org/10.1152/jn.00476.2014.
14. Freeman, J., Donner, T.H., and Heeger, D.J. (2011). Inter-area correlations in the ventral visual pathway reflect feature integration. J. Vis. *11*, 15. https://doi.org/10.1167/11.4.15.
15. He, S., Cavanagh, P., and Intriligator, J. (1996). Attentional resolution and the locus of visual awareness. Nature *383*, 334–337. https://doi.org/10.1038/383334a0.

16. Parkes, L., Lund, J., Angelucci, A., Solomon, J.A., and Morgan, M. (2001). Compulsory averaging of crowded orientation signals in human vision. Nat. Neurosci. *4*, 739–744. https://doi.org/10.1038/89532.

17. Pelli, D.G. (2008). Crowding: a cortical constraint on object recognition. Curr. Opin. Neurobiol. *18*, 445–451. https://doi.org/10.1016/j.conb.2008.09.008.

18. Levi, D.M., and Carney, T. (2009). Crowding in Peripheral Vision: Why Bigger Is Better. Curr. Biol. *19*, 1988–1993. https://doi.org/10.1016/j.cub.2009.09.056.

19. Greenwood, J.A., Bex, P.J., and Dakin, S.C. (2009). Positional averaging explains crowding with letter-like stimuli. Proc. Natl. Acad. Sci. USA *106*, 13130–13135. https://doi.org/10.1073/pnas.0901352106.

20. Freeman, J., and Simoncelli, E.P. (2011). Metamers of the ventral stream. Nat. Neurosci. *14*, 1195–1201. https://doi.org/10.1038/nn.2889.

21. Nandy, A.S., and Tjan, B.S. (2012). Saccade-confounded image statistics explain visual crowding. Nat. Neurosci. *15*, 463–469. https://doi.org/10.1038/nn.3021.

22. Balas, B., Nakano, L., and Rosenholtz, R. (2009). A summary-statistic representation in peripheral vision explains visual crowding. J. Vis. *9*, 13.1–1318. https://doi.org/10.1167/9.12.13.

23. Ester, E.F., Zilber, E., and Serences, J.T. (2015). Substitution and pooling in visual crowding induced by similar and dissimilar distractors. J. Vis. *15*, 15.1.4. https://doi.org/10.1167/15.1.4.

24. Motter, B.C., and Simoni, D.A. (2007). The roles of cortical image separation and size in active visual search performance. J. Vis. *7*, 6.1–615. https://doi.org/10.1167/7.2.6.

25. Petrov, Y., and Popple, A.V. (2007). Crowding is directed to the fovea and preserves only feature contrast. J. Vis. *7*, 8.1–8.9. https://doi.org/10.1167/7.2.8.

26. van den Berg, R., Roerdink, J.B.T.M., and Cornelissen, F.W. (2010). A neurophysiologically plausible population code model for feature integration explains visual crowding. PLoS Comput. Biol. *6*, e1000646. https://doi.org/10.1371/journal.pcbi.1000646.

27. Mountcastle, V.B. (1997). The columnar organization of the neocortex. Brain *120*, 701–722. https://doi.org/10.1093/brain/120.4.701.

28. Callaway, E.M. (1998). Local circuits in primary visual cortex of the macaque monkey. Annu. Rev. Neurosci. *21*, 47–74. https://doi.org/10.1146/annurev.neuro.21.1.47.

29. Lund, J.S. (1973). Organization of neurons in the visual cortex, area 17, of the monkey (Macaca mulatta). J. Comp. Neurol. *147*, 455–496. https://doi.org/10.1002/cne.901470404.

30. Douglas, R.J., and Martin, K.A.C. (2004). Neuronal circuits of the neocortex. Annu. Rev. Neurosci. *27*, 419–451. https://doi.org/10.1146/annurev.neuro.27.070203.144152.

31. Hubel, D.H., and Wiesel, T.N. (1965). Receptive fields and functional architecture in two nonstriate visual areas (18 and 19) of the cat. J. Neurophysiol. *28*, 229–289. https://doi.org/10.1152/jn.1965.28.2.229.

32. Blakemore, C., and Tobin, E.A. (1972). Lateral inhibition between orientation detectors in the cat's visual cortex. Exp. Brain Res. *15*, 439–440. https://doi.org/10.1007/BF00234129.

33. Cavanaugh, J.R., Bair, W., and Movshon, J.A. (2002). Nature and Interaction of Signals From the Receptive Field Center and Surround in Macaque V1 Neurons. J. Neurophysiol. *88*, 2530–2546. https://doi.org/10.1152/jn.00692.2001.

34. Shushruth, S., Ichida, J.M., Levitt, J.B., and Angelucci, A. (2009). Comparison of Spatial Summation Properties of Neurons in Macaque V1 and V2. J. Neurophysiol. *102*, 2069–2083. https://doi.org/10.1152/jn.00512.2009.

35. Angelucci, A., Levitt, J.B., Walton, E.J.S., Hupe, J.M., Bullier, J., and Lund, J.S. (2002). Circuits for Local and Global Signal Integration in Primary Visual Cortex. J. Neurosci. *22*, 8633–8646. https://doi.org/10.1523/JNEUROSCI.22-19-08633.2002.

36. Henry, C.A., Joshi, S., Xing, D., Shapley, R.M., and Hawken, M.J. (2013). Functional Characterization of the Extraclassical Receptive Field in Macaque V1: Contrast, Orientation, and Temporal Dynamics. J. Neurosci. *33*, 6230–6242. https://doi.org/10.1523/JNEUROSCI.4155-12.2013.

37. Bijanzadeh, M., Nurminen, L., Merlin, S., Clark, A.M., and Angelucci, A. (2018). Distinct Laminar Processing of Local and Global Context in Primate Primary Visual Cortex. Neuron *100*, 259–274.e4. https://doi.org/10.1016/j.neuron.2018.08.020.

38. Ichida, J.M., Schwabe, L., Bressloff, P.C., and Angelucci, A. (2007). Response Facilitation From the "Suppressive" Receptive Field Surround of Macaque V1 Neurons. J. Neurophysiol. *98*, 2168–2181. https://doi.org/10.1152/jn.00298.2007.

39. Sceniak, M.P., Hawken, M.J., and Shapley, R. (2001). Visual Spatial Characterization of Macaque V1 Neurons. J. Neurophysiol. *85*, 1873–1887. https://doi.org/10.1152/jn.2001.85.5.1873.

40. Shushruth, S., Nurminen, L., Bijanzadeh, M., Ichida, J.M., Vanni, S., and Angelucci, A. (2013). Different Orientation Tuning of Near- and Far-Surround Suppression in Macaque Primary Visual Cortex Mirrors Their Tuning in Human Perception. J. Neurosci. *33*, 106–119. https://doi.org/10.1523/JNEUROSCI.2518-12.2013.

41. Angelucci, A., Bijanzadeh, M., Nurminen, L., Federer, F., Merlin, S., and Bressloff, P.C. (2017). Circuits and Mechanisms for Surround Modulation in Visual Cortex. Annu. Rev. Neurosci. *40*, 425–451. https://doi.org/10.1146/annurev-neuro-072116-031418.

42. Semedo, J.D., Zandvakili, A., Machens, C.K., Yu, B.M., and Kohn, A. (2019). Cortical Areas Interact through a Communication Subspace. Neuron *102*, 249–259.e4. https://doi.org/10.1016/j.neuron.2019.01.026.

43. Mitzdorf, U. (1985). Current source-density method and application in cat cerebral cortex: investigation of evoked potentials and EEG phenomena. Physiol. Rev. *65*, 37–100. https://doi.org/10.1152/physrev.1985.65.1.37.

44. Srinath, R., Ruff, D.A., and Cohen, M.R. (2021). Attention improves information flow between neuronal populations without changing the communication subspace. Curr. Biol. *31*, 5299–5313.e4. https://doi.org/10.1016/j.cub.2021.09.076.

45. Izenman, A.J. (1975). Reduced-rank regression for the multivariate linear model. J. Multivariate Anal. *5*, 248–264. https://doi.org/10.1016/0047-259X(75)90042-1.

46. Kobak, D., Brendel, W., Constantinidis, C., Feierstein, C.E., Kepecs, A., Mainen, Z.F., Qi, X.-L., Romo, R., Uchida, N., and Machens, C.K. (2016). Demixed principal component analysis of neural population data. eLife *5*, e10989. https://doi.org/10.7554/eLife.10989.

47. Williamson, R.C., Cowley, B.R., Litwin-Kumar, A., Doiron, B., Kohn, A., Smith, M.A., and Yu, B.M. (2016). Scaling Properties of Dimensionality Reduction for Neural Populations and Network Models. PLoS Comput. Biol. *12*, e1005141. https://doi.org/10.1371/journal.pcbi.1005141.

48. Semedo, J.D., Jasper, A.I., Zandvakili, A., Krishna, A., Aschner, A., Machens, C.K., Kohn, A., and Yu, B.M. (2022). Feedforward and feedback interactions between visual cortical areas use different population activity patterns. Nat. Commun. *13*, 1099. https://doi.org/10.1038/s41467-022-28552-w.

49. Mitzdorf, U., and Singer, W. (1979). Excitatory synaptic ensemble properties in the visual cortex of the macaque monkey: A current source density analysis of electrically evoked potentials. J. Comp. Neurol. *187*, 71–83. https://doi.org/10.1002/cne.901870105.

50. Morton, M.P., Denagamage, S., Hudson, N.V., and Nandy, A.S. (2024). Geometry of anisotropic contextual interactions in the visual cortex places fundamental limits on spatial vision. J. Vis. *24*, 1432. https://doi.org/10.1167/jov.24.10.1432.

51. Stettler, D.D., Das, A., Bennett, J., and Gilbert, C.D. (2002). Lateral Connectivity and Contextual Interactions in Macaque Primary Visual Cortex. Neuron *36*, 739–750. https://doi.org/10.1016/S0896-6273(02)01029-2.

52. Adesnik, H., Bruns, W., Taniguchi, H., Huang, Z.J., and Scanziani, M. (2012). A neural circuit for spatial summation in visual cortex. Nature *490*, 226–231. https://doi.org/10.1038/nature11526.

53. Nurminen, L., Merlin, S., Bijanzadeh, M., Federer, F., and Angelucci, A. (2018). Top-down feedback controls spatial summation and response amplitude in primate visual cortex. Nat. Commun. *9*, 2281. https://doi.org/10.1038/s41467-018-04500-5.

54. Solomon, S.G., White, A.J.R., and Martin, P.R. (2002). Extraclassical Receptive Field Properties of Parvocellular, Magnocellular, and Koniocellular Cells in the Primate Lateral Geniculate Nucleus. J. Neurosci. *22*, 338–349. https://doi.org/10.1523/JNEUROSCI.22-01-00338.2002.

55. Bonin, V., Mante, V., and Carandini, M. (2005). The Suppressive Field of Neurons in Lateral Geniculate Nucleus. J. Neurosci. *25*, 10844–10856. https://doi.org/10.1523/JNEUROSCI.3562-05.2005.

56. Ozeki, H., Sadakane, O., Akasaki, T., Naito, T., Shimegi, S., and Sato, H. (2004). Relationship between Excitation and Inhibition Underlying Size Tuning and Contextual Response Modulation in the Cat Primary Visual Cortex. J. Neurosci. *24*, 1428–1438. https://doi.org/10.1523/JNEUROSCI.3852-03.2004.

57. Angelucci, A., and Sainsbury, K. (2006). Contribution of feedforward thalamic afferents and corticogeniculate feedback to the spatial summation area of macaque V1 and LGN. J. Comp. Neurol. *498*, 330–351. https://doi.org/10.1002/cne.21060.

58. Gilbert, C.D., and Li, W. (2013). Top-down influences on visual processing. Nat. Rev. Neurosci. *14*, 350–363. https://doi.org/10.1038/nrn3476.

59. Muckli, L., De Martino, F., Vizioli, L., Petro, L.S., Smith, F.W., Ugurbil, K., Goebel, R., and Yacoub, E. (2015). Contextual Feedback to Superficial Layers of V1. Curr. Biol. *25*, 2690–2695. https://doi.org/10.1016/j.cub.2015.08.057.

60. Harris, K.D., and Mrsic-Flogel, T.D. (2013). Cortical connectivity and sensory coding. Nature *503*, 51–58. https://doi.org/10.1038/nature12654.

61. van Kerkoerle, T., Self, M.W., Dagnino, B., Gariel-Mathis, M.A., Poort, J., van der Togt, C., and Roelfsema, P.R. (2014). Alpha and gamma oscillations characterize feedback and feedforward processing in monkey visual cortex. Proc. Natl. Acad. Sci. USA *111*, 14332–14341. https://doi.org/10.1073/pnas.1402773111.

62. Tauste Campo, A., Martinez-Garcia, M., Nácher, V., Luna, R., Romo, R., and Deco, G. (2015). Task-driven intra- and interarea communications in primate cerebral cortex. Proc. Natl. Acad. Sci. USA *112*, 4761–4766. https://doi.org/10.1073/pnas.1503937112.

63. Zandvakili, A., and Kohn, A. (2015). Coordinated Neuronal Activity Enhances Corticocortical Communication. Neuron *87*, 827–839. https://doi.org/10.1016/j.neuron.2015.07.026.

64. Jia, X., Tanabe, S., and Kohn, A. (2013). Gamma and the Coordination of Spiking Activity in Early Visual Cortex. Neuron *77*, 762–774. https://doi.org/10.1016/j.neuron.2012.12.036.

65. Nowak, L.G., Munk, M.H.J., James, A.C., Girard, P., and Bullier, J. (1999). Cross-Correlation Study of the Temporal Interactions Between Areas V1 and V2 of the Macaque Monkey. J. Neurophysiol. *81*, 1057–1074. https://doi.org/10.1152/jn.1999.81.3.1057.

66. Roe, A.W., and Ts'o, D.Y. (1999). Specificity of Color Connectivity Between Primate V1 and V2. J. Neurophysiol. *82*, 2719–2730. https://doi.org/10.1152/jn.1999.82.5.2719.

67. Gregoriou, G.G., Gotts, S.J., Zhou, H., and Desimone, R. (2009). High-Frequency, Long-Range Coupling Between Prefrontal and Visual Cortex During Attention. Science *324*, 1207–1210. https://doi.org/10.1126/science.1171402.

68. Salazar, R.F., Dotson, N.M., Bressler, S.L., and Gray, C.M. (2012). Content-Specific Fronto-Parietal Synchronization During Visual Working Memory. Science *338*, 1097–1100. https://doi.org/10.1126/science.1224000.

69. Bastos, A.M., Vezoli, J., and Fries, P. (2015). Communication through coherence with inter-areal delays. Curr. Opin. Neurobiol. *31*, 173–180. https://doi.org/10.1016/j.conb.2014.11.001.

70. de Lafuente, V., and Romo, R. (2006). Neural correlate of subjective sensory experience gradually builds up across cortical areas. Proc. Natl. Acad. Sci. USA *103*, 14266–14271. https://doi.org/10.1073/pnas.0605826103.

71. Siegel, M., Buschman, T.J., and Miller, E.K. (2015). Cortical information flow during flexible sensorimotor decisions. Science *348*, 1352–1355. https://doi.org/10.1126/science.aab0551.

72. Schmolesky, M.T., Wang, Y., Hanes, D.P., Thompson, K.G., Leutgeb, S., Schall, J.D., and Leventhal, A.G. (1998). Signal Timing Across the Macaque Visual System. J. Neurophysiol. *79*, 3272–3278. https://doi.org/10.1152/jn.1998.79.6.3272.

73. Freeman, J., Ziemba, C.M., Heeger, D.J., Simoncelli, E.P., and Movshon, J.A. (2013). A functional and perceptual signature of the second visual area in primates. Nat. Neurosci. *16*, 974–981. https://doi.org/10.1038/nn.3402.

74. Chen, M., Yan, Y., Gong, X., Gilbert, C.D., Liang, H., and Li, W. (2014). Incremental Integration of Global Contours through Interplay between Visual Cortical Areas. Neuron *82*, 682–694. https://doi.org/10.1016/j.neuron.2014.03.023.

75. Schwiedrzik, C.M., and Freiwald, W.A. (2017). High-Level Prediction Signals in a Low-Level Area of the Macaque Face-Processing Hierarchy. Neuron *96*, 89–97.e4. https://doi.org/10.1016/j.neuron.2017.09.007.

76. Issa, E.B., Cadieu, C.F., and DiCarlo, J.J. (2018). Neural dynamics at successive stages of the ventral visual stream are consistent with hierarchical error signals. eLife *7*, e42870. https://doi.org/10.7554/eLife.42870.

77. Callaway, E.M., and Wiser, A.K. (1996). Contributions of individual layer 2-5 spiny neurons to local circuits in macaque primary visual cortex. Vis. Neurosci. *13*, 907–922. https://doi.org/10.1017/s0952523800009159.

78. Wiser, A.K., and Callaway, E.M. (1996). Contributions of individual layer 6 pyramidal neurons to local circuitry in macaque primary visual cortex. J. Neurosci. *16*, 2724–2739. https://doi.org/10.1523/JNEUROSCI.16-08-02724.1996.

79. Briggs, F., and Callaway, E.M. (2001). Layer-Specific Input to Distinct Cell Types in Layer 6 of Monkey Primary Visual Cortex. J. Neurosci. *21*, 3600–3608. https://doi.org/10.1523/JNEUROSCI.21-10-03600.2001.

80. Nandy, A.S., Nassi, J.J., and Reynolds, J.H. (2017). Laminar Organization of Attentional Modulation in Macaque Visual Area V4. Neuron *93*, 235–246. https://doi.org/10.1016/j.neuron.2016.11.029.

81. Nassi, J.J., Avery, M.C., Cetin, A.H., Roe, A.W., and Reynolds, J.H. (2015). Optogenetic Activation of Normalization in Alert Macaque Visual Cortex. Neuron *86*, 1504–1517. https://doi.org/10.1016/j.neuron.2015.05.040.

82. Ruiz, O., Lustig, B.R., Nassi, J.J., Cetin, A., Reynolds, J.H., Albright, T.D., Callaway, E.M., Stoner, G.R., and Roe, A.W. (2013). Optogenetics through windows on the brain in the nonhuman primate. J. Neurophysiol. *110*, 1455–1467. https://doi.org/10.1152/jn.00153.2013.

83. Stringer, C., Pachitariu, M., Steinmetz, N., Reddy, C.B., Carandini, M., and Harris, K.D. (2019). Spontaneous behaviors drive multidimensional, brainwide activity. Science *364*, 255. https://doi.org/10.1126/science.aav7893.

84. Steinmetz, N.A., Aydin, C., Lebedeva, A., Okun, M., Pachitariu, M., Bauza, M., Beau, M., Bhagat, J., Böhm, C., Broux, M., et al. (2021). Neuropixels 2.0: A miniaturized high-density probe for stable, long-term brain recordings. Science *372*, eabf4588. https://doi.org/10.1126/science.abf4588.

85. Hwang, J., Mitz, A.R., and Murray, E.A. (2019). NIMH MonkeyLogic: Behavioral control and data acquisition in MATLAB. J. Neurosci. Methods *323*, 13–21. https://doi.org/10.1016/j.jneumeth.2019.05.002.

86. Bouma, H. (1970). Interaction Effects in Parafoveal Letter Recognition. Nature *226*, 177–178. https://doi.org/10.1038/226177a0.

87. Pelli, D.G., and Tillman, K.A. (2008). The uncrowded window of object recognition. Nat. Neurosci. *11*, 1129–1135. https://doi.org/10.1038/nn.2187.

88. Calin-Jageman, R.J., and Cumming, G. (2019). Estimation for Better Inference in Neuroscience. eNeuro *6*, ENEURO.0205-19.2019. https://doi.org/10.1523/eneuro.0205-19.2019.

89. Ho, J., Tumkaya, T., Aryal, S., Choi, H., and Claridge-Chang, A. (2019). Moving beyond P values: data analysis with estimation graphics. Nat. Methods *16*, 565–566. https://doi.org/10.1038/s41592-019-0470-3.

90. Everitt, B.S. (1984). Maximum Likelihood Estimation of the Parameters in a Mixture of Two Univariate Normal Distributions; A Comparison of Different Algorithms. J. R. Stat. Soc. D *33*, 205–215. https://doi.org/10.2307/2987851.

91. Yu, B.M., Cunningham, J.P., Santhanam, G., Ryu, S.I., Shenoy, K.V., and Sahani, M. (2009). Gaussian-Process Factor Analysis for Low-Dimensional Single-Trial Analysis of Neural Population Activity. J. Neurophysiol. *102*, 614–635. https://doi.org/10.1152/jn.90941.2008.

92. Björck, Å., and Golub, G.H. (1973). Numerical Methods for Computing Angles Between Linear Subspaces. Math. Comput. *27*, 579–594. https://doi.org/10.2307/2005662.

93. Gallego, J.A., Perich, M.G., Naufel, S.N., Ethier, C., Solla, S.A., and Miller, L.E. (2018). Cortical population activity within a preserved neural manifold underlies multiple motor behaviors. Nat. Commun. *9*, 4233. https://doi.org/10.1038/s41467-018-06560-z.

94. Hotelling, H. (1936). Relations Between Two Sets of Variates. Biometrika *28*, 321–377. https://doi.org/10.2307/2333955.

Please cite this article in press as: Xu et al., Spatial context non-uniformly modulates inter-laminar information flow in the primary visual cortex, Neuron (2024), https://doi.org/10.1016/j.neuron.2024.09.021

STAR★METHODS

KEY RESOURCES TABLE

REAGENT or RESOURCE	SOURCE	IDENTIFIER
Experimental models: Organisms/strains		
Rhesus Macaques (Macaca mulatta)	Worldwide Primates	N/A
Chemicals, peptides, and recombinant proteins		
PEDOT:PSS	Sigma-Aldrich	655201
Deposited data		
Figure data	This paper	https://doi.org/10.6084/m9.figshare.27055252
Software and algorithms		
MATLAB	Mathworks	R2021b
Kilosort2	Pachitariu & MouseLand	https://github.com/MouseLand/Kilosort
phy (spike curation GUI)	Rossant & cortex-lab	https://github.com/cortex-lab/phy
Custom code	This paper	https://doi.org/10.6084/m9.figshare.27055252
Other		
Silicon probes	NeuroNexus	a2x32_6mm35_200_177
RHD 512 channel recording controller	Intan	C3004
64 channel recording headstages	Intan	C3115
nanoZ	White Matter LLC	N/A

EXPERIMENTAL MODEL AND STUDY PARTICIPANT DETAILS

Two male rhesus macaques (Macaca mulatta, D: age 6 years, M: age 8 years) were used as subjects in this study. Animals were pair-housed on a 12:12 h light-dark cycle. Water intake was controlled during the experimental period. All experimental procedures were approved by the Institutional Animal Care and Use Committee at Yale University and conformed to NIH guidelines.

METHOD DETAILS

Surgical procedures

Surgical procedures were similar to those described previously.[80–82] We placed low-profile titanium recording chambers in two rhesus macaques so that the chambers allowed access to V1 (both left and right hemispheres in monkey M, right hemisphere in monkey D). Chambers were targeted based on sulcus reconstructions created using preoperative structural MRI. After chamber implantation, we removed the native dura mater and replaced it with a transparent silicone artificial dura (AD). The AD allowed for the visualization of cortical sites in V1 for probe targeting. All procedures were approved by the Yale University Institutional Animal Care and Use Committee and conformed to NIH guidelines.

Electrophysiology

Prior to a series of recordings, we electroplated (nanoZ, White Matter LLC) 64-channel electrode arrays (“laminar probes,” NeuroNexus Technologies, Inc., 2 shanks, 32 channels/shank, 70 μm spacing between sites, 200 μm between shanks) with PEDOT (poly(3,4-ethylene dioxythiophene)). At the beginning of each recording session, we inserted a laminar probe in V1. Laminar probes were attached to a titanium mounting stage that was screwed into the chamber. We positioned the laminar probes using an electronic micromanipulator (Narishige Inc.) and ensured that the probes were orthogonal to the surface of the cortex by visual inspection through a surgical microscope (Leica Microsystems). To position the probe within the brain, we first penetrated the AD, arachnoid, and pia by moving the probe downward at a high speed (>100 μm/s). After the tip of the probe entered the cortex, we inserted the remainder of the probe at a slow speed (2 μm/s). Once the entire probe was in the brain, we slowly (2μm/s) relieved the pressure on the brain by retracting the probe upward, relieving pressure on the brain but not moving the probe relative to the cortex.

Electrical signals from the laminar probe were collected at 30 kHz and digitized on a 64-channel digital headstage and sent to the recording system (RHD Recording System, Intan Technologies). Action potential waveforms were extracted offline using Kilosort2[83,84] and manually sorted into single and multi-unit clusters using Phy.[83,84] Clusters with peaks preceding the trough were

Please cite this article in press as: Xu et al., Spatial context non-uniformly modulates inter-laminar information flow in the primary visual cortex, Neuron (2024), https://doi.org/10.1016/j.neuron.2024.09.021

identified as axonal spikes and excluded. Recordings were collected over the course of 22 sessions (14 in monkey M, 8 in monkey D) with hundreds of units recorded in each subject (693 single units and 430 multi-unit clusters in monkey M, 400 single units and 277 multi-unit clusters in monkey D).

Behavioral control and eye tracking

We controlled behavioral experiments using NIMH MonkeyLogic.[85] Eye position and pupil diameter were sampled at 120Hz (ETL-200, ISCAN Inc.) and sent to the behavioral control system. Stimuli were presented on a monitor positioned 57cm from the monkey with a 60 Hz refresh rate. Trials were aborted if the eye position deviated more than 1.2-1.5 degrees of visual angle (dva; 1.2 for monkey D, 1.5 for monkey M) from the central fixation point.

Receptive field mapping

We mapped RFs of the column by presenting Gabor patch stimuli (2-4 cycles/degree, 0.25-1 degree Gaussian half-width, 100% luminance contrast) on a square grid spanning the lower visual quadrant of interest (both left and right in monkey M, left in monkey D) while the monkey maintained fixation on the center of the screen. Grid spacing parameters were optimized each session and ranged from 0.25-1 dva. A stimulus was presented at a random location and orientation on the grid during each frame. We calculated the LFP power for each recording channel 40-200 ms after stimulus presentation in each location. The LFP power at each location was smoothed using a Gaussian kernel (sigma = 0.75 dva), and the peak location averaged across all recording sites was defined as the receptive field center. Spatial receptive field maps for each channel were plotted as stacked contours for each shank for visualization.

Current source density mapping

We used CSD mapping[43] to identify laminar boundaries in our recordings and estimated the relative strength of the signal targeting the superficial layer across visual conditions.

While monkeys maintained fixation on the screen, 100% luminance contrast white annular stimuli were flashed for 32 ms, positioned at the center of the RF. The LFP signal following the stimulus onset was averaged across trials and spatially smoothed using a Gaussian kernel (sigma = 140 μm). The CSD was calculated as the second spatial derivative of the LFP:

$$CSD(x,t) = -\sigma * \frac{v(x+h,t) - 2v(x,t)+v(x-h,t)}{h^2}$$

where x is the position in the extracellular medium at which CSD is calculated, t the time following the stimulus onset (advancing in 1 ms), h the spacing between recording sites on the linear probe (here 70 μm), v the voltage, σ the conductivity of the cortical tissue (0.4 S/m). We interpolated the CSD every 7 μm. The input layer was identified by the boundaries of the early current sink characterizing feedforward input into layer IV. Channels above and below this sink were classified as superficial and deep, respectively.

CSD provides a link between LFP and neuronal ensemble activities by approximating the net local transmembrane currents that generate the local LFP. The identified current sinks (negative deflections, visualized in red in Figures 7A–7C) in the extracellular medium reflect integrated subthreshold input to neuronal ensembles.[43,49] We used CSD response to flanker-only stimuli (radial-out, radial-in, tangential) to estimate the relative strength of the signal targeting the superficial layer evoked by contextual stimuli at different locations. In particular, for each shank on the laminar probe, we first identified the early current sink (within 200 ms following stimulus onset) in its CSD response. At each depth along the superficial layer, we calculated the level of charge sinks by integrating the current sink over time and then averaged the result across the depth of the superficial layer. We compared the level of charge sinks evoked by flankers-only stimuli at different locations to quantify the relative strength of contextual signals targeting the superficial layer.

Experimental task

While monkeys maintained fixation on a point at the center of the screen, stimulus arrays were presented on the screen for 100 ms. In between stimulus presentations, there was a 200-250 ms inter-stimulus interval in which the screen was blank other than the fixation point. The arrays consisted of a probe stimulus in the receptive field center either in isolation (probe condition) or together with a flanking stimulus (flanked condition). There were four different conditions (probe, tangentially flanked, radially inward flanked, and radially outward flanked) of stimulus arrays presented during a trial. This was repeated 4-6 times during each trial depending on the monkey's ability to hold fixation. The stimulus conditions were randomly interleaved from flash to flash. The center of the probe was aligned with the center of the average of the RFs of each recording site. The four flanker locations were positioned on the radial or tangential axes. The radial axis was defined as the axis connecting the probe (and RF) center and the fixation point at the center of the monitor. The tangential axis was defined as the line orthogonal to the radial axis and passing through the probe center. The tangential flanked condition occurred when the probe was presented along with a flanker on the tangential axis, either in the clockwise or counterclockwise direction. The radial-in flanked condition occurred when the probe was presented along with a flanker on the radial axis and between the probe center and the fixation point. The radial-out condition was similar to the radial-in condition, except the flanker was placed on the radial axis further from the fixation point than the probe. Probe-flanker spacing was identical across stimulus conditions.

Please cite this article in press as: Xu et al., Spatial context non-uniformly modulates inter-laminar information flow in the primary visual cortex, Neuron (2024), https://doi.org/10.1016/j.neuron.2024.09.021

The probe condition was presented on 10% of flashes. On 80% of flashes, flanked stimuli were presented. In the flanked condition, the flanker was positioned at a tangential, radial-in, or radial-out location with equal probability. If the flanker was presented tangential to the probe, it was positioned clockwise or counterclockwise to the probe with equal probability. In the remaining 10% of trials, a stimulus was presented exclusively at one of the four flanker locations. Probe stimuli were sine Gabor patches (25% luminance contrast, 3.5 cycles/degree, 0.5-1.0 degree Gaussian half-width) presented at 6 evenly spaced orientations and 2 opposing phases. Flankers were presented at 100% luminance contrast but were otherwise identical to the probe stimuli. The center-to-center distance between the probe and flankers (Δe, Figure 1D1) was 0.6 (monkey D) or 0.85 dva (monkey M) depending on e_{probe}. Target and flanker stimuli were 0.5 (monkey D) or 0.75 dva (monkey M) in diameter. The ratio between Δe and e_{probe} was 0.46 ± 0.02 SEM, which matched the spatial scaling of crowding zones (critical spacing for crowding in the visual field ≈ 0.5 x target eccentricity).[86,87] The edge-to-edge gap between probe and flanker was 0.1-0.2 deg depending on e_{probe}. In the flanked condition, flankers were presented at the same orientation as the probe or orthogonal to the probe with equal probability. When flankers were presented alone, they were shown with the same orientation distribution as the probes.

QUANTIFICATION AND STATISTICAL ANALYSIS

Wherever possible, instead of relying on null-hypothesis testing, we show bootstrapped estimations of differences between conditions using the estimation statistics framework,[88,89] which provides a principled way to measure effect sizes coupled with estimates of uncertainty, yielding interval estimates of uncertainty. The experiment assigned substantially different presentation probabilities for the probe (10%) and each of the flanked conditions (26.7%). On average, our dataset contained 504.5 ± 29.1 SEM, 1348.8 ± 77.9 SEM, 1306.6 ± 87.6 SEM, 1321.5 ± 90.9 SEM trials for the probe, radial-in, radial-out, and tangential conditions, respectively. When comparing inter-laminar information flows for a pair of visual conditions, we drew the same number of trials under each condition multiple times and conducted the prediction analysis with 20-fold cross-validation. Consequently, when comparing the properties of inter-laminar information flow under the probe condition against any of the flanked conditions (Figures 2, 3, 4, 5A, 6C, and 6D), the number of trials from each draw was capped by the number of trials under the probe condition, which led to the exclusion of a large fraction of trials under each of the flanked conditions. When calculating the properties for individual conditions (Figures 1G–1L) without comparison across conditions, we did not match the number of trials.

Normalized peri-stimulus time histograms (PSTHs)

PSTHs were generated based on spike counts in 30 ms bins shifted by 10 ms. The PSTH for each neuron was calculated separately for each visual condition and normalized between the maximal PSTH over time under the probe condition and the baseline firing rate taken as the PSTH from -30 ms to 30 ms relative to stimulus onset. Neurons whose PSTHs never surpassed the 95% confidence interval of their baseline firing rates were excluded. The averaged normalized PSTH exhibits a maximum less than 1 because of the variability in the peak time across neurons.

Response onset estimation

For every recorded unit, we estimated its response onset for each visual condition. We took the PSTH from -30 ms to 30 ms relative to stimulus onset as the baseline firing rate. The response onset was identified as the time when the PSTH surpassed the 95% confidence interval of the baseline firing rate. Units whose PSTH never crossed the threshold were taken as non-responsive units. For each session, the response onset of the simultaneously recorded population in a specific layer was estimated by taking the average of response onsets of all responsive units. An interval of 100 ms following the response onset of the input layer population was considered as the stimulus processing range (referred to as 'responsive period') of V1 for the purpose of characterizing the inter-laminar information flow between the input and superficial layers.

Unit selection for regression analysis

For comparison of the inter-laminar prediction accuracy across visual conditions, we only included those units in the superficial layer well predicted by the recorded population in the input layer, which were identified by employing a Lasso regression with 20-fold cross-validation to each recorded unit in the superficial layer within the estimated responsive period. The prediction performance was calculated under the largest λ value such that the normalized squared error (*NSE*) was within one standard error of the minimum *NSE* across λ parameters. Units in the superficial layer with a normalized squared error smaller than 1 were identified as being well predicted.

Data preparation for regression analysis

We counted spikes in a sliding window of 50 ms within the estimated responsive period. We investigated how the neuronal activities in the input and superficial layers were related by assessing the extent to which trial-to-trial fluctuations of population responses in the superficial layer could be predicted by that in the input layer of V1. Therefore, for each type of visual stimuli (orientation, spatial configuration, orientation difference between probe and flanker), we subtracted the appropriate peri-stimulus time histogram (i.e., average

time-varying signal; PSTH) from each single-trial response and z-scored the residual. For all analyses, we excluded units with low firing rates (less than 0.2 spikes/s on average). Our results are qualitatively similar for larger 100 ms bins, which corresponded to the stimuli duration in the experiment.

Regression

To assess the extent to which trial-to-trial fluctuations of population responses in the superficial layer could be predicted by that in the input layer of V1, we first applied a linear model of the form $Y = XB$ using ridge regression, which was referred to as the full regression model. To test whether the inter-laminar information propagation occurred through a 'communication subspace', we used reduced-rank regression (RRR), which constrains the linear weight matrix B to be of a given rank. The optimal dimensionality (Dim_{opt}) was defined as the lowest number of predictive dimensions for which prediction performance was within one SEM of peak performance. The details of this analysis can be found in Semedo et al.[42]

Both ridge regression and RRR were applied to a sliding window of 50 ms (advancing in 2 ms) in both layers with 20-fold cross-validation. The prediction accuracy was calculated as $1 - NSE$, where NSE is the mean normalized squared error between the test data and the predictions across folds. For RRR, we took the smallest number of dimensions for which predictive performance was within one SEM of the peak performance as the optimal dimensionality. To study the effect of the spatial configuration of visual stimuli on prediction accuracy, we analyzed the temporal evolution of the prediction accuracies at optimal dimensionality across visual conditions. For each pair of visual conditions, we first aligned the temporal evolutions of corresponding prediction accuracies to compensate for the difference in the response onsets across visual conditions and computed a prediction modulation index, which was calculated as:

$$\mathrm{PMI(t)} = \frac{P_1(t) - P_2(t)}{\sum_t (P_1(t)+P_2(t))/N_t}$$

Where $P_1(t)$ and $P_2(t)$ are the prediction accuracies at optimal dimensionalities obtained by RRR at time t after response onset under visual conditions 1 and 2, respectively. N_t is the number of time points involved in the analysis.

Factor analysis

We quantified the complexity of neural activity in the superficial layer of V1 by using factor analysis (FA), a dimensionality reduction technique which allows spiking variability to vary across neurons and calculates the dimensionality of covariance. The details of this analysis can be found in Williamson et al.,[47] Everitt et al.,[90] and Yu et al.[91] We followed the same steps as previously published work[42,44] to estimate the dimensionality: We first determined the number of dimensions m_{peak} that maximized the cross-validated log-likelihood of the observed residuals. Then we fitted an FA model with m_{peak} dimensions and chose m, by the eigenvalue decomposition, as the smallest dimensionality that captured 95% of the variance in the shared covariance matrix. These population dimensions (m) and predictive dimensions as determined from RRR are based on different techniques.

Principal angle

We characterized the relative alignment of two communication subspaces identified from different visual conditions by using the measure of principal angle, which computes angles between sequentially aligned pairs of basis vectors, each within one of the subspaces, so as to minimize the angle between them. Notably, this measure does not require the compared subspaces to have the same rank. The smallest angle obtained was taken as the 'leading principal angle'. The details of this method can be found in Björck and Golub[92] and Gallego et al.[93] A small leading principal angle implies similar orientations of the communication subspaces identified from different conditions. To verify that the experimentally obtained leading principal angles were significantly different from chance, we compared them to a null distribution of principal angles. These were obtained from 5000 pairs of subspaces that were generated randomly but with preserved ranks (as that of the empirical communication subspaces under different visual conditions). The confidence intervals of the null distribution were obtained from estimation statistics. Moreover, to efficiently assess the extent of similarity in the measure of the principal angle between communication subspaces identified from different visual conditions, we constructed an estimate of the minimal principal angle that could be obtained. This was achieved by computing the principal angle between subspaces identified from pairs of disjoint sets of trials within the same visual condition. To ensure a fair comparison with the cross-condition principal angles, each set was composed of the same number of trials as those used to identify cross-condition communication subspaces. This number was capped by the number of trials under the probe condition, as the experiment assigned a significantly smaller presentation probability to the probe condition (10%) compared to any of the flanked conditions (26.7%). Consequently, the ratio of the number of trials in any of the flanked conditions and the probe condition exceeded 2, which allowed us to compute the within-condition principal angle for the radial-in, radial-out, and tangential conditions when compared with the probe condition. In Figure S2A where we computed the principal angle between any pair of flanked conditions, the number of trials used to identify communication subspaces was only capped by the smallest number of trials across all flanked conditions, which was larger than the half of number of trials under any flanked condition. We were therefore unable to construct an estimate of within-condition principal angles that could be fairly compared with existing curves.

Please cite this article in press as: Xu et al., Spatial context non-uniformly modulates inter-laminar information flow in the primary visual cortex, Neuron (2024), https://doi.org/10.1016/j.neuron.2024.09.021

Cross-prediction analysis

An additional analysis to compare the communication subspaces was based on measuring the inter-laminar prediction performance under a given visual condition when the corresponding input layer data was projected onto the communication subspace identified from a different visual condition. We computed the prediction performance for when projecting the input layer data from the communication subspace identified from condition A onto that identified from condition B (across-condition prediction performance). Then we compared it to the prediction performance when the input layer data was projected onto the original communication subspace of condition A (within-condition prediction performance; obtained from RRR by definition). Comparable cross-condition and within-condition prediction performance implies a similarity between the structure of communication subspaces identified from different conditions. To verify whether the computed cross-condition and within-condition prediction performances were significantly close to each other, we compared them to the prediction performance obtained by chance, where the input layer data in a given condition was projected onto subspaces randomly generated as in the principal angle analysis. Note that this analysis was performed twice for each pair of visual conditions, considering either condition as the within-condition communication subspace.

Population correlation analysis

We used canonical correlation analysis (CCA)[94] to capture the population correlation between the input and superficial layers at different time delays on a moment-by-moment basis. CCA finds pairs of dimensions, one each in the neuronal activity space in each layer, such that the correlation between the projected activity onto these dimensions is maximally correlated. The exact description and formulation of CCA can be found in Semedo et al.[48] We took two windows of activity, one in each layer. Window length was 50 ms and the window was advanced in 10 ms steps. The activity within each window was then binned using 10 ms bins. The reported results were robust over a reasonable range of window and binning lengths chosen. We reported correlation associated with the first two canonical pairs (correlations associated with the third were on average 60% lower and close to chance level).

The correlations along the feedforward (FF) and the effective feedback (FB) signaling pathways were calculated as the mean correlation at positive and negative delays, respectively:

$$C_{FF}(t) = \frac{\sum_{dt>0} C(t,dt)}{N_{dt>0}}$$

$$C_{FB}(t) = \frac{\sum_{dt<0} C(t,dt)}{N_{dt<0}}$$

where t is the time following response onset, dt is the inter-laminar delay involved between windows from two layers, $C(t,dt)$ is the corresponding correlation. $N_{dt>0}$ is the number of positive delays investigated, which is equal to the number of negative delays, $N_{dt<0}$.

The direction dominance index was calculated as:

$$DDI(t) = \frac{C_{FF}(t) - C_{FB}(t)}{\sum_t \sum_{dt} C(t,dt) \Big/ N_{dt} \Big/ N_t}$$

where N_t and N_{dt} are the number of time points and delay involved in the analysis, respectively. A positive DDI indicates the dominance of feedforward signaling and a negative DDI indicates the dominance of effective feedback signaling.

Neuron, Volume *112*

Supplemental information

Spatial context non-uniformly modulates inter-laminar information flow in the primary visual cortex

Xize Xu (徐锡泽), Mitchell P. Morton, Sachira Denagamage, Nyomi V. Hudson, Anirvan S. Nandy, and Monika P. Jadi

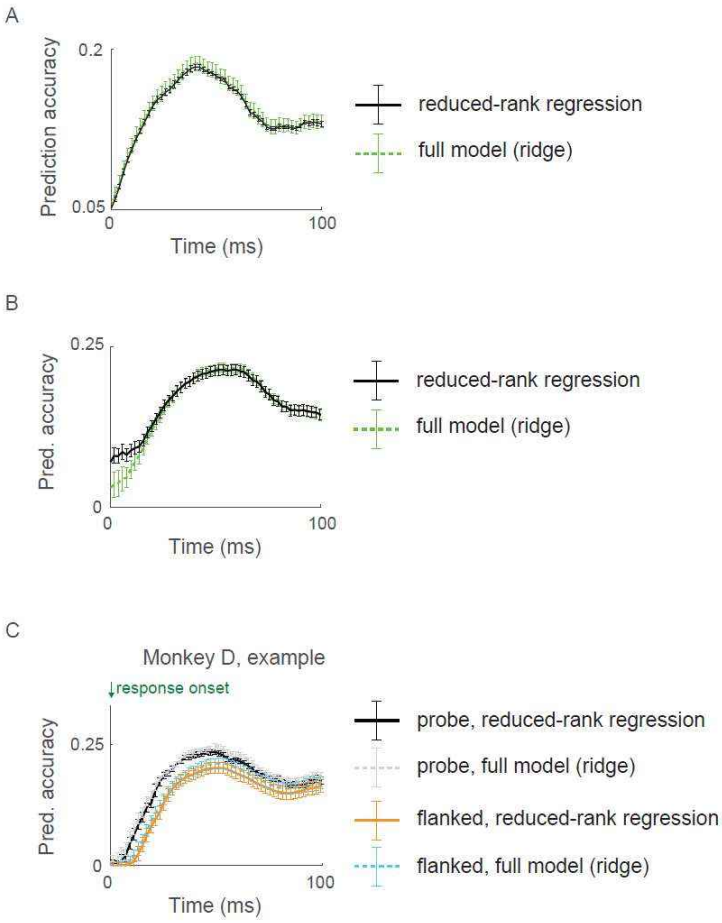

Figure S1. Comparing prediction accuracies calculated using reduced-rank regression (RRR) against the full regression model (ridge), related to Figure 1-3

(**A**) Temporal evolution of prediction accuracy as shown in Fig. 1H computed by RRR (solid curve) or the full regression model (dashed curve). (B) Temporal evolution of within-condition prediction accuracy as shown in black in Fig. 2C computed by RRR (solid curve) or the full regression model (dashed curve). (C) Temporal evolution of prediction accuracy under the probe and flanked conditions as shown in Fig. 3A computed by RRR (solid curves) or the full regression model (dashed curves). The full regression model always gives comparable predictive performance as RRR.

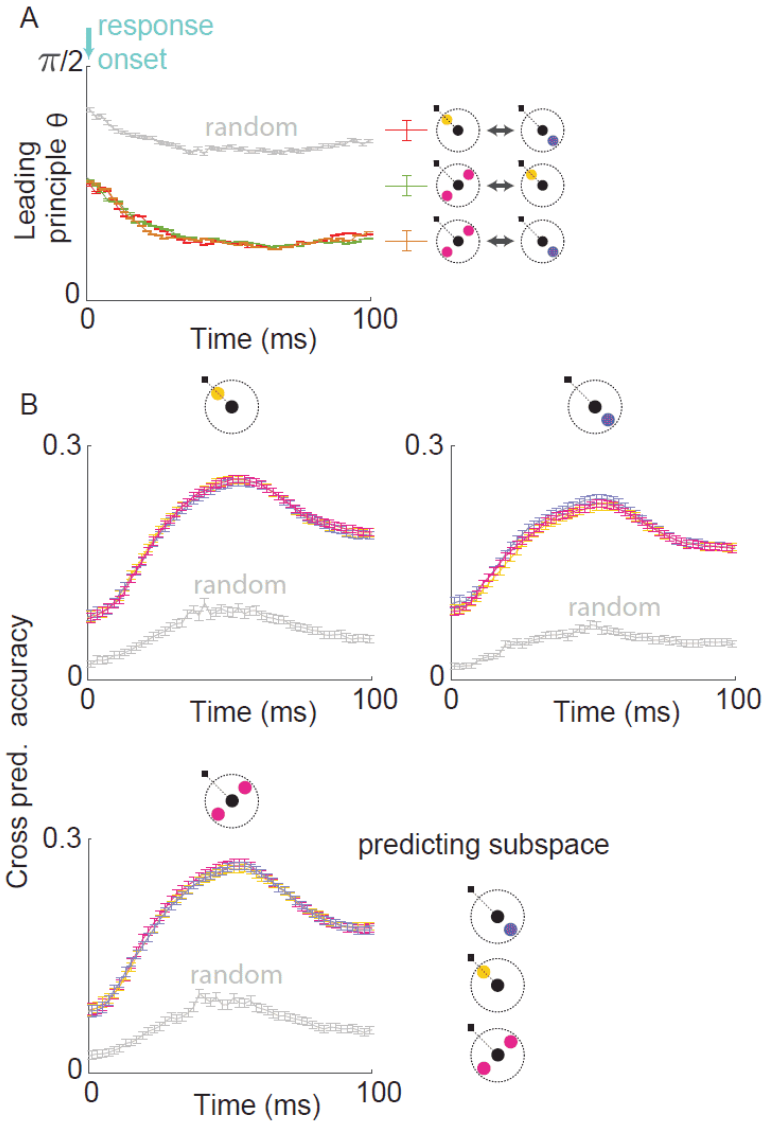

Figure S2. Comparing communication subspace across visual conditions, related to Figure 2

(**A**) The temporal evolution of leading principal angles between the communication subspaces identified from different types of flanked conditions during the corresponding visually responsive period (averaged across all sessions) and between random subspaces of comparable dimensions (grey; see Methods). (**B**) Cross-prediction analysis for input layer predicting superficial layer activity during a given flanked condition (shown at the top) and using subspaces identified for various conditions (as shown in the legend). Error bars indicate the 95% confidence interval for the mean.

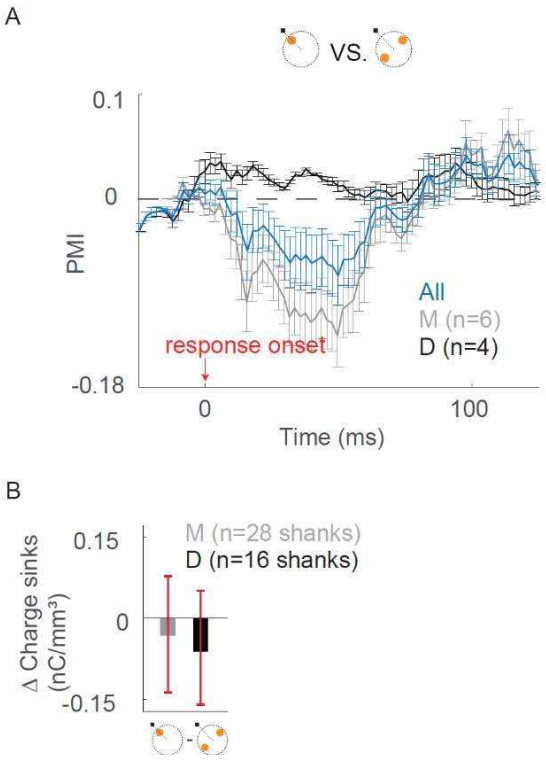

Figure S3. Comparing prediction accuracy across visual conditions, related to Figure 5, 7

(**A**) Same as Fig. 5B, comparing inter-laminar prediction accuracy under the radial-in condition to that under the tangential condition. Negative PMIs imply a degradation of prediction accuracy in the radial-in condition compared to the tangential condition. (**B**) The within-shank difference in the level of early charge sinks in the superficial layer, when compared between the radial-in and tangential conditions for all shanks from each monkey. Error bars indicate 95% confidence interval for the mean.

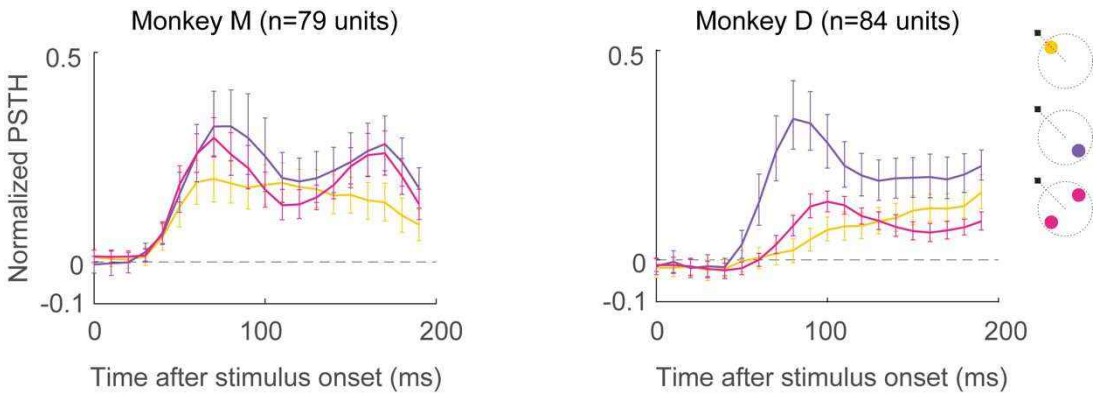

Figure S4. Comparing PSTH across flanker-only conditions, related to Figure 7

Normalized peri-stimulus time histograms (PSTHs; see Methods) for superficial layer units (separately for each monkey) under various flanker-only conditions. Error bars indicate the standard error across neurons. This analysis only included neurons that were visually responsive (see Methods) in the probe condition and exhibited significantly higher rates compared to all flanker-only conditions.

Neuron, Volume *112*

Supplemental information

Spatial context non-uniformly modulates inter-laminar information flow in the primary visual cortex

Xize Xu (徐锡泽), Mitchell P. Morton, Sachira Denagamage, Nyomi V. Hudson, Anirvan S. Nandy, and Monika P. Jadi

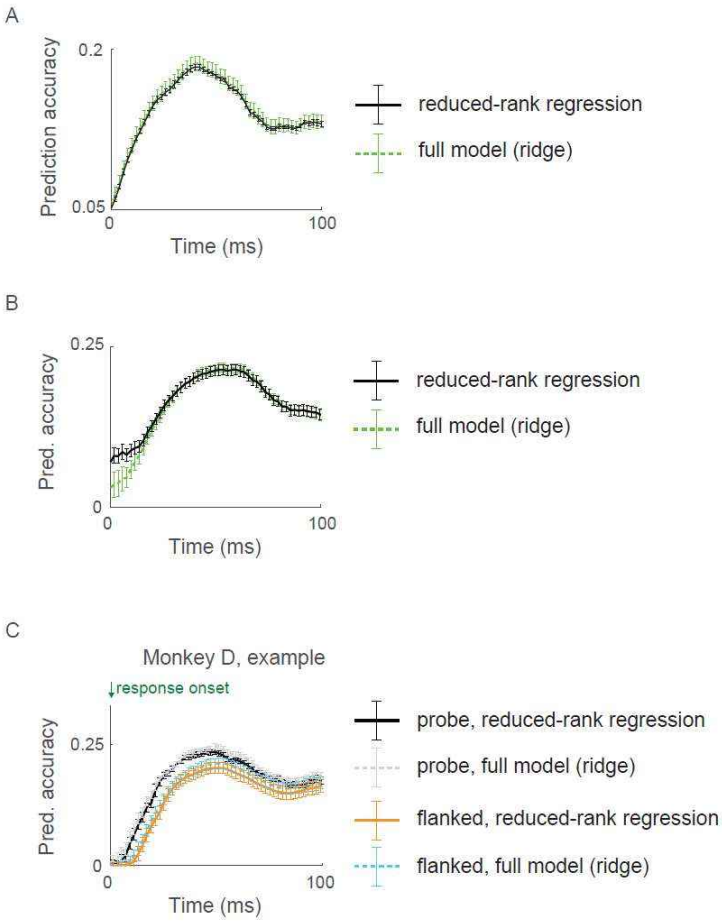

Figure S1. Comparing prediction accuracies calculated using reduced-rank regression (RRR) against the full regression model (ridge), related to Figure 1-3

(**A**) Temporal evolution of prediction accuracy as shown in Fig. 1H computed by RRR (solid curve) or the full regression model (dashed curve). (B) Temporal evolution of within-condition prediction accuracy as shown in black in Fig. 2C computed by RRR (solid curve) or the full regression model (dashed curve). (C) Temporal evolution of prediction accuracy under the probe and flanked conditions as shown in Fig. 3A computed by RRR (solid curves) or the full regression model (dashed curves). The full regression model always gives comparable predictive performance as RRR.

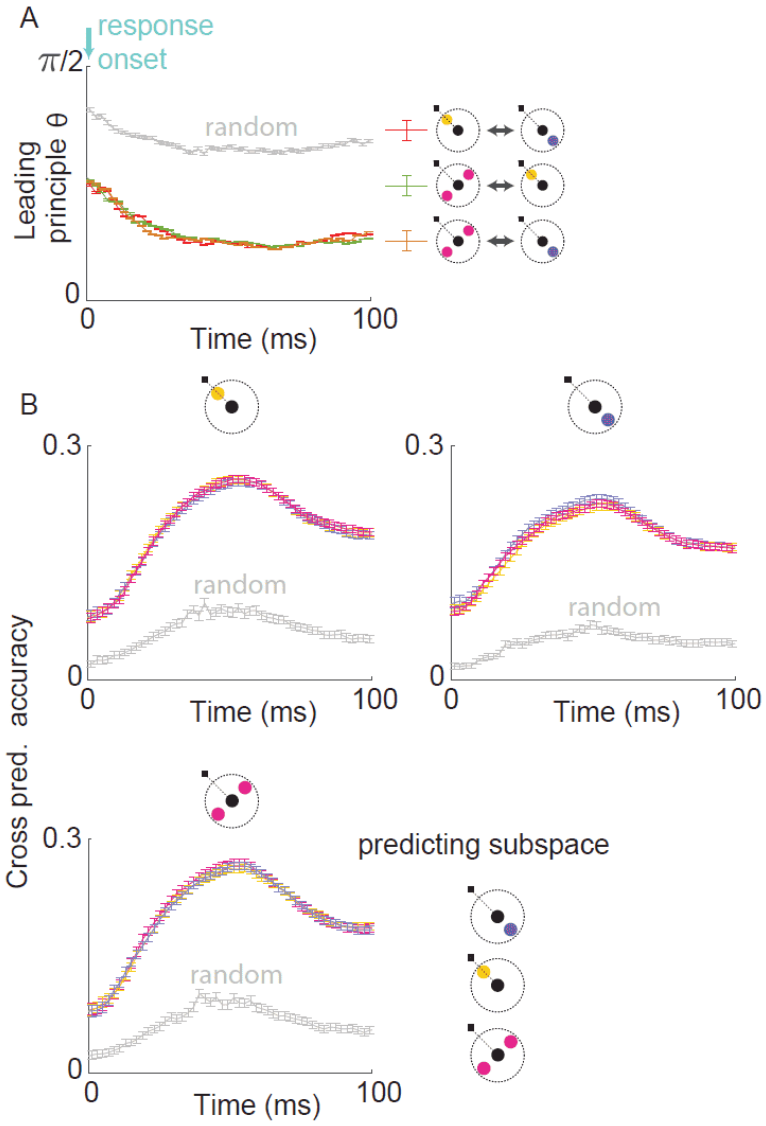

Figure S2. Comparing communication subspace across visual conditions, related to Figure 2

(**A**) The temporal evolution of leading principal angles between the communication subspaces identified from different types of flanked conditions during the corresponding visually responsive period (averaged across all sessions) and between random subspaces of comparable dimensions (grey; see Methods). (**B**) Cross-prediction analysis for input layer predicting superficial layer activity during a given flanked condition (shown at the top) and using subspaces identified for various conditions (as shown in the legend). Error bars indicate the 95% confidence interval for the mean.

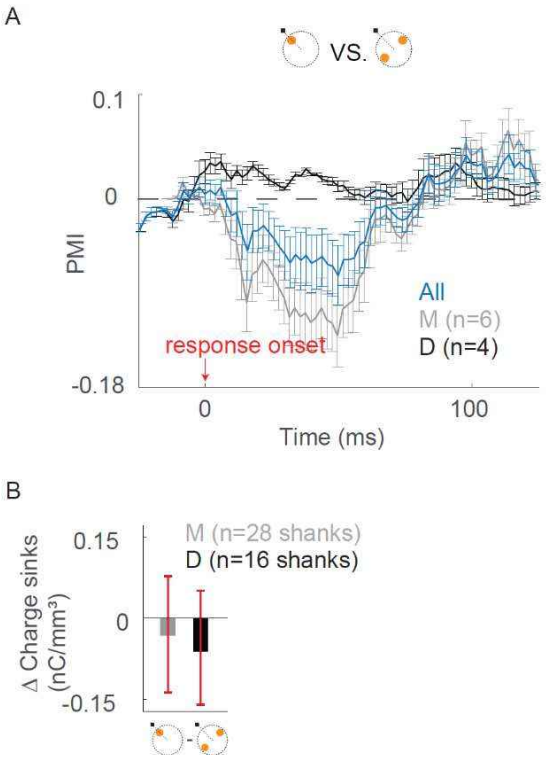

Figure S3. Comparing prediction accuracy across visual conditions, related to Figure 5, 7

(**A**) Same as Fig. 5B, comparing inter-laminar prediction accuracy under the radial-in condition to that under the tangential condition. Negative PMIs imply a degradation of prediction accuracy in the radial-in condition compared to the tangential condition. (**B**) The within-shank difference in the level of early charge sinks in the superficial layer, when compared between the radial-in and tangential conditions for all shanks from each monkey. Error bars indicate 95% confidence interval for the mean.

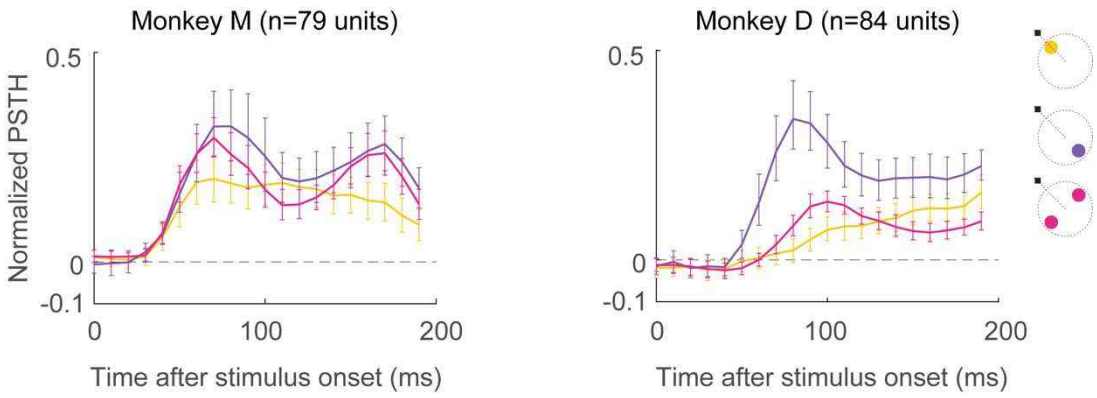

Figure S4. Comparing PSTH across flanker-only conditions, related to Figure 7

Normalized peri-stimulus time histograms (PSTHs; see Methods) for superficial layer units (separately for each monkey) under various flanker-only conditions. Error bars indicate the standard error across neurons. This analysis only included neurons that were visually responsive (see Methods) in the probe condition and exhibited significantly higher rates compared to all flanker-only conditions.

Neuron

Article

Spatial context non-uniformly modulates inter-laminar information flow in the primary visual cortex

Graphical abstract

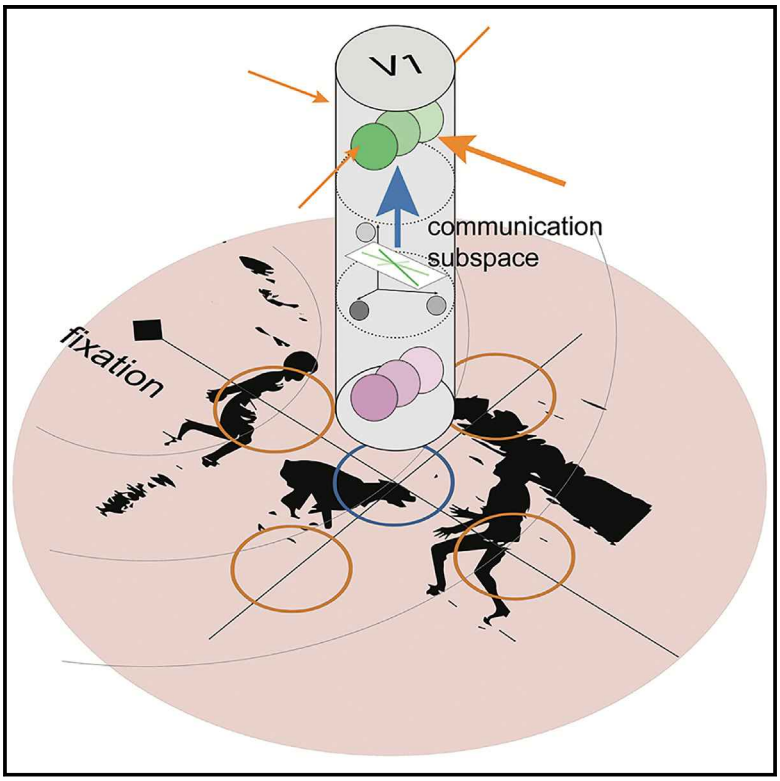

Authors

Xize Xu (徐锡泽), Mitchell P. Morton, Sachira Denagamage, Nyomi V. Hudson, Anirvan S. Nandy, Monika P. Jadi

Correspondence

xize.xu@yale.edu (X.X.), anirvan.nandy@yale.edu (A.S.N.), monika.jadi@yale.edu (M.P.J.)

In brief

Using simultaneous, layer-specific population recordings from primate primary visual area V1, Xu, Morton, et al. show that the spatial configuration of contextual stimuli differentially modulates inter-laminar information flow by changing its efficacy but not its structure. This non-uniform modulation is mediated by a location-dependent output-layer-targeting signal.

Highlights

- Inter-laminar information flow in V1 occurs along communication subspaces
- Structure of inter-laminar subspace is preserved across spatial locations of visual context
- Visual context degrades efficacy of information flow in a location-dependent manner
- The degradation is driven by a novel signal targeting the output layers

Xu et al., 2024, Neuron *112*, 1–15
December 18, 2024
https://doi.org/10.1016/j.neuron.2024.09.021

CellPress

Please cite this article in press as: Xu et al., Spatial context non-uniformly modulates inter-laminar information flow in the primary visual cortex, Neuron (2024), https://doi.org/10.1016/j.neuron.2024.09.021

Neuron

CellPress

Article

Spatial context non-uniformly modulates inter-laminar information flow in the primary visual cortex

Xize Xu (徐锡泽),[1,2,5,7,*] Mitchell P. Morton,[1,4,7] Sachira Denagamage,[1,4] Nyomi V. Hudson,[1] Anirvan S. Nandy,[1,3,4,5,6,8,*] and Monika P. Jadi[1,2,4,6,8,9,*]

[1]Department of Neuroscience, Yale University, New Haven, CT 06510, USA
[2]Department of Psychiatry, Yale University, New Haven, CT 06510, USA
[3]Department of Psychology, Yale University, New Haven, CT 06511, USA
[4]Interdepartmental Neuroscience Program, Yale University, New Haven, CT 06510, USA
[5]Kavli Institute for Neuroscience, Yale University, New Haven, CT 06510, USA
[6]Wu Tsai Institute, Yale University, New Haven, CT 06510, USA
[7]These authors contributed equally
[8]Senior author
[9]Lead contact
*Correspondence: xize.xu@yale.edu (X.X.), anirvan.nandy@yale.edu (A.S.N.), monika.jadi@yale.edu (M.P.J.)
https://doi.org/10.1016/j.neuron.2024.09.021

SUMMARY

Our visual experience is a result of the concerted activity of neuronal ensembles in the sensory hierarchy. Yet, how the spatial organization of objects influences this activity remains poorly understood. We investigate how inter-laminar information flow within the primary visual cortex (V1) is affected by visual stimuli in isolation or with flankers at spatial configurations that are known to cause non-uniform degradation of perception. By employing dimensionality reduction approaches to simultaneous, layer-specific population recordings, we establish that information propagation between cortical layers occurs along a structurally stable communication subspace. The spatial configuration of contextual stimuli differentially modulates inter-laminar communication efficacy, the balance of feedforward and effective feedback signaling, and contextual signaling in the superficial layers. Remarkably, these modulations mirror the spatially non-uniform aspects of perceptual degradation. Our results suggest a model of retinotopically non-uniform cortical connectivity in the output layers of V1 that influences information flow in the sensory hierarchy.

INTRODUCTION

Spatial vision is the ability to perceive visual objects within three-dimensional space, and its dysfunction is detrimental to our ability to interact with the visual world. Our visual experience relies on the coordinated activity of neuronal ensembles in the sensory hierarchy of the cortex.[1] Yet, how the spatial organization of objects influences information flow between neuronal populations in this hierarchy remains incompletely understood.

Visual perceptual performance varies as a function of visual field location, which is best at the center of gaze, degrades with eccentricity, and varies with radial angle. This asymmetry is paralleled by the asymmetric neural organization at multiple stages of the visual system (see Himmelberg et al.[2] for a review). Thus, a comprehensive characterization of the neural correlates of spatial vision requires empirical investigations without the assumption of spatial isotropy. Phenomena such as visual crowding—the inability to recognize objects among clutter—offer a powerful framework for such investigations. Visual crowding is thought to be the primary limitation on object perception in peripheral vision.[3] The crowding zone, which refers to the spatial extent over which flankers affect target identification, shows distinct spatially non-uniform characteristics, as identified by psychophysical studies.[4,5] This suggests non-uniform information processing along the visual hierarchy.

Understanding the neural basis of spatially non-uniform context integration requires identification of where the effects arise in the visual hierarchy and how information flow along this hierarchy is modulated by context. Neuronal spiking activity recorded from anesthetized monkeys indicates that visual crowding impairs feature representations as early as the primary visual cortex (area V1).[6,7] Human imaging studies show modulation of activity in V1[8,9] as well as in higher visual areas.[10–13] More importantly, inter-areal correlations are disrupted by spatial context integration,[14] suggesting modulation of information flow along the hierarchy. Despite extensive psychophysical

Please cite this article in press as: Xu et al., Spatial context non-uniformly modulates inter-laminar information flow in the primary visual cortex, Neuron (2024), https://doi.org/10.1016/j.neuron.2024.09.021

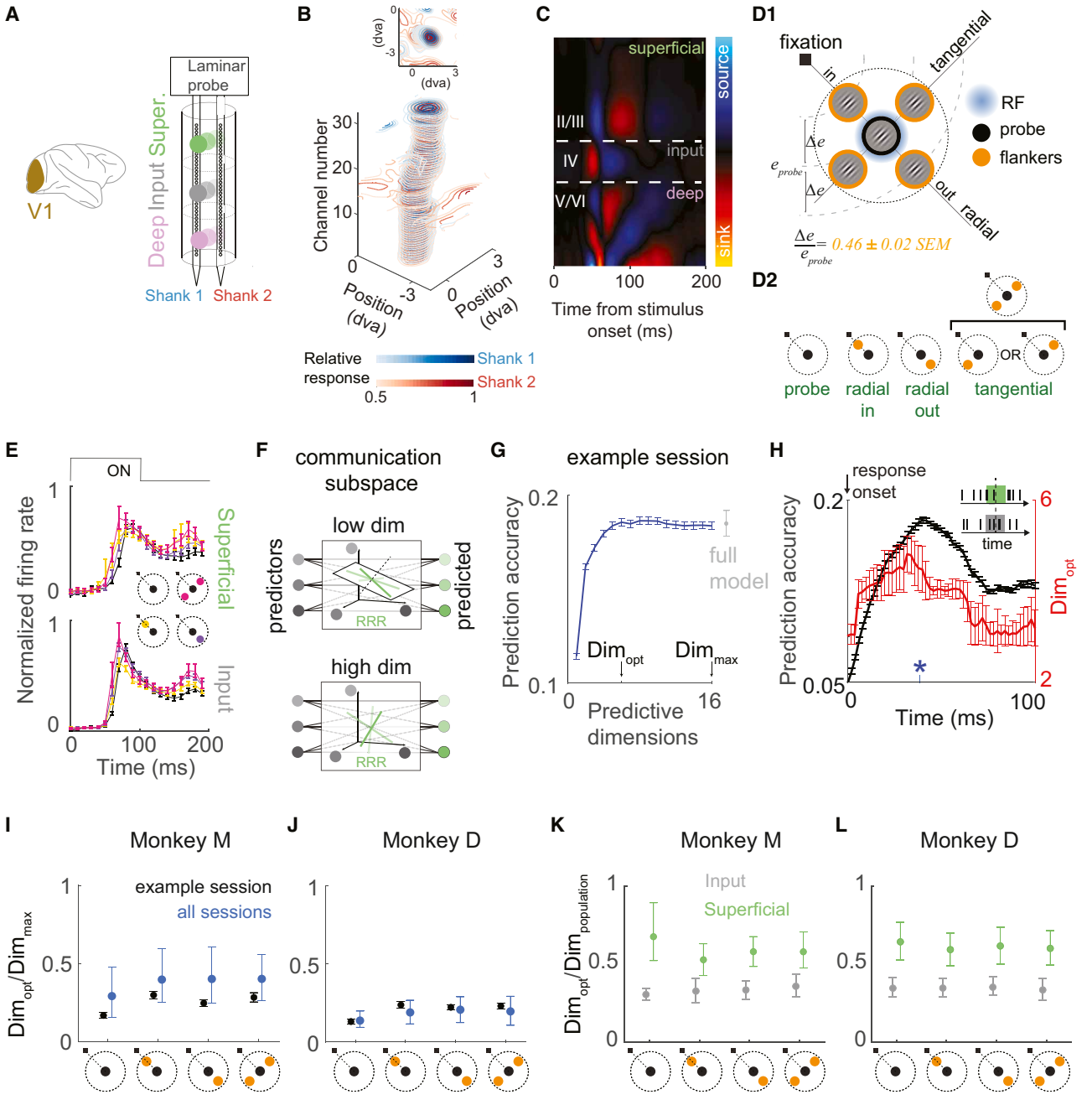

Figure 1. Characterization of inter-laminar information flow in V1

(A) Illustration of electrophysiological recordings with high-density 2-shank laminar probes.

(B) Example receptive field contours along the two shanks on the laminar probe. Top: vertical view. Dva, degrees of visual angle.

(C) Example current source density (CSD).

(D) Visual stimulation protocol. (D1) Schematic of visual stimulation for the passive fixation task. e_{probe}, parafoveal eccentricity of probe presentation; Δe, center-to-center distance between the probe and flankers. D2: summary of stimulus conditions. In subsequent results, "tangential" refers to one of the two tangential locations shown in (D1), indicated by a common symbol shown here.

(E) Normalized peri-stimulus time histograms (PSTHs; see STAR Methods) of recorded units in the superficial (top) and input (bottom) layers under various visual conditions. Top: visual stimulation protocol.

(F) Illustration of a low-dimensional communication subspace between cortical layers. The activity of each neuron in the superficial layer (illustrated by green circles) is predicted as a linear combination of the population activity in the input layer (illustrated by gray circles), which is equivalent to its projection onto a certain axis (shown as a green line/superficial neuron) in the activity space of input layer population. The axes for prediction either span the entire input layer activity space (bottom row) or are constrained in a low-dimensional subspace (top row), referred to as "communication subspace." The activity along the subspace is sufficient

(legend continued on next page)

Please cite this article in press as: Xu et al., Spatial context non-uniformly modulates inter-laminar information flow in the primary visual cortex, Neuron (2024), https://doi.org/10.1016/j.neuron.2024.09.021

studies and computational modeling,[15–26] the neural basis of the perceptual asymmetry of spatial context integration remains incompletely understood. Understanding how the organization of objects influences information flow along the visual hierarchy is thus critical to our understanding of spatial vision.

Information flow in the visual hierarchy is both inter-areal as well as inter-laminar because the laminar organization of neuronal populations,[1,27] with their stereotypical patterns of intra- and inter-areal projections,[28–30] is a canonical motif of cortical organization. The neurophysiological aspects of these lamina-specific circuits have been extensively characterized in the context of surround modulation, namely the change in neuronal activity in response to visual stimulation of classical and extra-classical receptive fields.[31–40] Geniculate feedforward connections, intra-V1 horizontal connections, and inter-areal feedback connections to V1 have all been shown to contribute to surround modulation in V1 at different spatiotemporal scales (see Angelucci et al.[41] for a review). However, a prevailing assumption in most of these studies has been the spatially uniform nature of the surrounding context. In V1, receptive field sizes and spatial frequency preference vary with eccentricity. In addition, the distribution of cortical tissue devoted to visual space varies with polar angle (see Himmelberg et al.[2] for a review). Such asymmetric neural organization suggests the possibility of non-uniform processing within V1 acting as a substrate for the non-uniform psychophysical effects observed in phenomena such as visual crowding.[4,5] In this study, we investigated how the spatial configuration of visual stimuli modulates inter-laminar information flow in V1 by analyzing functional communication between neuronal populations. We specifically focused on communication between two populations: input-layer neurons that receive geniculate inputs and project locally to superficial layers and superficial-layer neurons that project to higher-order visual areas as well as to local deep layers.

We performed laminar recordings from awake macaque V1 with visual stimuli presented either in isolation or with a flanking stimulus at various locations known to cause non-uniform perceptual impairment in peripheral vision. We characterized information flow from the input to the superficial layer, which is a key pathway in the feedforward propagation of sensory information. Using dimensionality reduction techniques to identify communication subspaces,[42] we found that the information flow from the input to superficial layers occurs along a structurally stable communication subspace under different visual conditions. Flanking stimuli modulated the efficacy of inter-laminar information flow in a location-specific manner by changing both its efficacy and the balance of feedforward and effective feedback signaling. Moreover, our analysis revealed a non-uniform contextual signal in the superficial layers triggered by flankers.

RESULTS

To characterize inter-laminar information flow in V1, we simultaneously recorded the spiking activity in the input layer (unit count: 27.9 ± 3.2 SEM) and in the primary downstream target, the superficial layer (unit count: 21.9 ± 5.0 SEM) in two awake macaque monkeys (Figure 1A; 14 sessions from monkey M, 8 sessions from monkey D). The recorded neurons consisted of well-isolated single units and multi-unit clusters, which had retinotopically aligned receptive fields (Figure 1B), implying a high probability of direct interactions. Laminar identity was established using current source density (CSD) analysis[43] (Figure 1C). Monkeys were trained to fixate on the center of the screen and passively view a probe stimulus (100 ms stimulus duration, 200–250 ms inter-stimulus interval) at the receptive field of the recording site, either in isolation (probe condition) or with a flanking stimulus (flanked condition) at one of four spatial locations relative to the probe (Figure 1D1), based on which three flanked conditions were defined (Figure 1D2). In both the radial-in and radial-out flanked conditions, the flanker was positioned on the radial axis connecting the probe and the fixation point, either between the probe and the fixation point or past the probe, respectively. In the tangential flanked condition, the flanker was positioned on either side of the probe along the axis orthogonal to the radial axis.

Given the rich temporal dynamics of the V1 units (Figure 1E), we hypothesized that the dynamics of inter-laminar information flow were also time variant and therefore conducted analysis on a moment-by-moment basis. Neuronal activity was measured as spike counts in 50-ms bins during the appropriate stimulus processing range of V1 neurons, which we refer to as the responsive period (see STAR Methods). Leveraging trial-to-trial response variabilities to repeated stimuli, we characterized inter-laminar information flow by assessing the extent to which variability of mean-subtracted neuronal activity in the superficial layer could be predicted by the correponding activity in the input layer.

Information propagation between cortical layers occurs along a communication subspace

Information propagation across cortical areas has been shown to occur along a ''communication subspace.''[42,44] That is, only a low-dimensional subspace of the upstream area neural

to capture the inter-laminar communication. Any perturbation of input layer activity orthogonal to this subspace (black dotted line) will not change the predicted population activity of the superficial layer.

(G) Predicting superficial layer population activity (16 units) from input layer population activity (34 units) using reduced-rank regression (RRR) with varying number of predictive dimensions (blue curve) or a full regression model (gray circle) for an example session. Error bars indicate the standard error across multiple draws of trials and the corresponding cross-validation folds. For all prediction analyses presented, the RRR model performs as well as the full model (Figure S1).

(H) Temporal evolution of the optimal dimensionality (red) and its prediction accuracy (black) computed by RRR for the example session used in (G) (see STAR Methods). Blue asterisk: time around which the window analyzed in (G) was centered. Error bars indicate the standard error across multiple draws of trials.

(I) The ratio between Dim_{opt} and Dim_{max} under various visual conditions for an example session (black) or across all sessions (blue) from monkey M. Error bars indicate the 95% confidence interval for the mean ratio averaged across the responsive period.

(J) Same as (I) for results from monkey D.

(K and L) The ratio between Dim_{opt} and the dimensionality of the population activity ($Dim_{population}$) in the superficial layer (green) or the input layer (gray) across all sessions from monkey M (K) and monkey D (L).

Please cite this article in press as: Xu et al., Spatial context non-uniformly modulates inter-laminar information flow in the primary visual cortex, Neuron (2024), https://doi.org/10.1016/j.neuron.2024.09.021

population activity space is informative of the downstream area activity (illustrated in Figure 1F). It is important to note that a subspace of neural activity is different from a subnetwork. Whereas a subnetwork comprises a subset of neurons, a subspace of neural activity corresponds to a subset of population activity patterns, which may involve non-trivial activities of all neurons within the network. The dimensionality of the communication subspace from V1 to V2 has been shown to be consistently lower than the dimensionality of the target population activity.[42] Based on these results, we hypothesized that inter-laminar information propagation also occurs along subspaces and that this is not simply due to the low dimensionality of either the source or target population activity. Specifically, we tested whether the inter-laminar interaction between the input and superficial layers in V1 was limited to a subspace of the neural activity space of the input layer by employing reduced-rank regression (RRR),[45,46] a multivariate linear regression model with a constraint enforcing a small number of latent predictive factors (see STAR Methods). For an example session under the radial-in condition (Figure 1G), only 6 dimensions (Dim_{opt}) were needed to achieve prediction performance that is as good as a full linear regression model (ridge regression; see STAR Methods), which was lower than the maximal possible prediction dimensionality (Dim_{max}) determined by the minimum between the number of units in the source and target populations. Moment-by-moment analysis for this session revealed that this result held throughout the responsive period of V1 (Figure 1H). Furthermore, this result was consistent across visual conditions, sessions, and monkeys (Figures 1I and 1J), implying that inter-laminar information flow in V1 shared the low-dimensional property exhibited by inter-areal information flow. We next tested whether this signature of inter-laminar information flow was due to a low complexity of population activity either in the source population (the input layer) or in the target population (the superficial layer). We used factor analysis to assess the complexity of population activity in either layer (see STAR Methods). The analysis revealed that the dimensionality of activity in either population was consistently higher than the number of predictive dimensions (Figures 1K and 1L). Thus, the observed low dimensionality of inter-laminar interactions cannot be explained by the complexity of population activity in the input or superficial layer but rather reflected the nature of inter-laminar information flow.

We next investigated the impact of stimulus configuration on the structure and efficacy of the communication subspace underlying inter-laminar information flow. Potentially, inter-laminar information flow can be modulated by the spatial configuration of stimuli in two ways that are not mutually exclusive: (1) the structure of the communication subspace is changed, which would be observable as the degraded prediction performance under a given visual condition when the corresponding input layer data were projected onto the communication subspace identified from a different visual condition, and (2) the efficacy of the communication subspace is changed, which would be observable as differential prediction accuracies across visual conditions. To test these possibilities, we performed RRR to characterize the communication subspace and computed its prediction accuracy on a moment-by-moment basis for each visual condition.

Structure of communication subspace is preserved across flanker locations

Testing whether the structure of inter-laminar information flow is changed requires characterizing the difference between communication subspaces identified from different visual conditions. To ensure a fair comparison across visual conditions, populations in the input and the superficial layers used to conduct prediction analysis were fixed and the sample sizes were matched across visual conditions. These protocols prevented the number of analyzed neurons and trials from differentially affecting the analysis result.[42,47] We first investigated the relative alignment between the subspaces across different visual conditions by using the measure of principal angle (Figure 2A), which computes angles between sequentially aligned pairs of basis vectors, each within one of the subspaces. The smallest principal angle is referred to as the "leading principal angle." Small principal angles indicate a similar orientation of subspaces and imply that much of the structure of the communication subspace is preserved across visual conditions. By performing RRR using data from a sliding time window of 50 ms, we identified the communication subspace for each visual condition and computed the principal angles between all possible pairs. To assess whether the obtained principal angles were significantly small, we compared them with the principal angles between randomly generated subspaces while preserving the dimensionalities of the computed communication subspaces (see STAR Methods). The leading principal angles between the communication subspaces identified from the probe and any of the flanked conditions were consistently below chance level (Figure 2B). The result held for all other visual condition comparisons (Figure S2A). Because the regression could be prone to overfitting, we calculated within-condition principal angles (see STAR Methods), which provided an estimate of the minimal principal angle that could be realistically obtained, and compared these with the cross-condition principal angles. The levels of the within-condition principal angles (Figure 2B, black curves) were consistently comparable with the cross-condition principal angles (Figure 2B, colored curves), providing further evidence for similar communication subspaces across visual conditions.

To characterize the influence of the relative alignment between communication subspaces across visual conditions on the strength of interaction, we performed cross-prediction analysis using the projection of the data from the source (input layer) population for a given visual condition onto the communication subspaces identified across different visual conditions using a multivariate linear regression model (Figure 2A). Throughout the responsive period, the projected data gave similar prediction performance across all visual conditions from which the communication subspace was identified, and these were significantly above what would be expected by chance (Figures 2C and S2B). Thus, the extent to which the input layer activity was informative of the superficial layer activity was similar among the communication subspaces identified from different visual conditions. Taken together, these two results indicate that the structure of inter-laminar information flow in a linear framework is preserved across different spatial configurations of visual stimuli.

Please cite this article in press as: Xu et al., Spatial context non-uniformly modulates inter-laminar information flow in the primary visual cortex, Neuron (2024), https://doi.org/10.1016/j.neuron.2024.09.021

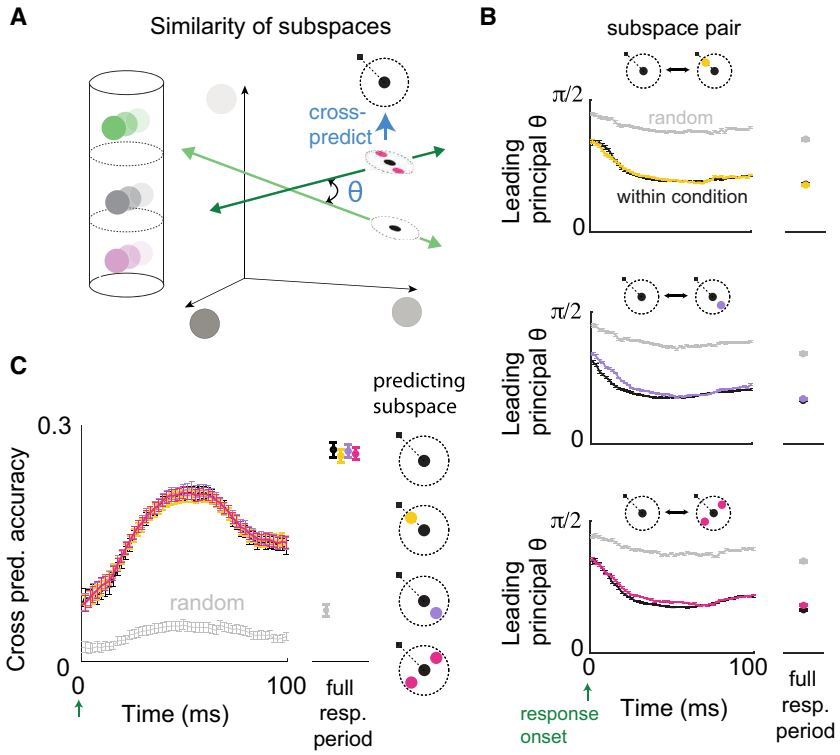

Figure 2. Similarity of inter-laminar communication subspace across visual conditions

(A) Illustration of principal angle measure and cross-prediction analysis for comparing two subspaces. Each axis represents the activity of an input layer neuron used to predict superficial layer activity. Green lines represent input-to-superficial communication subspaces identified from two visual conditions.

(B) Temporal evolution of leading principal angle between the communication subspaces identified for all visual conditions (averaged across all sessions). Gray: chance level alignment between subspaces (see STAR Methods). Black: within-condition leading principal angles (see STAR Methods).

(C) Cross-prediction analysis for neural activity in probe condition, using projection onto subspaces identified from one of the four visual conditions. Error bars indicate the 95% confidence interval for the mean. Difference between conditions was inferred using estimation statistics framework (see STAR Methods). Black: within-condition prediction. Yellow, purple, magenta: across-condition prediction. Gray: chance level (see STAR Methods). Also shown in (B) and (C) on the right, are the results calculated using the activities from the full responsive period (a 100-ms time bin starting from response onset). For other visual condition comparisons, see Figure S2.

Efficacy of inter-laminar information flow is degraded in the presence of flankers

We next investigated how the spatial configuration of visual stimuli influenced the efficacy of inter-laminar information flow, as characterized by inter-laminar prediction accuracies. We started by comparing the probe condition against the flanked condition (data pooled across all possible locations of flankers). Temporal dynamics of prediction accuracy were obtained as the predictive performance at optimal dimensionality under RRR employed on a moment-by-moment basis. As shown in Figure 3A for a representative session, under either visual condition, the inter-laminar prediction accuracy initially increased and then decayed during the responsive period. To quantify the difference in the prediction accuracies across visual conditions for each session, we introduced a prediction modulation index (PMI; see STAR Methods). For the example session in Figure 3A, the corresponding PMI was significantly negative during the entire responsive period (Figure 3B), indicating that the prediction accuracy was weakened in the presence of flankers. Despite an inter-subject difference in the initial temporal profile of the PMI, the degradation of inter-laminar prediction accuracy was consistent across sessions for both monkeys (Figure 3C), implying a weaker efficacy of information flow.

Degradation in the efficacy of inter-laminar information flow is mediated by layer-specific signals

We tested two non-mutually exclusive hypotheses about how the presence of flankers might weaken inter-laminar prediction accuracy (schematized in Figure 4A): hypothesis *I*, the flanked condition causes the activation of a novel signal targeting the input layer, or hypothesis *II*, the flanked condition causes the activation of a novel signal targeting the superficial layer. To disentangle these possibilities, we investigated the temporal relationship between layer-specific activity and the degradation in prediction accuracy. On a moment-by-moment basis, we performed the RRR analysis using data from the two layers at different temporal delays (Figure 4B1) and thereby determined the temporal evolution of PMI as a function of delay. It is important to note here that delays associated with both inter-laminar signal conduction and intra-laminar recurrent processing would factor into this temporal analysis. If hypothesis *I* were true, the timing of the degradation and hence the temporal profile of the PMI would be independent of the inter-laminar delay being considered (Figure 4B2, left). In contrast, if hypothesis *II* were true, i.e., if the novel signal targeted the superficial layer, the timing of the degradation would depend on the offset of the superficial layer data analyzed and therefore shift earlier with increasing temporal delay (Figure 4B2, right). Based on these observations, we estimated the time of degradation of prediction accuracy by determining the decrease onset time (DOT) of PMI followed by persistently negative components and related it with the temporal delay being considered. As shown in Figure 4C, for two representative sessions from the two monkeys, the DOTs of PMI became earlier with increasing temporal delay. Across sessions, the correlation between the DOTs of PMI and the temporal delay was consistently negative and close to −1 for both monkeys (Figure 4D), indicating a dependence as predicted by hypothesis *II*. This result suggests that the degradation of prediction accuracy in the presence of flankers was mainly due to a novel signal targeting the superficial layer.

Please cite this article in press as: Xu et al., Spatial context non-uniformly modulates inter-laminar information flow in the primary visual cortex, Neuron (2024), https://doi.org/10.1016/j.neuron.2024.09.021

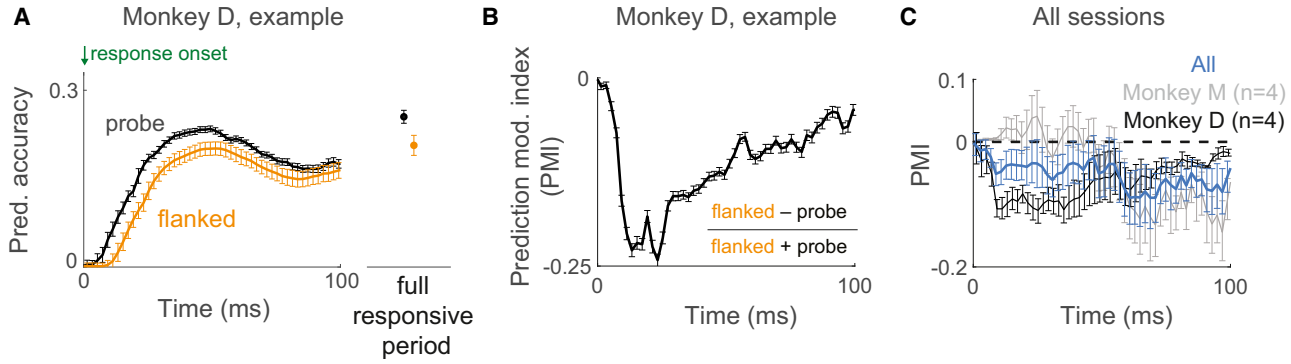

Figure 3. Efficacy of inter-laminar information flow across visual conditions

(A) The temporal evolution of input-superficial prediction accuracies under the probe (black) and the flanked conditions (orange) for an example session from monkey D. Error bars indicate the standard error across multiple draws of trials. Results calculated using the activities from the full responsive period (a 100-ms time bin starting from response onset) are shown on the right.

(B) The temporal evolution of the prediction modulation index (PMI; see STAR Methods). Error bars indicate 95% confidence interval for the mean. Difference between conditions was inferred using estimation statistics framework (see STAR Methods).

(C) Same as (B) for results across sessions from each monkey (gray: monkey M; black: monkey D) or across the two monkeys (blue).

Degradation in the efficacy of inter-laminar information flow is sensitive to flanker location

Two robust characteristics of visual crowding identified by psychophysical studies are the asymmetry and anisotropy of crowding zones, the spatial extent over which flankers affect target recognition. First, a flanker more eccentric than the target stimulus (radial-out condition) has a greater perceptual crowding effect than an equally spaced inward (less eccentric) flanker (radial-in condition).[5] Second, the crowding zone is elongated along the radial axis so that radially positioned flankers produce a stronger crowding effect than tangential ones (tangential condition).[4] We reasoned that these perceptual asymmetries could be due to asymmetries in inter-laminar prediction accuracy in V1. To investigate this possibility, we first compared the inter-laminar prediction accuracies between the probe and the different flanked conditions. The degradation due to the presence of flankers was consistent across all flanker locations, yet the extent of degradation varied (Figure 5A). To further characterize this, we compared the prediction accuracy under the flanked condition associated with the strongest perceptual crowding effects (the radial-out condition) against the other flanked conditions (the radial-in and the tangential conditions). To ensure a fair comparison across visual conditions, we additionally aligned the temporal prediction accuracy data to account for different response latencies across conditions. We found that the prediction accuracy degraded in the radial-out condition compared with the radial-in (Figure 5B) and the tangential conditions (Figure 5E) over most of the responsive period. Despite an inter-subject variability in the temporal profile of the prediction degradation caused by the radial-out condition relative to the radial-in condition, such degradation was consistent across all sessions for both monkeys. Moreover, applying the inter-laminar temporal delay analysis as above, we found that the prediction degradation with radial-out flankers emerged earlier with increasing temporal delay (Figures 5C, 5D, 5F, and 5G), consistent with a hypothesis of a superficial-layer-targeting signal that is dominant in the radial-out condition.

Bi-directional information flow depends on flanker location

Prediction analysis using RRR was motivated by the anatomical model of lamina-specific circuits, and thus assumed a direction of information flow from the input layer (source) to the superficial layer (target). We next sought to understand how information flow in either direction was affected by the spatial configuration of visual stimuli. We investigated this by employing canonical correlation analysis (CCA; see STAR Methods) to relate the population activities in the input and superficial layers at different time delays on a moment-by-moment basis (Figure 6A), which we refer to as population correlation. Positive or negative delays between the population activities from each layer allowed a bi-directional analysis of inter-laminar information flow. This methodology has been previously applied[48] to study the structure of interactions between cortical areas, finding that the balance was feedforward dominated shortly following stimulus onset and then became feedback dominated. For each visual condition, we calculated the population correlation between activities in the two layers as a function of time and time delay between layers (Figure 6B). To quantify the strength of interaction in each direction, we computed a "feedforward correlation" by taking the mean over correlations for all positive delays (input layer leading superficial layer; STAR Methods) and similarly for "effective feedback correlation" for negative delays (superficial layer leading input layer). For a representative example session under the probe condition (Figure 6B), whereas the feedforward correlation increased steadily from the time of response onset and then gradually decayed, the effective feedback correlation was consistently lower than the feedforward correlation, indicating a feedforward-dominant interaction throughout the responsive period.

We quantified the degree to which the inter-laminar interaction was dominant in either direction of signaling by defining a direction dominance index (DDI; see STAR Methods), where a positive DDI indicates the dominance of feedforward signaling and a negative DDI indicates the dominance of effective feedback

Please cite this article in press as: Xu et al., Spatial context non-uniformly modulates inter-laminar information flow in the primary visual cortex, Neuron (2024), https://doi.org/10.1016/j.neuron.2024.09.021

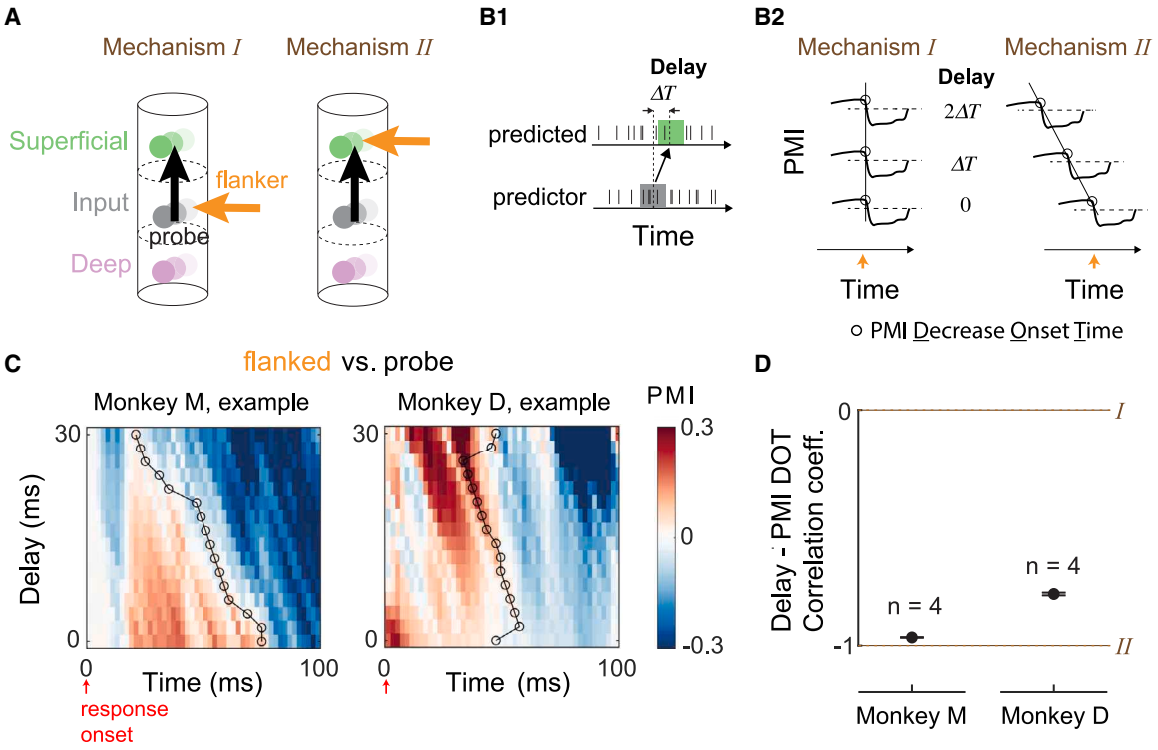

Figure 4. Mechanism of degradation in the efficacy of inter-laminar information flow

(A) Illustration of two possible mechanisms: flanker causes the activation of a novel signal (orange arrow) targeting the input (mechanism *I*) or superficial layer (mechanism *II*).

(B) Delay analysis protocol and potential outcomes. (B1) RRR was conducted on a moment-by-moment basis using input (at t) and superficial layer activity at non-negative temporal delays (t + delay). (B2) Illustration of delay-induced changes in PMI dynamics, as implied by mechanisms *I* and *II*. Orange arrows: the time when the hypothetical novel signal caused by the flanker arrived at the input (mechanism *I*) or superficial (mechanism *II*) layer.

(C) Temporal evolution of inter-laminar PMI under the probe and the flanked conditions at various inter-laminar temporal delays for example sessions from two monkeys. PMIs that are neither significantly positive nor negative are colored in white (the corresponding 95% confidence interval for the mean PMI includes zero). Black circles: decrease onset times (DOTs) of PMI at each level of delay.

(D) Correlation between inter-laminar temporal delay and the DOTs of PMI across all sessions from each monkey. Error bars indicate 95% confidence interval for the mean.

signaling. The larger the magnitude of DDI, the more biased the interaction was toward one direction. To investigate the impact of stimulus configuration on the balance of the inter-laminar feedforward and effective feedback signaling, we determined the temporal evolution of DDI separately for each visual condition. In the same example session as above, under both the probe and the flanked conditions, the DDI increased steadily and gradually decayed, remaining significantly positive throughout the responsive period (black and orange curves in Figure 6C). Thus, the interaction became more feedforward dominated in the early phase of the responsive period and then returned to a more balanced interaction. Remarkably, the DDI was less positive under the flanked condition, indicating that the balance was shifted away from the feedforward direction in the presence of a flanker. This result was robust across sessions for each monkey (Figure 6D). Furthermore, similar analysis revealed that this modulation was flanker-position dependent. In the visual condition associated with the strongest perceptual crowding effect (the radial-out condition), the balance was shifted away from the feedforward direction compared with both the radial-in and tangential conditions (Figure 6E). Thus, the non-uniformity in stimuli-specific prediction accuracy analysis (Figure 5) was mirrored by the modulation of the interplay between inter-laminar feedforward and effective feedback signaling. Interestingly, the inter-subject difference in the temporal profile of the difference in DDI across visual conditions (probe vs. flanked and radial-out vs. radial-in) was similar to that in PMI obtained from the prediction analysis, such that both the shift of balance (Figures 6D and 6E) and the degradation of inter-laminar prediction accuracy (Figures 3C and 5B) emerged later during the responsive period for monkey M compared with monkey D.

Strength of contextual drive to the superficial layer is location specific

To test the hypothesis that our observations are a reflection of a signal that targets the superficial layers and is sensitive to flanker locations, we next examined the relative strength of this signal evoked by flanker-only stimuli at different locations. For each flanker-only condition, we determined the level of charge sinks by integrating over time the early current sinks in the superficial

Please cite this article in press as: Xu et al., Spatial context non-uniformly modulates inter-laminar information flow in the primary visual cortex, Neuron (2024), https://doi.org/10.1016/j.neuron.2024.09.021

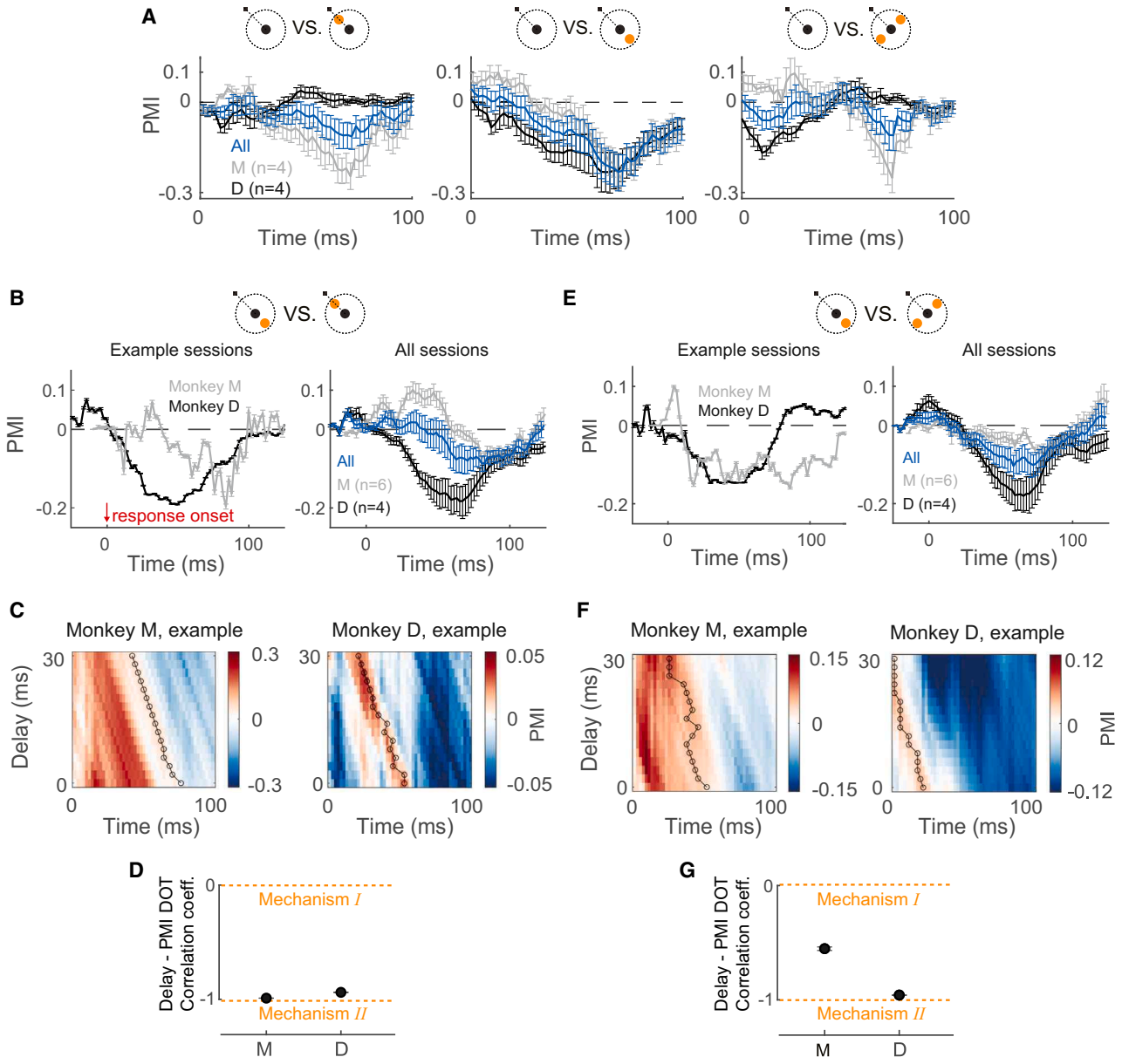

Figure 5. Efficacy of inter-laminar information flow as a function of flanker location

(A) Same as Figure 3C, comparing the prediction accuracy under the probe condition against each flanked condition (from left to right: radial-in, radial-out, and tangential).

(B) Temporal evolution of RRR PMI comparing the radial-out and radial-in conditions for example sessions (left) or across all sessions (right), from monkeys M (gray), D (black), or both (blue). Negative PMIs imply a degradation of prediction accuracy in the radial-out condition compared with the radial-in condition. Error bars indicate 95% confidence interval for the mean.

(C) Example sessions showing temporal evolution of PMI as a function of inter-laminar delay (see Figures 4B and 4C) for the visual conditions compared in (B).

(D) Correlation between inter-laminar temporal delay and the DOTs of PMI across all sessions from each monkey.

(E–G) Same as (B)–(D), comparing the modulation of inter-laminar prediction accuracy under the radial-out and tangential conditions. For comparison between the radial-in and tangential conditions, see Figure S3A.

layer obtained from the CSD response (Figures 7A–7C; see STAR Methods), which reflected the subthreshold integrated input to local neurons.[43,49] For both monkeys, flankers at the radial-out position evoked stronger charge sinks compared with flankers at the radial-in or tangential positions (Figure 7D), thus providing direct evidence for a location-dependent superficial-layer-targeting signal that differentially impacts the representation of the probe. Similar results were obtained from spike-based analysis, such that the radial-out flanker-only condition evoked higher levels of activity (Figure 7E). This provides

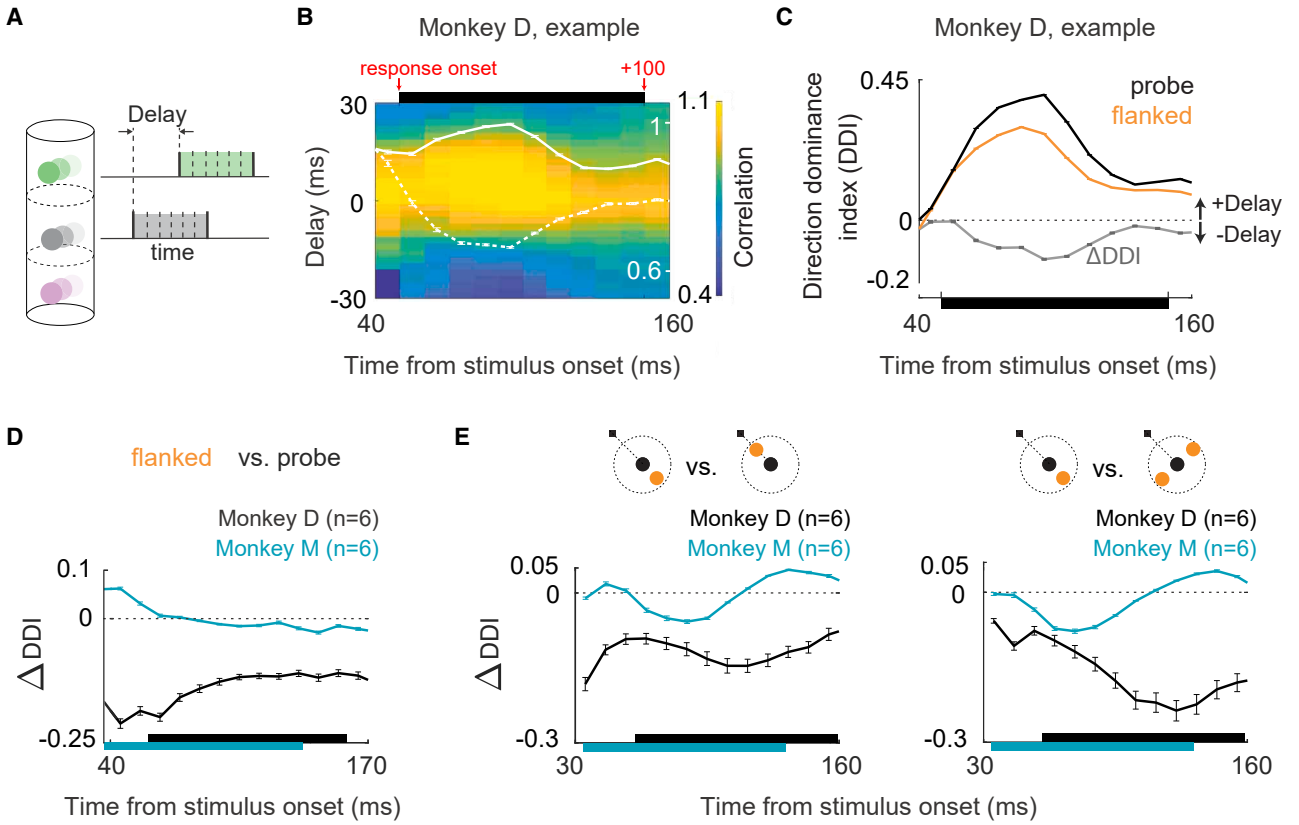

Figure 6. Balance of bi-directional inter-laminar information flow and its modulation in the presence of flankers

(A) Canonical correlation analysis (CCA) protocol for estimating temporal evolution of population correlations.

(B) CCA-based population correlation as a function of time and inter-laminar delay during the visually responsive period. Overlaid solid and dotted traces (white) show the average correlation at positive and negative sides of delay, respectively. Error bars indicate the standard error across multiple draws of trials.

(C) Temporal evolution of the direction dominance index (DDI; see STAR Methods) under the probe and the flanked conditions for an example session. Also shown is the difference between DDIs across conditions (gray trace).

(D) Temporal evolution of the difference in the DDIs under the probe and the flanked conditions for all sessions from each monkey.

(E and F) Same as (D) for results comparing DDIs separately under different types of flanked stimuli (E: radial-out vs. radial-in; F: radial-out vs. tangential). In (B)–(E), corresponding visually responsive periods estimated as 100 ms from the response onsets are marked by horizontal bars. In (C)–(E), error bars indicate 95% confidence interval for the mean.

further evidence for stronger inputs to the superficial layer as a potential mechanism underlying the observed non-uniformity. These results support a hypothesis that the observed degradation in the efficacy of inter-laminar information flow and the shift in feedforward-feedback signaling balance are mediated by retinotopically non-uniform cortical connectivity in the output layers of V1 (Figure 7F).

DISCUSSION

We leveraged simultaneous laminar recordings to understand how the spatial configuration of visual contextual stimuli affected inter-laminar information flow in V1 of the macaque. V1 activity has been extensively studied as a locus of surround modulation[34–41] and, more recently, has been implicated as a bottleneck impairing perception under visual crowding.[6–9,13] We established that information flow across V1 laminar populations is constrained to a communication subspace. We demonstrated that the efficacy of inter-laminar information flow was degraded in the presence of contextual stimuli. This degradation was not accompanied by changes in the structure of the subspace of neural activity along which the information flow occurs. Furthermore, we found that the balance between the inter-laminar feedforward and effective feedback signaling was non-uniformly shifted in the presence of flankers. Strikingly, these modulations matched the spatially non-uniform aspects of perceptual degradation, such that a greater degree of modulation was associated with a flanker at the visual location that is known to exert a stronger perceptual impairment. Finally, we found that the spatial configuration of contextual stimuli differentially modulated contextual signaling in the superficial layers. Our results suggest a model in which degraded information flow along the sensory hierarchy, mediated by retinotopically non-uniform connectivity in the output layers of V1, underlies the perceptual impairments in spatial vision.

Contextual modulation of information flow

Despite decades of research at the level of perception, investigation into the neural mechanisms of non-uniform perceptual

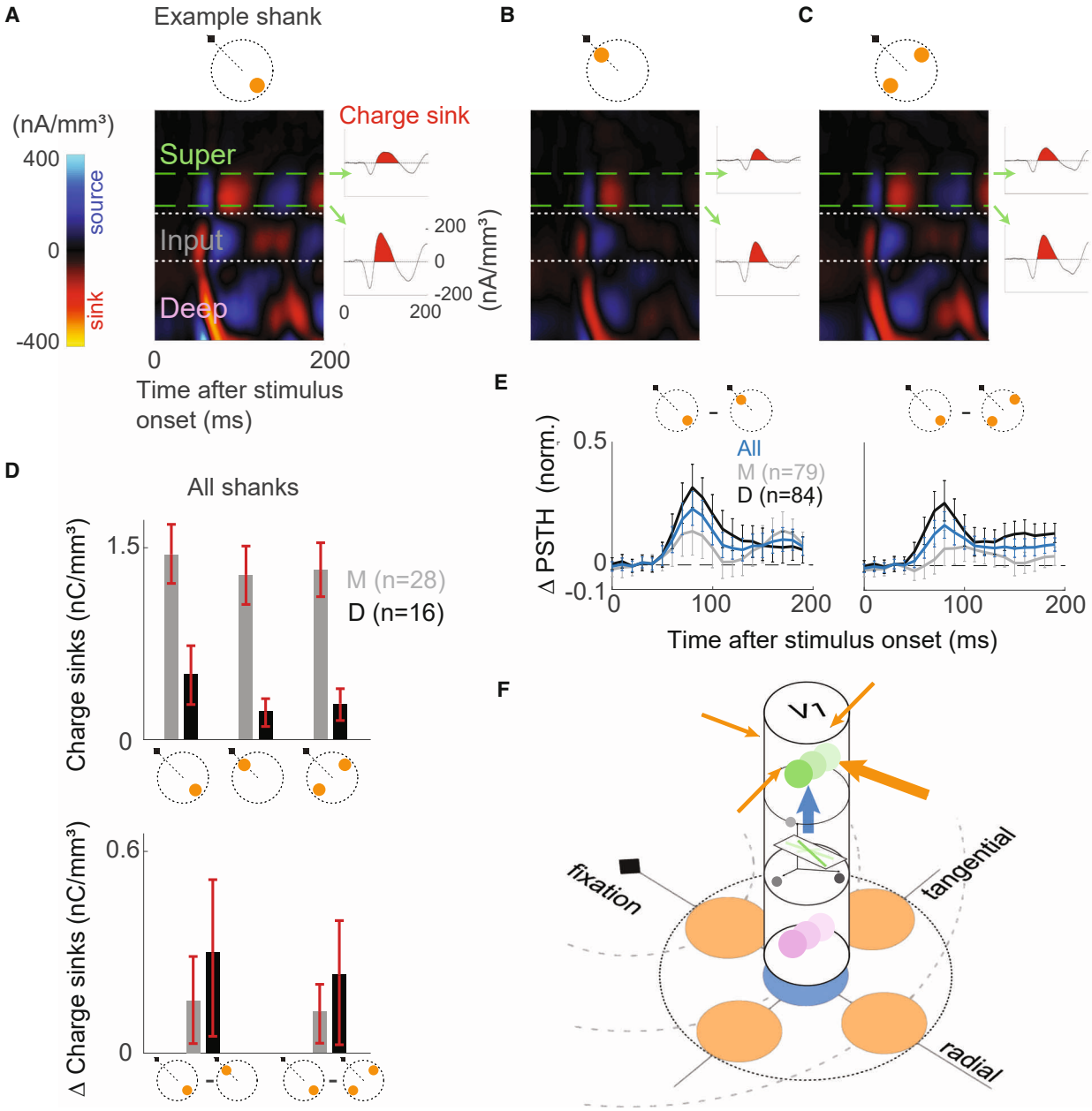

Figure 7. Retinotopically non-uniform context integration in V1

(A) An example of estimated CSD across V1 layers evoked by flanker presented by itself at the radial-out position. Dotted white lines indicate laminar boundaries (see STAR Methods). Traces on the right show temporal evolution of the CSD signal at two recording sites on the example shank, marked by the green dashed lines. Red shade: the earliest charge sink.

(B and C) Same as (A), with the flanker presented at the radial-in and tangential positions, respectively.

(D) Top: level of early charge sinks under different flanker-only conditions across all sessions from each monkey. Bottom: within-shank difference in the level of early charge sinks between the radial-out and radial-in conditions (left) and the radial-out and tangential conditions (right). Error bars indicate 95% confidence interval for the mean. Difference between conditions was inferred using estimation statistics framework (see STAR Methods). For comparison between the radial-in and tangential conditions, see Figure S3B.

(E) Difference in the normalized PSTH of superficial layer units between the radial-out flanker-only and radial-in flanker-only conditions (left) and the radial-out flanker-only and tangential flanker-only conditions (right). Error bars indicate 95% confidence interval for the mean difference (see STAR Methods). Normalized PSTHs for each condition are shown in Figure S4.

(F) Summary of findings.

Please cite this article in press as: Xu et al., Spatial context non-uniformly modulates inter-laminar information flow in the primary visual cortex, Neuron (2024), https://doi.org/10.1016/j.neuron.2024.09.021

degradation in peripheral vision has received limited attention. The most studied hypothesis is that the perceptual degradation is mediated by changes in the tuning properties of neurons and therefore leads to information loss about target features as early as the input and superficial layers of V1.[6,7,50] The observed impairment of information encoding has been shown to be greater with flankers positioned at visual configurations that exert stronger crowding effects, either with shorter target-flanker distance or at a radial-out location relative to the target stimulus. However, modulation of neural responses and changes in information coding do not necessarily imply changes in signaling efficacy along processing stages in the visual hierarchy. Our results demonstrate that inter-laminar information flow in V1, a key mechanism of hierarchical signaling, is disrupted by spatial context, which may account for the accumulation of information loss along the visual hierarchy.

Although we address degraded inter-laminar information flow in V1, our results do not rule out the possibility of additional mechanisms responsible for visual crowding in higher visual areas. A stronger information loss in area V4 has been observed with crowding due to the summation of signals within the larger receptive fields of V4 neurons compared with V1.[7] Other relevant studies relying on coarser measures of neural activity, such as fMRI, found that inter-areal temporal correlations (between V1, V2, V3, V4, and the visual word form area) are lower with crowded letters compared with uncrowded letters.[14] Such deterioration in the extrastriate cortex can only compound the degradation of signaling that we identified within V1, as higher visual areas ultimately rely on V1 inputs for their computations.[1] Given reports of the similar extents of anatomical horizontal (recurrent within V1) and feedback (from V2 to V1) projections in the visual cortex,[51] cortical magnification can partially explain the inward-outward asymmetry of perceptual degradation due to crowding but not the full extent of the radial-tangential anisotropy.[21] This suggests the existence of additional "functional" non-uniformities in the peri-columnar network.

Source of non-uniform context signal

The dependence of the PMI temporal profile on the inter-laminar delay suggested that the degradation of prediction accuracy in the presence of flankers was mainly due to a novel signal targeting the superficial layer. This result is broadly consistent with a recent study[37] that examined the laminar profile of current sinks in the CSD upon stimulation of the receptive field surround with isotropic annular gratings and found, based on onset latency measurements, that the processing of such spatial context initiates in the superficial and deep layers. Our results significantly extend this prior work by (1) characterizing the effect of such a mechanism on information propagation along the intra-V1 hierarchy and (2) showing that such a mechanism could also be a template for non-uniform contextual modulation. Further experiments are needed to be able to pinpoint the source of this implicated input, which could non-exclusively be horizontal connections from superficial-layer neurons outside the recorded V1 column or feedback connections from higher visual areas. Both possibilities are supported by previous studies in the context of surround modulation where optogenetic inactivation of horizontal connections in mouse L2/3 V1[52] or marmoset V2 feedback connections to V1[53] reduced the amplitude of surround modulation. Moreover, each type of connection was shown to contribute to the processing of spatial context at different spatiotemporal scales.[37,41] It is important to note that our results do not conflict with previous work suggesting the contribution of geniculate feedforward connections, which primarily terminate in the input layer of V1, to the processing of contextual stimuli,[34,40,54–57] but imply a weaker effect of such connections on the efficacy of input-superficial information flow compared with connections terminating in the superficial layers. Interestingly, our observation of an intermediate level of negative correlation (close to neither 0 nor −1) between the time when degradation emerged and the temporal delay being considered for the comparison between the tangential and radial-out conditions from one monkey (Figure 5G), suggests the influence of potentially both types of connections on the anisotropy. Thus, the mechanism underlying the non-uniform aspect of the modulation of inter-laminar information flow by contextual stimuli could vary with the specific locations of flankers being compared.

Features of inter-laminar information flow

Our study has identified two signatures of inter-laminar flow in V1: low-dimensionality and effective feedback signaling. By employing RRR, we demonstrated that the interaction between the input and superficial layers occurred through a low-dimensional communication subspace, akin to inter-areal interactions[42,44] but in contrast to interactions within the superficial layer of V1.[42] The low-dimensional structure could confer the computational benefit of flexible and selective routing of activity to downstream targets.

The interplay of feedforward and feedback signaling is a hallmark of cortical information processing.[58–60] Such interplay is not only prominent at the inter-areal level but is also implicated at the local circuit level within V1.[40,53,61] Extensive studies have attempted to infer feedback interactions between brain areas by relating activities between areas with temporal delay,[48,62–66] computing phase delays in local field potentials (LFPs) or multi-unit neuronal activity (MUA)[61,67–69] and comparing the timing of neuronal response onsets[70–72] as well as the emergence of certain neuronal response properties[73–76] across areas. Yet, feedback interactions among within-area laminar circuits in general, and between the input and superficial layers in particular, remain unknown. Here, we characterized inter-laminar interactions along both feedforward and feedback directions by applying CCA with varying temporal delay between layers. Notably, we observed substantial levels of correlation over a range of negative delays, especially at the initial and late phases of the responsive period, implying an effective feedback component (superficial leading input) in the inter-laminar interaction. This result is consistent with the implication of a previous study that examined the laminar profile of the MUA for the alpha rhythm and found that MUA in the superficial and deep layers preceded MUA in the input layer.[61] Given that the dendritic arbors of the input layer (L4C) neurons are locally confined, and the descending axons of the superficial-layer neurons mainly pass through the input layer with very weak branching,[28,29,77] the identified effective feedback signaling is less likely to be

relayed via a direct superficial-input anatomical connection. Instead, certain types of neurons in the deep layer, the primary target of projections from neurons in the superficial layer, have been shown to send extensive axonal projections into the input layer,[28,78,79] which form an indirect superficial-input pathway via the deep layer and could serve as an anatomical substrate for the identified effective feedback signaling.

RESOURCE AVAILABILITY

Lead contact

Further information and requests for resources should be directed to and will be fulfilled by the lead contact, Monika P. Jadi (monika.jadi@yale.edu).

Materials availability

This study did not generate new unique reagents.

Data and code availability

All data tables have been deposited to Figshare (https://doi.org/10.6084/m9.figshare.27055252). Raw electrophysiology data are available upon request. All analysis was performed using MATLAB software from MathWorks.

ACKNOWLEDGMENTS

This research was supported by NIH/NEI R01 EY032555, a NARSAD Young Investigator grant, a Ziegler Foundation grant, and Yale Orthwein Scholar funds to A.S.N.; NIH/NEI R01 EY034605 and R00 EY025026 to M.P.J.; Kavli postdoctoral fellowship and Swartz postdoctoral fellowship in theoretical neuroscience to X.X.; NIH/NINDS training grants T32-NS007224 and T32-NS041228 to M.P.M. and S.D.; and an NIH/NEI core grant for vision research P30 EY026878 to Yale University. We want to thank the veterinary and husbandry staff at Yale for excellent animal care. We would like to dedicate this to the memory of Bosco S. Tjan.

AUTHOR CONTRIBUTIONS

X.X., A.S.N., and M.P.J. conceptualized the project. M.P.M. and A.S.N. designed the experiments, and A.S.N. supervised the data collection. M.P.M., N.V.H., and S.D. collected data and performed preliminary analyses. X.X. conducted the statistical analysis. M.P.J. supervised the analysis. X.X., A.S.N., and M.P.J. wrote the manuscript.

DECLARATION OF INTERESTS

The authors declare no competing interests.

STAR★METHODS

Detailed methods are provided in the online version of this paper and include the following:

- KEY RESOURCES TABLE
- EXPERIMENTAL MODEL AND STUDY PARTICIPANT DETAILS
- METHOD DETAILS
  - Surgical procedures
  - Electrophysiology
  - Behavioral control and eye tracking
  - Receptive field mapping
  - Current source density mapping
  - Experimental task
- QUANTIFICATION AND STATISTICAL ANALYSIS
  - Normalized peri-stimulus time histograms (PSTHs)
  - Response onset estimation
  - Unit selection for regression analysis
  - Data preparation for regression analysis
  - Regression
  - Factor analysis
  - Principal angle
  - Cross-prediction analysis
  - Population correlation analysis

SUPPLEMENTAL INFORMATION

Supplemental information can be found online at https://doi.org/10.1016/j.neuron.2024.09.021.

Received: March 9, 2024
Revised: August 19, 2024
Accepted: September 25, 2024
Published: October 22, 2024

REFERENCES

1. Felleman, D.J., and Van Essen, D.C. (1991). Distributed Hierarchical Processing in the Primate Cerebral Cortex. Cereb. Cortex *1*, 1–47. https://doi.org/10.1093/cercor/1.1.1-a.
2. Himmelberg, M.M., Winawer, J., and Carrasco, M. (2023). Polar angle asymmetries in visual perception and neural architecture. Trends Neurosci. *46*, 445–458. https://doi.org/10.1016/j.tins.2023.03.006.
3. Levi, D.M. (2008). Crowding—An essential bottleneck for object recognition: A mini-review. Vision Res. *48*, 635–654. https://doi.org/10.1016/j.visres.2007.12.009.
4. Toet, A., and Levi, D.M. (1992). The two-dimensional shape of spatial interaction zones in the parafovea. Vision Res. *32*, 1349–1357. https://doi.org/10.1016/0042-6989(92)90227-A.
5. Petrov, Y., Popple, A.V., and McKee, S.P. (2007). Crowding and surround suppression: Not to be confused. J. Vis. *7*, 12.1–12.9. https://doi.org/10.1167/7.2.12.
6. Henry, C.A., and Kohn, A. (2020). Spatial contextual effects in primary visual cortex limit feature representation under crowding. Nat. Commun. *11*, 1687. https://doi.org/10.1038/s41467-020-15386-7.
7. Henry, C.A., and Kohn, A. (2022). Feature representation under crowding in macaque V1 and V4 neuronal populations. Curr. Biol. *32*, 5126–5137.e3. https://doi.org/10.1016/j.cub.2022.10.049.
8. Millin, R., Arman, A.C., Chung, S.T.L., and Tjan, B.S. (2014). Visual Crowding in V1. Cereb. Cortex *24*, 3107–3115.
9. Chen, J., He, Y., Zhu, Z., Zhou, T., Peng, Y., Zhang, X., and Fang, F. (2014). Attention-Dependent Early Cortical Suppression Contributes to Crowding. J. Neurosci. *34*, 10465–10474. https://doi.org/10.1523/JNEUROSCI.1140-14.2014.
10. Chicherov, V., Plomp, G., and Herzog, M.H. (2014). Neural correlates of visual crowding. NeuroImage *93*, 23–31. https://doi.org/10.1016/j.neuroimage.2014.02.021.
11. Bi, T., Cai, P., Zhou, T., and Fang, F. (2009). The effect of crowding on orientation-selective adaptation in human early visual cortex. J. Vis. *9*, 13.1–1310. https://doi.org/10.1167/9.11.13.
12. Anderson, E.J., Dakin, S.C., Schwarzkopf, D.S., Rees, G., and Greenwood, J.A. (2012). The neural correlates of crowding-induced changes in appearance. Curr. Biol. *22*, 1199–1206. https://doi.org/10.1016/j.cub.2012.04.063.
13. Kwon, M., Bao, P., Millin, R., and Tjan, B.S. (2014). Radial-tangential anisotropy of crowding in the early visual areas. J. Neurophysiol. *112*, 2413–2422. https://doi.org/10.1152/jn.00476.2014.
14. Freeman, J., Donner, T.H., and Heeger, D.J. (2011). Inter-area correlations in the ventral visual pathway reflect feature integration. J. Vis. *11*, 15. https://doi.org/10.1167/11.4.15.
15. He, S., Cavanagh, P., and Intriligator, J. (1996). Attentional resolution and the locus of visual awareness. Nature *383*, 334–337. https://doi.org/10.1038/383334a0.

16. Parkes, L., Lund, J., Angelucci, A., Solomon, J.A., and Morgan, M. (2001). Compulsory averaging of crowded orientation signals in human vision. Nat. Neurosci. *4*, 739–744. https://doi.org/10.1038/89532.

17. Pelli, D.G. (2008). Crowding: a cortical constraint on object recognition. Curr. Opin. Neurobiol. *18*, 445–451. https://doi.org/10.1016/j.conb.2008.09.008.

18. Levi, D.M., and Carney, T. (2009). Crowding in Peripheral Vision: Why Bigger Is Better. Curr. Biol. *19*, 1988–1993. https://doi.org/10.1016/j.cub.2009.09.056.

19. Greenwood, J.A., Bex, P.J., and Dakin, S.C. (2009). Positional averaging explains crowding with letter-like stimuli. Proc. Natl. Acad. Sci. USA *106*, 13130–13135. https://doi.org/10.1073/pnas.0901352106.

20. Freeman, J., and Simoncelli, E.P. (2011). Metamers of the ventral stream. Nat. Neurosci. *14*, 1195–1201. https://doi.org/10.1038/nn.2889.

21. Nandy, A.S., and Tjan, B.S. (2012). Saccade-confounded image statistics explain visual crowding. Nat. Neurosci. *15*, 463–469. https://doi.org/10.1038/nn.3021.

22. Balas, B., Nakano, L., and Rosenholtz, R. (2009). A summary-statistic representation in peripheral vision explains visual crowding. J. Vis. *9*, 13.1–1318. https://doi.org/10.1167/9.12.13.

23. Ester, E.F., Zilber, E., and Serences, J.T. (2015). Substitution and pooling in visual crowding induced by similar and dissimilar distractors. J. Vis. *15*, 15.1.4. https://doi.org/10.1167/15.1.4.

24. Motter, B.C., and Simoni, D.A. (2007). The roles of cortical image separation and size in active visual search performance. J. Vis. *7*, 6.1–615. https://doi.org/10.1167/7.2.6.

25. Petrov, Y., and Popple, A.V. (2007). Crowding is directed to the fovea and preserves only feature contrast. J. Vis. *7*, 8.1–8.9. https://doi.org/10.1167/7.2.8.

26. van den Berg, R., Roerdink, J.B.T.M., and Cornelissen, F.W. (2010). A neurophysiologically plausible population code model for feature integration explains visual crowding. PLoS Comput. Biol. *6*, e1000646. https://doi.org/10.1371/journal.pcbi.1000646.

27. Mountcastle, V.B. (1997). The columnar organization of the neocortex. Brain *120*, 701–722. https://doi.org/10.1093/brain/120.4.701.

28. Callaway, E.M. (1998). Local circuits in primary visual cortex of the macaque monkey. Annu. Rev. Neurosci. *21*, 47–74. https://doi.org/10.1146/annurev.neuro.21.1.47.

29. Lund, J.S. (1973). Organization of neurons in the visual cortex, area 17, of the monkey (Macaca mulatta). J. Comp. Neurol. *147*, 455–496. https://doi.org/10.1002/cne.901470404.

30. Douglas, R.J., and Martin, K.A.C. (2004). Neuronal circuits of the neocortex. Annu. Rev. Neurosci. *27*, 419–451. https://doi.org/10.1146/annurev.neuro.27.070203.144152.

31. Hubel, D.H., and Wiesel, T.N. (1965). Receptive fields and functional architecture in two nonstriate visual areas (18 and 19) of the cat. J. Neurophysiol. *28*, 229–289. https://doi.org/10.1152/jn.1965.28.2.229.

32. Blakemore, C., and Tobin, E.A. (1972). Lateral inhibition between orientation detectors in the cat's visual cortex. Exp. Brain Res. *15*, 439–440. https://doi.org/10.1007/BF00234129.

33. Cavanaugh, J.R., Bair, W., and Movshon, J.A. (2002). Nature and Interaction of Signals From the Receptive Field Center and Surround in Macaque V1 Neurons. J. Neurophysiol. *88*, 2530–2546. https://doi.org/10.1152/jn.00692.2001.

34. Shushruth, S., Ichida, J.M., Levitt, J.B., and Angelucci, A. (2009). Comparison of Spatial Summation Properties of Neurons in Macaque V1 and V2. J. Neurophysiol. *102*, 2069–2083. https://doi.org/10.1152/jn.00512.2009.

35. Angelucci, A., Levitt, J.B., Walton, E.J.S., Hupe, J.M., Bullier, J., and Lund, J.S. (2002). Circuits for Local and Global Signal Integration in Primary Visual Cortex. J. Neurosci. *22*, 8633–8646. https://doi.org/10.1523/JNEUROSCI.22-19-08633.2002.

36. Henry, C.A., Joshi, S., Xing, D., Shapley, R.M., and Hawken, M.J. (2013). Functional Characterization of the Extraclassical Receptive Field in Macaque V1: Contrast, Orientation, and Temporal Dynamics. J. Neurosci. *33*, 6230–6242. https://doi.org/10.1523/JNEUROSCI.4155-12.2013.

37. Bijanzadeh, M., Nurminen, L., Merlin, S., Clark, A.M., and Angelucci, A. (2018). Distinct Laminar Processing of Local and Global Context in Primate Primary Visual Cortex. Neuron *100*, 259–274.e4. https://doi.org/10.1016/j.neuron.2018.08.020.

38. Ichida, J.M., Schwabe, L., Bressloff, P.C., and Angelucci, A. (2007). Response Facilitation From the "Suppressive" Receptive Field Surround of Macaque V1 Neurons. J. Neurophysiol. *98*, 2168–2181. https://doi.org/10.1152/jn.00298.2007.

39. Sceniak, M.P., Hawken, M.J., and Shapley, R. (2001). Visual Spatial Characterization of Macaque V1 Neurons. J. Neurophysiol. *85*, 1873–1887. https://doi.org/10.1152/jn.2001.85.5.1873.

40. Shushruth, S., Nurminen, L., Bijanzadeh, M., Ichida, J.M., Vanni, S., and Angelucci, A. (2013). Different Orientation Tuning of Near- and Far-Surround Suppression in Macaque Primary Visual Cortex Mirrors Their Tuning in Human Perception. J. Neurosci. *33*, 106–119. https://doi.org/10.1523/JNEUROSCI.2518-12.2013.

41. Angelucci, A., Bijanzadeh, M., Nurminen, L., Federer, F., Merlin, S., and Bressloff, P.C. (2017). Circuits and Mechanisms for Surround Modulation in Visual Cortex. Annu. Rev. Neurosci. *40*, 425–451. https://doi.org/10.1146/annurev-neuro-072116-031418.

42. Semedo, J.D., Zandvakili, A., Machens, C.K., Yu, B.M., and Kohn, A. (2019). Cortical Areas Interact through a Communication Subspace. Neuron *102*, 249–259.e4. https://doi.org/10.1016/j.neuron.2019.01.026.

43. Mitzdorf, U. (1985). Current source-density method and application in cat cerebral cortex: investigation of evoked potentials and EEG phenomena. Physiol. Rev. *65*, 37–100. https://doi.org/10.1152/physrev.1985.65.1.37.

44. Srinath, R., Ruff, D.A., and Cohen, M.R. (2021). Attention improves information flow between neuronal populations without changing the communication subspace. Curr. Biol. *31*, 5299–5313.e4. https://doi.org/10.1016/j.cub.2021.09.076.

45. Izenman, A.J. (1975). Reduced-rank regression for the multivariate linear model. J. Multivariate Anal. *5*, 248–264. https://doi.org/10.1016/0047-259X(75)90042-1.

46. Kobak, D., Brendel, W., Constantinidis, C., Feierstein, C.E., Kepecs, A., Mainen, Z.F., Qi, X.-L., Romo, R., Uchida, N., and Machens, C.K. (2016). Demixed principal component analysis of neural population data. eLife *5*, e10989. https://doi.org/10.7554/eLife.10989.

47. Williamson, R.C., Cowley, B.R., Litwin-Kumar, A., Doiron, B., Kohn, A., Smith, M.A., and Yu, B.M. (2016). Scaling Properties of Dimensionality Reduction for Neural Populations and Network Models. PLoS Comput. Biol. *12*, e1005141. https://doi.org/10.1371/journal.pcbi.1005141.

48. Semedo, J.D., Jasper, A.I., Zandvakili, A., Krishna, A., Aschner, A., Machens, C.K., Kohn, A., and Yu, B.M. (2022). Feedforward and feedback interactions between visual cortical areas use different population activity patterns. Nat. Commun. *13*, 1099. https://doi.org/10.1038/s41467-022-28552-w.

49. Mitzdorf, U., and Singer, W. (1979). Excitatory synaptic ensemble properties in the visual cortex of the macaque monkey: A current source density analysis of electrically evoked potentials. J. Comp. Neurol. *187*, 71–83. https://doi.org/10.1002/cne.901870105.

50. Morton, M.P., Denagamage, S., Hudson, N.V., and Nandy, A.S. (2024). Geometry of anisotropic contextual interactions in the visual cortex places fundamental limits on spatial vision. J. Vis. *24*, 1432. https://doi.org/10.1167/jov.24.10.1432.

51. Stettler, D.D., Das, A., Bennett, J., and Gilbert, C.D. (2002). Lateral Connectivity and Contextual Interactions in Macaque Primary Visual Cortex. Neuron *36*, 739–750. https://doi.org/10.1016/S0896-6273(02)01029-2.

52. Adesnik, H., Bruns, W., Taniguchi, H., Huang, Z.J., and Scanziani, M. (2012). A neural circuit for spatial summation in visual cortex. Nature *490*, 226–231. https://doi.org/10.1038/nature11526.

53. Nurminen, L., Merlin, S., Bijanzadeh, M., Federer, F., and Angelucci, A. (2018). Top-down feedback controls spatial summation and response amplitude in primate visual cortex. Nat. Commun. *9*, 2281. https://doi.org/10.1038/s41467-018-04500-5.

54. Solomon, S.G., White, A.J.R., and Martin, P.R. (2002). Extraclassical Receptive Field Properties of Parvocellular, Magnocellular, and Koniocellular Cells in the Primate Lateral Geniculate Nucleus. J. Neurosci. *22*, 338–349. https://doi.org/10.1523/JNEUROSCI.22-01-00338.2002.

55. Bonin, V., Mante, V., and Carandini, M. (2005). The Suppressive Field of Neurons in Lateral Geniculate Nucleus. J. Neurosci. *25*, 10844–10856. https://doi.org/10.1523/JNEUROSCI.3562-05.2005.

56. Ozeki, H., Sadakane, O., Akasaki, T., Naito, T., Shimegi, S., and Sato, H. (2004). Relationship between Excitation and Inhibition Underlying Size Tuning and Contextual Response Modulation in the Cat Primary Visual Cortex. J. Neurosci. *24*, 1428–1438. https://doi.org/10.1523/JNEUROSCI.3852-03.2004.

57. Angelucci, A., and Sainsbury, K. (2006). Contribution of feedforward thalamic afferents and corticogeniculate feedback to the spatial summation area of macaque V1 and LGN. J. Comp. Neurol. *498*, 330–351. https://doi.org/10.1002/cne.21060.

58. Gilbert, C.D., and Li, W. (2013). Top-down influences on visual processing. Nat. Rev. Neurosci. *14*, 350–363. https://doi.org/10.1038/nrn3476.

59. Muckli, L., De Martino, F., Vizioli, L., Petro, L.S., Smith, F.W., Ugurbil, K., Goebel, R., and Yacoub, E. (2015). Contextual Feedback to Superficial Layers of V1. Curr. Biol. *25*, 2690–2695. https://doi.org/10.1016/j.cub.2015.08.057.

60. Harris, K.D., and Mrsic-Flogel, T.D. (2013). Cortical connectivity and sensory coding. Nature *503*, 51–58. https://doi.org/10.1038/nature12654.

61. van Kerkoerle, T., Self, M.W., Dagnino, B., Gariel-Mathis, M.A., Poort, J., van der Togt, C., and Roelfsema, P.R. (2014). Alpha and gamma oscillations characterize feedback and feedforward processing in monkey visual cortex. Proc. Natl. Acad. Sci. USA *111*, 14332–14341. https://doi.org/10.1073/pnas.1402773111.

62. Tauste Campo, A., Martinez-Garcia, M., Nácher, V., Luna, R., Romo, R., and Deco, G. (2015). Task-driven intra- and interarea communications in primate cerebral cortex. Proc. Natl. Acad. Sci. USA *112*, 4761–4766. https://doi.org/10.1073/pnas.1503937112.

63. Zandvakili, A., and Kohn, A. (2015). Coordinated Neuronal Activity Enhances Corticocortical Communication. Neuron *87*, 827–839. https://doi.org/10.1016/j.neuron.2015.07.026.

64. Jia, X., Tanabe, S., and Kohn, A. (2013). Gamma and the Coordination of Spiking Activity in Early Visual Cortex. Neuron *77*, 762–774. https://doi.org/10.1016/j.neuron.2012.12.036.

65. Nowak, L.G., Munk, M.H.J., James, A.C., Girard, P., and Bullier, J. (1999). Cross-Correlation Study of the Temporal Interactions Between Areas V1 and V2 of the Macaque Monkey. J. Neurophysiol. *81*, 1057–1074. https://doi.org/10.1152/jn.1999.81.3.1057.

66. Roe, A.W., and Ts'o, D.Y. (1999). Specificity of Color Connectivity Between Primate V1 and V2. J. Neurophysiol. *82*, 2719–2730. https://doi.org/10.1152/jn.1999.82.5.2719.

67. Gregoriou, G.G., Gotts, S.J., Zhou, H., and Desimone, R. (2009). High-Frequency, Long-Range Coupling Between Prefrontal and Visual Cortex During Attention. Science *324*, 1207–1210. https://doi.org/10.1126/science.1171402.

68. Salazar, R.F., Dotson, N.M., Bressler, S.L., and Gray, C.M. (2012). Content-Specific Fronto-Parietal Synchronization During Visual Working Memory. Science *338*, 1097–1100. https://doi.org/10.1126/science.1224000.

69. Bastos, A.M., Vezoli, J., and Fries, P. (2015). Communication through coherence with inter-areal delays. Curr. Opin. Neurobiol. *31*, 173–180. https://doi.org/10.1016/j.conb.2014.11.001.

70. de Lafuente, V., and Romo, R. (2006). Neural correlate of subjective sensory experience gradually builds up across cortical areas. Proc. Natl. Acad. Sci. USA *103*, 14266–14271. https://doi.org/10.1073/pnas.0605826103.

71. Siegel, M., Buschman, T.J., and Miller, E.K. (2015). Cortical information flow during flexible sensorimotor decisions. Science *348*, 1352–1355. https://doi.org/10.1126/science.aab0551.

72. Schmolesky, M.T., Wang, Y., Hanes, D.P., Thompson, K.G., Leutgeb, S., Schall, J.D., and Leventhal, A.G. (1998). Signal Timing Across the Macaque Visual System. J. Neurophysiol. *79*, 3272–3278. https://doi.org/10.1152/jn.1998.79.6.3272.

73. Freeman, J., Ziemba, C.M., Heeger, D.J., Simoncelli, E.P., and Movshon, J.A. (2013). A functional and perceptual signature of the second visual area in primates. Nat. Neurosci. *16*, 974–981. https://doi.org/10.1038/nn.3402.

74. Chen, M., Yan, Y., Gong, X., Gilbert, C.D., Liang, H., and Li, W. (2014). Incremental Integration of Global Contours through Interplay between Visual Cortical Areas. Neuron *82*, 682–694. https://doi.org/10.1016/j.neuron.2014.03.023.

75. Schwiedrzik, C.M., and Freiwald, W.A. (2017). High-Level Prediction Signals in a Low-Level Area of the Macaque Face-Processing Hierarchy. Neuron *96*, 89–97.e4. https://doi.org/10.1016/j.neuron.2017.09.007.

76. Issa, E.B., Cadieu, C.F., and DiCarlo, J.J. (2018). Neural dynamics at successive stages of the ventral visual stream are consistent with hierarchical error signals. eLife *7*, e42870. https://doi.org/10.7554/eLife.42870.

77. Callaway, E.M., and Wiser, A.K. (1996). Contributions of individual layer 2-5 spiny neurons to local circuits in macaque primary visual cortex. Vis. Neurosci. *13*, 907–922. https://doi.org/10.1017/s0952523800009159.

78. Wiser, A.K., and Callaway, E.M. (1996). Contributions of individual layer 6 pyramidal neurons to local circuitry in macaque primary visual cortex. J. Neurosci. *16*, 2724–2739. https://doi.org/10.1523/JNEUROSCI.16-08-02724.1996.

79. Briggs, F., and Callaway, E.M. (2001). Layer-Specific Input to Distinct Cell Types in Layer 6 of Monkey Primary Visual Cortex. J. Neurosci. *21*, 3600–3608. https://doi.org/10.1523/JNEUROSCI.21-10-03600.2001.

80. Nandy, A.S., Nassi, J.J., and Reynolds, J.H. (2017). Laminar Organization of Attentional Modulation in Macaque Visual Area V4. Neuron *93*, 235–246. https://doi.org/10.1016/j.neuron.2016.11.029.

81. Nassi, J.J., Avery, M.C., Cetin, A.H., Roe, A.W., and Reynolds, J.H. (2015). Optogenetic Activation of Normalization in Alert Macaque Visual Cortex. Neuron *86*, 1504–1517. https://doi.org/10.1016/j.neuron.2015.05.040.

82. Ruiz, O., Lustig, B.R., Nassi, J.J., Cetin, A., Reynolds, J.H., Albright, T.D., Callaway, E.M., Stoner, G.R., and Roe, A.W. (2013). Optogenetics through windows on the brain in the nonhuman primate. J. Neurophysiol. *110*, 1455–1467. https://doi.org/10.1152/jn.00153.2013.

83. Stringer, C., Pachitariu, M., Steinmetz, N., Reddy, C.B., Carandini, M., and Harris, K.D. (2019). Spontaneous behaviors drive multidimensional, brainwide activity. Science *364*, 255. https://doi.org/10.1126/science.aav7893.

84. Steinmetz, N.A., Aydin, C., Lebedeva, A., Okun, M., Pachitariu, M., Bauza, M., Beau, M., Bhagat, J., Böhm, C., Broux, M., et al. (2021). Neuropixels 2.0: A miniaturized high-density probe for stable, long-term brain recordings. Science *372*, eabf4588. https://doi.org/10.1126/science.abf4588.

85. Hwang, J., Mitz, A.R., and Murray, E.A. (2019). NIMH MonkeyLogic: Behavioral control and data acquisition in MATLAB. J. Neurosci. Methods *323*, 13–21. https://doi.org/10.1016/j.jneumeth.2019.05.002.

86. Bouma, H. (1970). Interaction Effects in Parafoveal Letter Recognition. Nature *226*, 177–178. https://doi.org/10.1038/226177a0.

87. Pelli, D.G., and Tillman, K.A. (2008). The uncrowded window of object recognition. Nat. Neurosci. *11*, 1129–1135. https://doi.org/10.1038/nn.2187.

88. Calin-Jageman, R.J., and Cumming, G. (2019). Estimation for Better Inference in Neuroscience. eNeuro *6*, ENEURO.0205-19.2019. https://doi.org/10.1523/eneuro.0205-19.2019.

89. Ho, J., Tumkaya, T., Aryal, S., Choi, H., and Claridge-Chang, A. (2019). Moving beyond P values: data analysis with estimation graphics. Nat. Methods *16*, 565–566. https://doi.org/10.1038/s41592-019-0470-3.

90. Everitt, B.S. (1984). Maximum Likelihood Estimation of the Parameters in a Mixture of Two Univariate Normal Distributions; A Comparison of Different Algorithms. J. R. Stat. Soc. D *33*, 205–215. https://doi.org/10.2307/2987851.

91. Yu, B.M., Cunningham, J.P., Santhanam, G., Ryu, S.I., Shenoy, K.V., and Sahani, M. (2009). Gaussian-Process Factor Analysis for Low-Dimensional Single-Trial Analysis of Neural Population Activity. J. Neurophysiol. *102*, 614–635. https://doi.org/10.1152/jn.90941.2008.

92. Björck, Å., and Golub, G.H. (1973). Numerical Methods for Computing Angles Between Linear Subspaces. Math. Comput. *27*, 579–594. https://doi.org/10.2307/2005662.

93. Gallego, J.A., Perich, M.G., Naufel, S.N., Ethier, C., Solla, S.A., and Miller, L.E. (2018). Cortical population activity within a preserved neural manifold underlies multiple motor behaviors. Nat. Commun. *9*, 4233. https://doi.org/10.1038/s41467-018-06560-z.

94. Hotelling, H. (1936). Relations Between Two Sets of Variates. Biometrika *28*, 321–377. https://doi.org/10.2307/2333955.

Please cite this article in press as: Xu et al., Spatial context non-uniformly modulates inter-laminar information flow in the primary visual cortex, Neuron (2024), https://doi.org/10.1016/j.neuron.2024.09.021

STAR★METHODS

KEY RESOURCES TABLE

REAGENT or RESOURCE	SOURCE	IDENTIFIER
Experimental models: Organisms/strains		
Rhesus Macaques (Macaca mulatta)	Worldwide Primates	N/A
Chemicals, peptides, and recombinant proteins		
PEDOT:PSS	Sigma-Aldrich	655201
Deposited data		
Figure data	This paper	https://doi.org/10.6084/m9.figshare.27055252
Software and algorithms		
MATLAB	Mathworks	R2021b
Kilosort2	Pachitariu & MouseLand	https://github.com/MouseLand/Kilosort
phy (spike curation GUI)	Rossant & cortex-lab	https://github.com/cortex-lab/phy
Custom code	This paper	https://doi.org/10.6084/m9.figshare.27055252
Other		
Silicon probes	NeuroNexus	a2x32_6mm35_200_177
RHD 512 channel recording controller	Intan	C3004
64 channel recording headstages	Intan	C3115
nanoZ	White Matter LLC	N/A

EXPERIMENTAL MODEL AND STUDY PARTICIPANT DETAILS

Two male rhesus macaques (Macaca mulatta, D: age 6 years, M: age 8 years) were used as subjects in this study. Animals were pair-housed on a 12:12 h light-dark cycle. Water intake was controlled during the experimental period. All experimental procedures were approved by the Institutional Animal Care and Use Committee at Yale University and conformed to NIH guidelines.

METHOD DETAILS

Surgical procedures

Surgical procedures were similar to those described previously.[80–82] We placed low-profile titanium recording chambers in two rhesus macaques so that the chambers allowed access to V1 (both left and right hemispheres in monkey M, right hemisphere in monkey D). Chambers were targeted based on sulcus reconstructions created using preoperative structural MRI. After chamber implantation, we removed the native dura mater and replaced it with a transparent silicone artificial dura (AD). The AD allowed for the visualization of cortical sites in V1 for probe targeting. All procedures were approved by the Yale University Institutional Animal Care and Use Committee and conformed to NIH guidelines.

Electrophysiology

Prior to a series of recordings, we electroplated (nanoZ, White Matter LLC) 64-channel electrode arrays (“laminar probes,” NeuroNexus Technologies, Inc., 2 shanks, 32 channels/shank, 70 μm spacing between sites, 200 μm between shanks) with PEDOT (poly(3,4-ethylene dioxythiophene)). At the beginning of each recording session, we inserted a laminar probe in V1. Laminar probes were attached to a titanium mounting stage that was screwed into the chamber. We positioned the laminar probes using an electronic micromanipulator (Narishige Inc.) and ensured that the probes were orthogonal to the surface of the cortex by visual inspection through a surgical microscope (Leica Microsystems). To position the probe within the brain, we first penetrated the AD, arachnoid, and pia by moving the probe downward at a high speed (>100 μm/s). After the tip of the probe entered the cortex, we inserted the remainder of the probe at a slow speed (2 μm/s). Once the entire probe was in the brain, we slowly (2μm/s) relieved the pressure on the brain by retracting the probe upward, relieving pressure on the brain but not moving the probe relative to the cortex.

Electrical signals from the laminar probe were collected at 30 kHz and digitized on a 64-channel digital headstage and sent to the recording system (RHD Recording System, Intan Technologies). Action potential waveforms were extracted offline using Kilosort2[83,84] and manually sorted into single and multi-unit clusters using Phy.[83,84] Clusters with peaks preceding the trough were

Please cite this article in press as: Xu et al., Spatial context non-uniformly modulates inter-laminar information flow in the primary visual cortex, Neuron (2024), https://doi.org/10.1016/j.neuron.2024.09.021

identified as axonal spikes and excluded. Recordings were collected over the course of 22 sessions (14 in monkey M, 8 in monkey D) with hundreds of units recorded in each subject (693 single units and 430 multi-unit clusters in monkey M, 400 single units and 277 multi-unit clusters in monkey D).

Behavioral control and eye tracking

We controlled behavioral experiments using NIMH MonkeyLogic.[85] Eye position and pupil diameter were sampled at 120Hz (ETL-200, ISCAN Inc.) and sent to the behavioral control system. Stimuli were presented on a monitor positioned 57cm from the monkey with a 60 Hz refresh rate. Trials were aborted if the eye position deviated more than 1.2-1.5 degrees of visual angle (dva; 1.2 for monkey D, 1.5 for monkey M) from the central fixation point.

Receptive field mapping

We mapped RFs of the column by presenting Gabor patch stimuli (2-4 cycles/degree, 0.25-1 degree Gaussian half-width, 100% luminance contrast) on a square grid spanning the lower visual quadrant of interest (both left and right in monkey M, left in monkey D) while the monkey maintained fixation on the center of the screen. Grid spacing parameters were optimized each session and ranged from 0.25-1 dva. A stimulus was presented at a random location and orientation on the grid during each frame. We calculated the LFP power for each recording channel 40-200 ms after stimulus presentation in each location. The LFP power at each location was smoothed using a Gaussian kernel (sigma = 0.75 dva), and the peak location averaged across all recording sites was defined as the receptive field center. Spatial receptive field maps for each channel were plotted as stacked contours for each shank for visualization.

Current source density mapping

We used CSD mapping[43] to identify laminar boundaries in our recordings and estimated the relative strength of the signal targeting the superficial layer across visual conditions.

While monkeys maintained fixation on the screen, 100% luminance contrast white annular stimuli were flashed for 32 ms, positioned at the center of the RF. The LFP signal following the stimulus onset was averaged across trials and spatially smoothed using a Gaussian kernel (sigma = 140 μm). The CSD was calculated as the second spatial derivative of the LFP:

$$CSD(x,t) = -\sigma * \frac{v(x+h,t) - 2v(x,t)+v(x-h,t)}{h^2}$$

where x is the position in the extracellular medium at which CSD is calculated, t the time following the stimulus onset (advancing in 1 ms), h the spacing between recording sites on the linear probe (here 70 μm), v the voltage, σ the conductivity of the cortical tissue (0.4 S/m). We interpolated the CSD every 7 μm. The input layer was identified by the boundaries of the early current sink characterizing feedforward input into layer IV. Channels above and below this sink were classified as superficial and deep, respectively.

CSD provides a link between LFP and neuronal ensemble activities by approximating the net local transmembrane currents that generate the local LFP. The identified current sinks (negative deflections, visualized in red in Figures 7A–7C) in the extracellular medium reflect integrated subthreshold input to neuronal ensembles.[43,49] We used CSD response to flanker-only stimuli (radial-out, radial-in, tangential) to estimate the relative strength of the signal targeting the superficial layer evoked by contextual stimuli at different locations. In particular, for each shank on the laminar probe, we first identified the early current sink (within 200 ms following stimulus onset) in its CSD response. At each depth along the superficial layer, we calculated the level of charge sinks by integrating the current sink over time and then averaged the result across the depth of the superficial layer. We compared the level of charge sinks evoked by flankers-only stimuli at different locations to quantify the relative strength of contextual signals targeting the superficial layer.

Experimental task

While monkeys maintained fixation on a point at the center of the screen, stimulus arrays were presented on the screen for 100 ms. In between stimulus presentations, there was a 200-250 ms inter-stimulus interval in which the screen was blank other than the fixation point. The arrays consisted of a probe stimulus in the receptive field center either in isolation (probe condition) or together with a flanking stimulus (flanked condition). There were four different conditions (probe, tangentially flanked, radially inward flanked, and radially outward flanked) of stimulus arrays presented during a trial. This was repeated 4-6 times during each trial depending on the monkey's ability to hold fixation. The stimulus conditions were randomly interleaved from flash to flash. The center of the probe was aligned with the center of the average of the RFs of each recording site. The four flanker locations were positioned on the radial or tangential axes. The radial axis was defined as the axis connecting the probe (and RF) center and the fixation point at the center of the monitor. The tangential axis was defined as the line orthogonal to the radial axis and passing through the probe center. The tangential flanked condition occurred when the probe was presented along with a flanker on the tangential axis, either in the clockwise or counterclockwise direction. The radial-in flanked condition occurred when the probe was presented along with a flanker on the radial axis and between the probe center and the fixation point. The radial-out condition was similar to the radial-in condition, except the flanker was placed on the radial axis further from the fixation point than the probe. Probe-flanker spacing was identical across stimulus conditions.

Please cite this article in press as: Xu et al., Spatial context non-uniformly modulates inter-laminar information flow in the primary visual cortex, Neuron (2024), https://doi.org/10.1016/j.neuron.2024.09.021

The probe condition was presented on 10% of flashes. On 80% of flashes, flanked stimuli were presented. In the flanked condition, the flanker was positioned at a tangential, radial-in, or radial-out location with equal probability. If the flanker was presented tangential to the probe, it was positioned clockwise or counterclockwise to the probe with equal probability. In the remaining 10% of trials, a stimulus was presented exclusively at one of the four flanker locations. Probe stimuli were sine Gabor patches (25% luminance contrast, 3.5 cycles/degree, 0.5-1.0 degree Gaussian half-width) presented at 6 evenly spaced orientations and 2 opposing phases. Flankers were presented at 100% luminance contrast but were otherwise identical to the probe stimuli. The center-to-center distance between the probe and flankers (Δe, Figure 1D1) was 0.6 (monkey D) or 0.85 dva (monkey M) depending on e_{probe}. Target and flanker stimuli were 0.5 (monkey D) or 0.75 dva (monkey M) in diameter. The ratio between Δe and e_{probe} was 0.46 ± 0.02 SEM, which matched the spatial scaling of crowding zones (critical spacing for crowding in the visual field ≈ 0.5 x target eccentricity).[86,87] The edge-to-edge gap between probe and flanker was 0.1-0.2 deg depending on e_{probe}. In the flanked condition, flankers were presented at the same orientation as the probe or orthogonal to the probe with equal probability. When flankers were presented alone, they were shown with the same orientation distribution as the probes.

QUANTIFICATION AND STATISTICAL ANALYSIS

Wherever possible, instead of relying on null-hypothesis testing, we show bootstrapped estimations of differences between conditions using the estimation statistics framework,[88,89] which provides a principled way to measure effect sizes coupled with estimates of uncertainty, yielding interval estimates of uncertainty. The experiment assigned substantially different presentation probabilities for the probe (10%) and each of the flanked conditions (26.7%). On average, our dataset contained 504.5 ± 29.1 SEM, 1348.8 ± 77.9 SEM, 1306.6 ± 87.6 SEM, 1321.5 ± 90.9 SEM trials for the probe, radial-in, radial-out, and tangential conditions, respectively. When comparing inter-laminar information flows for a pair of visual conditions, we drew the same number of trials under each condition multiple times and conducted the prediction analysis with 20-fold cross-validation. Consequently, when comparing the properties of inter-laminar information flow under the probe condition against any of the flanked conditions (Figures 2, 3, 4, 5A, 6C, and 6D), the number of trials from each draw was capped by the number of trials under the probe condition, which led to the exclusion of a large fraction of trials under each of the flanked conditions. When calculating the properties for individual conditions (Figures 1G–1L) without comparison across conditions, we did not match the number of trials.

Normalized peri-stimulus time histograms (PSTHs)

PSTHs were generated based on spike counts in 30 ms bins shifted by 10 ms. The PSTH for each neuron was calculated separately for each visual condition and normalized between the maximal PSTH over time under the probe condition and the baseline firing rate taken as the PSTH from -30 ms to 30 ms relative to stimulus onset. Neurons whose PSTHs never surpassed the 95% confidence interval of their baseline firing rates were excluded. The averaged normalized PSTH exhibits a maximum less than 1 because of the variability in the peak time across neurons.

Response onset estimation

For every recorded unit, we estimated its response onset for each visual condition. We took the PSTH from -30 ms to 30 ms relative to stimulus onset as the baseline firing rate. The response onset was identified as the time when the PSTH surpassed the 95% confidence interval of the baseline firing rate. Units whose PSTH never crossed the threshold were taken as non-responsive units. For each session, the response onset of the simultaneously recorded population in a specific layer was estimated by taking the average of response onsets of all responsive units. An interval of 100 ms following the response onset of the input layer population was considered as the stimulus processing range (referred to as 'responsive period') of V1 for the purpose of characterizing the inter-laminar information flow between the input and superficial layers.

Unit selection for regression analysis

For comparison of the inter-laminar prediction accuracy across visual conditions, we only included those units in the superficial layer well predicted by the recorded population in the input layer, which were identified by employing a Lasso regression with 20-fold cross-validation to each recorded unit in the superficial layer within the estimated responsive period. The prediction performance was calculated under the largest λ value such that the normalized squared error (*NSE*) was within one standard error of the minimum *NSE* across λ parameters. Units in the superficial layer with a normalized squared error smaller than 1 were identified as being well predicted.

Data preparation for regression analysis

We counted spikes in a sliding window of 50 ms within the estimated responsive period. We investigated how the neuronal activities in the input and superficial layers were related by assessing the extent to which trial-to-trial fluctuations of population responses in the superficial layer could be predicted by that in the input layer of V1. Therefore, for each type of visual stimuli (orientation, spatial configuration, orientation difference between probe and flanker), we subtracted the appropriate peri-stimulus time histogram (i.e., average

time-varying signal; PSTH) from each single-trial response and z-scored the residual. For all analyses, we excluded units with low firing rates (less than 0.2 spikes/s on average). Our results are qualitatively similar for larger 100 ms bins, which corresponded to the stimuli duration in the experiment.

Regression

To assess the extent to which trial-to-trial fluctuations of population responses in the superficial layer could be predicted by that in the input layer of V1, we first applied a linear model of the form $Y = XB$ using ridge regression, which was referred to as the full regression model. To test whether the inter-laminar information propagation occurred through a 'communication subspace', we used reduced-rank regression (RRR), which constrains the linear weight matrix B to be of a given rank. The optimal dimensionality (Dim_{opt}) was defined as the lowest number of predictive dimensions for which prediction performance was within one SEM of peak performance. The details of this analysis can be found in Semedo et al.[42]

Both ridge regression and RRR were applied to a sliding window of 50 ms (advancing in 2 ms) in both layers with 20-fold cross-validation. The prediction accuracy was calculated as $1 - NSE$, where NSE is the mean normalized squared error between the test data and the predictions across folds. For RRR, we took the smallest number of dimensions for which predictive performance was within one SEM of the peak performance as the optimal dimensionality. To study the effect of the spatial configuration of visual stimuli on prediction accuracy, we analyzed the temporal evolution of the prediction accuracies at optimal dimensionality across visual conditions. For each pair of visual conditions, we first aligned the temporal evolutions of corresponding prediction accuracies to compensate for the difference in the response onsets across visual conditions and computed a prediction modulation index, which was calculated as:

$$\mathrm{PMI(t)} = \frac{P_1(t) - P_2(t)}{\sum_t (P_1(t)+P_2(t))/N_t}$$

Where $P_1(t)$ and $P_2(t)$ are the prediction accuracies at optimal dimensionalities obtained by RRR at time t after response onset under visual conditions 1 and 2, respectively. N_t is the number of time points involved in the analysis.

Factor analysis

We quantified the complexity of neural activity in the superficial layer of V1 by using factor analysis (FA), a dimensionality reduction technique which allows spiking variability to vary across neurons and calculates the dimensionality of covariance. The details of this analysis can be found in Williamson et al.,[47] Everitt et al.,[90] and Yu et al.[91] We followed the same steps as previously published work[42,44] to estimate the dimensionality: We first determined the number of dimensions m_{peak} that maximized the cross-validated log-likelihood of the observed residuals. Then we fitted an FA model with m_{peak} dimensions and chose m, by the eigenvalue decomposition, as the smallest dimensionality that captured 95% of the variance in the shared covariance matrix. These population dimensions (m) and predictive dimensions as determined from RRR are based on different techniques.

Principal angle

We characterized the relative alignment of two communication subspaces identified from different visual conditions by using the measure of principal angle, which computes angles between sequentially aligned pairs of basis vectors, each within one of the subspaces, so as to minimize the angle between them. Notably, this measure does not require the compared subspaces to have the same rank. The smallest angle obtained was taken as the 'leading principal angle'. The details of this method can be found in Björck and Golub[92] and Gallego et al.[93] A small leading principal angle implies similar orientations of the communication subspaces identified from different conditions. To verify that the experimentally obtained leading principal angles were significantly different from chance, we compared them to a null distribution of principal angles. These were obtained from 5000 pairs of subspaces that were generated randomly but with preserved ranks (as that of the empirical communication subspaces under different visual conditions). The confidence intervals of the null distribution were obtained from estimation statistics. Moreover, to efficiently assess the extent of similarity in the measure of the principal angle between communication subspaces identified from different visual conditions, we constructed an estimate of the minimal principal angle that could be obtained. This was achieved by computing the principal angle between subspaces identified from pairs of disjoint sets of trials within the same visual condition. To ensure a fair comparison with the cross-condition principal angles, each set was composed of the same number of trials as those used to identify cross-condition communication subspaces. This number was capped by the number of trials under the probe condition, as the experiment assigned a significantly smaller presentation probability to the probe condition (10%) compared to any of the flanked conditions (26.7%). Consequently, the ratio of the number of trials in any of the flanked conditions and the probe condition exceeded 2, which allowed us to compute the within-condition principal angle for the radial-in, radial-out, and tangential conditions when compared with the probe condition. In Figure S2A where we computed the principal angle between any pair of flanked conditions, the number of trials used to identify communication subspaces was only capped by the smallest number of trials across all flanked conditions, which was larger than the half of number of trials under any flanked condition. We were therefore unable to construct an estimate of within-condition principal angles that could be fairly compared with existing curves.

Please cite this article in press as: Xu et al., Spatial context non-uniformly modulates inter-laminar information flow in the primary visual cortex, Neuron (2024), https://doi.org/10.1016/j.neuron.2024.09.021

Cross-prediction analysis

An additional analysis to compare the communication subspaces was based on measuring the inter-laminar prediction performance under a given visual condition when the corresponding input layer data was projected onto the communication subspace identified from a different visual condition. We computed the prediction performance for when projecting the input layer data from the communication subspace identified from condition A onto that identified from condition B (across-condition prediction performance). Then we compared it to the prediction performance when the input layer data was projected onto the original communication subspace of condition A (within-condition prediction performance; obtained from RRR by definition). Comparable cross-condition and within-condition prediction performance implies a similarity between the structure of communication subspaces identified from different conditions. To verify whether the computed cross-condition and within-condition prediction performances were significantly close to each other, we compared them to the prediction performance obtained by chance, where the input layer data in a given condition was projected onto subspaces randomly generated as in the principal angle analysis. Note that this analysis was performed twice for each pair of visual conditions, considering either condition as the within-condition communication subspace.

Population correlation analysis

We used canonical correlation analysis (CCA)[94] to capture the population correlation between the input and superficial layers at different time delays on a moment-by-moment basis. CCA finds pairs of dimensions, one each in the neuronal activity space in each layer, such that the correlation between the projected activity onto these dimensions is maximally correlated. The exact description and formulation of CCA can be found in Semedo et al.[48] We took two windows of activity, one in each layer. Window length was 50 ms and the window was advanced in 10 ms steps. The activity within each window was then binned using 10 ms bins. The reported results were robust over a reasonable range of window and binning lengths chosen. We reported correlation associated with the first two canonical pairs (correlations associated with the third were on average 60% lower and close to chance level).

The correlations along the feedforward (FF) and the effective feedback (FB) signaling pathways were calculated as the mean correlation at positive and negative delays, respectively:

$$C_{FF}(t) = \frac{\sum_{dt>0} C(t,dt)}{N_{dt>0}}$$

$$C_{FB}(t) = \frac{\sum_{dt<0} C(t,dt)}{N_{dt<0}}$$

where t is the time following response onset, dt is the inter-laminar delay involved between windows from two layers, $C(t,dt)$ is the corresponding correlation. $N_{dt>0}$ is the number of positive delays investigated, which is equal to the number of negative delays, $N_{dt<0}$.

The direction dominance index was calculated as:

$$DDI(t) = \frac{C_{FF}(t) - C_{FB}(t)}{\sum_t \sum_{dt} C(t,dt) \Big/ N_{dt} \Big/ N_t}$$

where N_t and N_{dt} are the number of time points and delay involved in the analysis, respectively. A positive DDI indicates the dominance of feedforward signaling and a negative DDI indicates the dominance of effective feedback signaling.

Neuron, Volume *112*

Supplemental information

Spatial context non-uniformly modulates inter-laminar information flow in the primary visual cortex

Xize Xu (徐锡泽), Mitchell P. Morton, Sachira Denagamage, Nyomi V. Hudson, Anirvan S. Nandy, and Monika P. Jadi

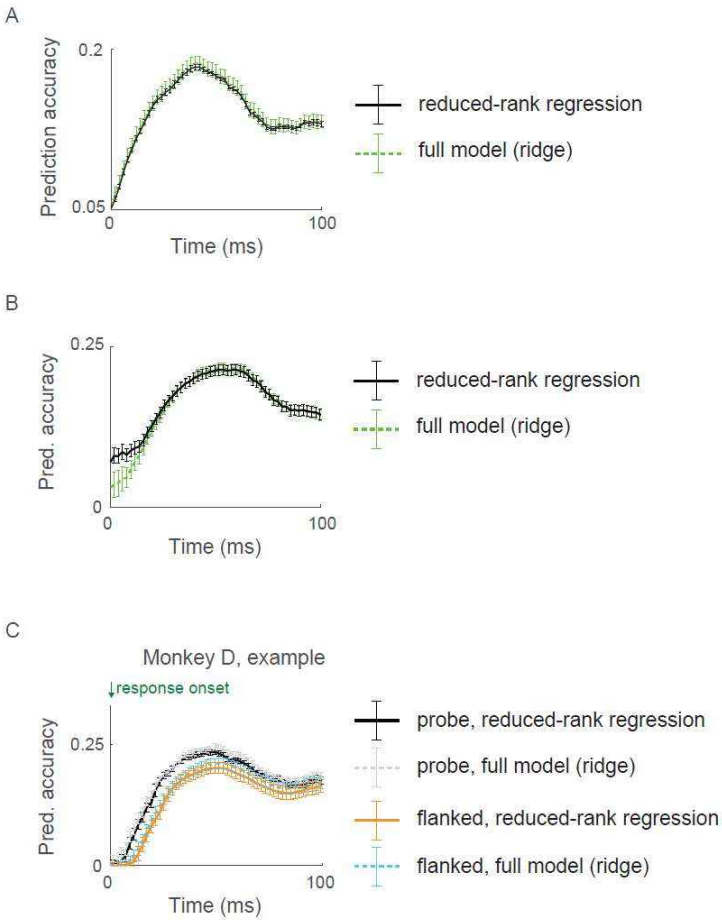

Figure S1. Comparing prediction accuracies calculated using reduced-rank regression (RRR) against the full regression model (ridge), related to Figure 1-3

(**A**) Temporal evolution of prediction accuracy as shown in Fig. 1H computed by RRR (solid curve) or the full regression model (dashed curve). (B) Temporal evolution of within-condition prediction accuracy as shown in black in Fig. 2C computed by RRR (solid curve) or the full regression model (dashed curve). (C) Temporal evolution of prediction accuracy under the probe and flanked conditions as shown in Fig. 3A computed by RRR (solid curves) or the full regression model (dashed curves). The full regression model always gives comparable predictive performance as RRR.

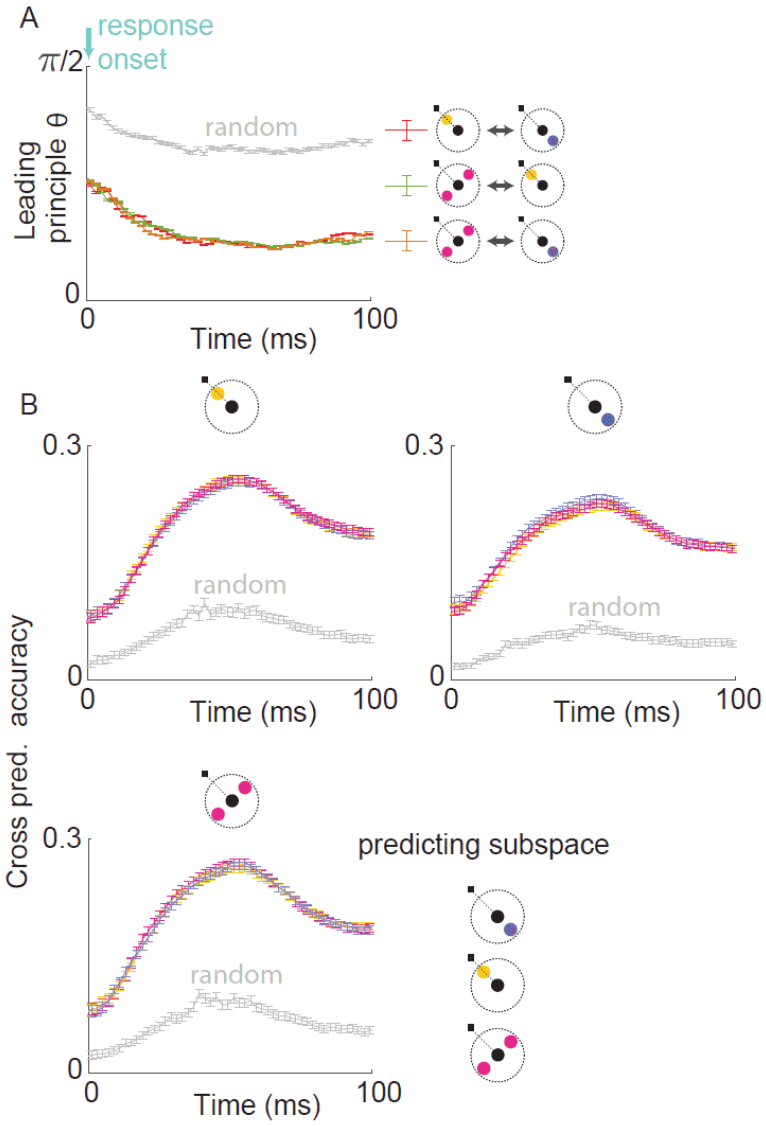

Figure S2. Comparing communication subspace across visual conditions, related to Figure 2

(**A**) The temporal evolution of leading principal angles between the communication subspaces identified from different types of flanked conditions during the corresponding visually responsive period (averaged across all sessions) and between random subspaces of comparable dimensions (grey; see Methods). (**B**) Cross-prediction analysis for input layer predicting superficial layer activity during a given flanked condition (shown at the top) and using subspaces identified for various conditions (as shown in the legend). Error bars indicate the 95% confidence interval for the mean.

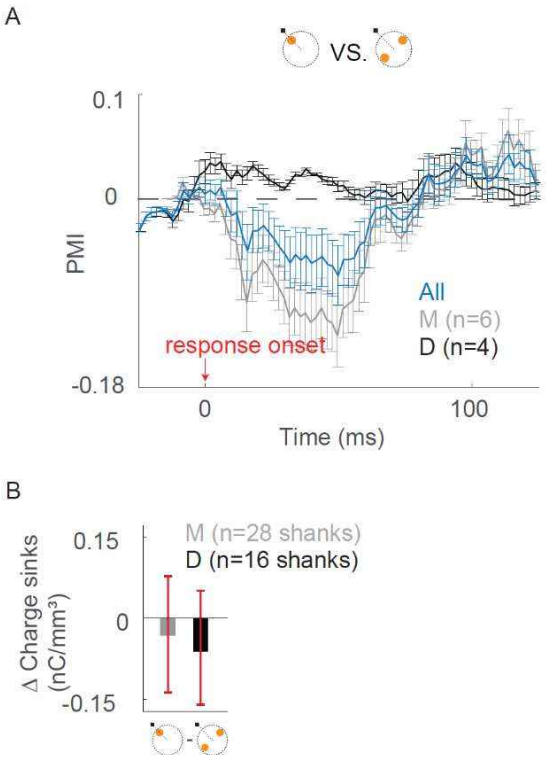

Figure S3. Comparing prediction accuracy across visual conditions, related to Figure 5, 7

(**A**) Same as Fig. 5B, comparing inter-laminar prediction accuracy under the radial-in condition to that under the tangential condition. Negative PMIs imply a degradation of prediction accuracy in the radial-in condition compared to the tangential condition. (**B**) The within-shank difference in the level of early charge sinks in the superficial layer, when compared between the radial-in and tangential conditions for all shanks from each monkey. Error bars indicate 95% confidence interval for the mean.

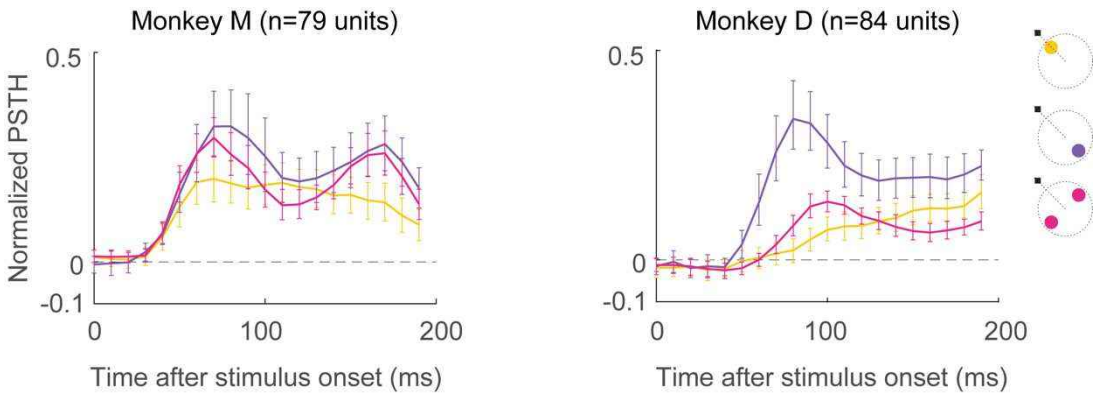

Figure S4. Comparing PSTH across flanker-only conditions, related to Figure 7

Normalized peri-stimulus time histograms (PSTHs; see Methods) for superficial layer units (separately for each monkey) under various flanker-only conditions. Error bars indicate the standard error across neurons. This analysis only included neurons that were visually responsive (see Methods) in the probe condition and exhibited significantly higher rates compared to all flanker-only conditions.